Genetics of Antibiotic Synergy in Mycobacterium tuberculosis

HARVARD UNIVERSITY
Graduate School of Arts and Sciences

DISSERTATION ACCEPTANCE CERTIFICATE

The undersigned, appointed by the

Committee on Higher Degrees in Biological Sciences in Public Health

have examined a dissertation entitled

Genetics of Antibiotic Synergy in *Mycobacterium tuberculosis*

presented by Francesca Guglielmini Tomasi

candidate for the degree of Doctor of Philosophy and hereby certify that it is worthy of acceptance.

Signature _____

Typed name: Prof. Yonatan Grad

Signature _____

Typed name: Prof. Dyann Wirth

Signature _____

Typed name: Prof. Simon Dove

Signature _____

Typed name: Prof. Valerie Mizrahi

Date: August 12, 2022

Genetics of Antibiotic Synergy in *Mycobacterium tuberculosis*

A dissertation presented

by

Francesca Guglielmini Tomasi

to

The Committee on Higher Degrees in Biological Sciences in Public Health

in partial fulfillment of the requirements

for the degree of

Doctor of Philosophy

in the subject of

Biological Sciences in Public Health

Harvard University

Cambridge, Massachusetts

August 2022

Dissertation Advisor: Eric J. Rubin Francesca Guglielmini Tomasi

Genetics of antibiotic synergy in *Mycobacterium tuberculosis*

Abstract

Tuberculosis (TB) is an infectious disease caused by the bacterium *Mycobacterium tuberculosis* (*Mtb*), which has been around for millennia and continues to affect millions of people every year. Successful TB treatment requires months of combination antibiotics, which complicates the ability to treat all cases quickly and effectively. Expanding our antibiotic arsenal against TB and optimizing drug combinations are two important steps to reducing treatment failure. In Chapter One of this dissertation, we examine the research tools available to identify new antibiotic targets in *Mtb* and to characterize the mechanisms of action of anti-tubercular compounds. New targets can be discovered through small molecule screens as well as target-based discovery using genetic methods. We can furthermore apply these tools to identify synergies between experimental treatments and optimize the effects of different antibiotics.

We have applied multiple genetic tools to identify and characterize promising candidates for target-based drug discovery against *Mtb*. The bulk of our work presented here focuses on a specific enzyme, peptidyl tRNA hydrolase (Pth). We find that while Pth could be investigated as a new antibiotic target on its own, its added appeal is as an enzyme whose inhibition would lend additional efficacy to existing drugs.

In Chapter Two, we identify two distinct biological roles for Pth in *Mtb*. We demonstrate that while one is required for bacterial survival, the other is not. Understanding the essential function of a protein is critical for assessing whether cells could quickly develop resistance against an inhibitor of that protein simply by reducing the need for it. In Chapter Three, we dive deeper into Pth's essential role in *Mtb* and probe the vulnerability of protein synthesis in this pathogen by assessing how Pth

interacts with tRNA in cells. We develop new experimental strategies to study tRNA in *Mtb* and lay a groundwork for future work on tRNA dynamics.

By examining Pth through a therapeutic lens, we next discover that drugs targeting this enzyme would synergize with two existing classes of antibiotics that are not currently used to treat TB: macrolides and aminoacyl tRNA synthetase inhibitors. Macrolides are inexpensive, well-tolerated drugs used to treat other bacterial infections but are not effective on their own against TB. Aminoacyl tRNA synthetase inhibitors have seen success in other types of infections and are currently being developed to target *Mtb*.

In the final chapter of this thesis, we discuss the implications of our work and lingering questions that would further improve our understanding of *Mtb* biology. We also present ongoing work that builds on tools and findings presented in this dissertation. Altogether, our goal is to contribute to a growing body of knowledge on *Mtb* physiology and the development of new strategies against an age-old disease.

Table of Contents

List of figures and tables

Chapter Two

Chapter Three

Chapter Four

Chapter Five

Appendix I

Appendix II

Acknowledgements

There are many, many people to thank. To start, thank you to my thesis advisor (and wedding officiant!) Eric for five years of intellectual curiosity, creativity, and support of a healthy work-life balance. I am grateful for the kind-hearted, goofy, and collaborative environment in which I completed my PhD, and that kind of positive culture comes from the top.

To all members of the Rubin and Fortune labs, past and present, thank you for your scientific and social contributions. Jess, you know that these pages would not exist without you. Thank you for sharing your discoveries with me. Satoshi, your mentorship, scientific knowledge, and generosity are unparalleled. I cannot thank you enough for your guidance, feedback, and patience. Junhao, your enthusiasm is contagious. Thank you for your genuine care, and for all your experimental and computational support. Xin, thank you for always having an answer to any lab question I had, and for being a great person to discuss ideas (and life!) with. Skye, thank you for imparting so much wisdom and love for the ribosome and for helping me out even after your time in the Rubin lab. Katie, thank you for literally putting a roof over my head and for being such a wonderful friend and (albeit briefly) lab mate. If I have attained half of your work ethic or communication skills, I will consider myself a successful scientist. Chidi, thank you for all your wisdom on mycobacterial genetics and experiment troubleshooting, and for all the laughs over the years. Kerry, you are a wonderful cat parent and scientist, and I am excited to watch you cross the PhD finish line soon!

To all my collaborators named throughout this dissertation, thank you for working with me and for being so friendly, communicative, and enthusiastic throughout the process. Alex, thank you for all the work you did in Chapter Two of this thesis, and for all your patience when explaining mass spec and basic protein structures to me.

To my DAC (Yonatan, Marcia, Matt, and Mike), thank you for your feedback as I planned, executed, re-planned, re-executed, analyzed, and re-analyzed experiments. Matt, thank you for your generosity also as a close collaborator. It was always fun running into you and catching up on experiments.

To Richard Cash: it was an absolute honor and joy to work with you and learn from you in GHP 539 for five years. Thank you for so many fascinating conversations, and for keeping me grounded in the broader global health context of even the most hyper-focused molecular research.

It has been a long academic road and I must thank all the teachers, professors, and mentors who encouraged my love of learning over 3 decades of school from Hoover to Durham Academy, to the University of Chicago, to the National Institutes of Health, and to Harvard.

Maddy, Harry, and Ian, I don't think I have to say anything for you to know how much our friendship has meant to me on and off campus. Harry and Ian, our hours in the BL3 were some of my favorite lab moments. Maddy, meeting you during other PhD program interviews was fate. You are such a wise and hard-working scientist, and an even kinder and funnier friend. I can't wait for all our paths to continue crossing. See you all on the next boat!

Thank you to every friend with whom I have shared even a single mile on the roads. I'm not going to check my Strava to see how many miles I have run since starting this PhD (but the data are out there). Through each of those N miles, you all gave me the physical endurance, emotional confidence, and mental clarity to complete this special type of scientific marathon.

Alissa and Jon, thank you for being our go-to besties in Boston. From boiling lobster in Maine to a flawless Iceland trip (I mean come on), our adventures kept my batteries charged during the most challenging years of my PhD. See you in Denver!

Mom and Dad: I could not have asked for better parents who got me curious about the world so early on. Thank you for everything: the science kits and homework help, the trips that opened our eyes to the world, your high expectations of us both academically and as human beings, and your love of life, adventures, and cultures. Luca and Ale: you are the best siblings ever and I am so proud of us! "Remember the potato" is still a more important lesson than all the science I have done. Stay witty.

Rachel, Jordan, Sixto, Zach, Brittany, and Remy: I'm so lucky to be able to call you my siblings now too, and to have shared this journey with you. To all the Rices and Camps: Thank you for being some of my loudest cheerleaders and for always showing up. Abel: thank you for helping me write my DAC reports in 2020. You're going to crush it in kindergarten next year. Demi: I can't wait to bribe you with science kits in a few years.

Thank you to all the pets in my life who have given me so much joy and unconditional love, especially my dearest Charlotte, Duke, Peyton, Muffins, Winston (the dog), Winston (the cat), and Stevie.

James: My academic career was made possible by so many people over so many years, but this thesis is dedicated to you (even if you don't read the whole thing – that's okay). Thank you for being my strongest supporter, for fiercely believing in me even when my own confidence slipped, and for always reminding me of what is most important at the end of the day. Your service to our country

enabled me to follow my own passions: your selflessness and desire to make the world a better place through genuine action continue to inspire me every day. I love our life together and am so excited for our next adventure.

A Note About This Dissertation

The discussion of scientific findings with audiences beyond those who are in the lab is critical for an entire society to be able to have open, productive discussions about these findings, their implications, and shortfalls. The final chapter of this thesis provides a summary that has been written for a general audience.

Chapter One: Introduction to genetic tools for tuberculosis (TB) antibiotic discovery

Tuberculosis: a pandemic of the past, present, and future

Tuberculosis (TB) is a deadly infectious disease that has plagued humans for at least ten thousand years and continues to be a leading infectious cause of death worldwide [1, 2]. Over time it has been called many different names, from *phthisis* in ancient Greece and *tabes* in ancient Rome, to *the white plague* in the 1700s and *consumption* through the nineteenth century. Despite its many designations, TB is caused by a single bacterium: *Mycobacterium tuberculosis* (*Mtb*). This pathogen spreads from person to person via aerosol and predominantly infects the lungs, where it establishes itself in alveolar macrophages. Its signature pathology is the granuloma, a conglomerate of immune cells and infected macrophages that are partitioned from the rest of the lung [3]. Within these niches, *Mtb* encounters many environmental pressures including variable nutrient availability, oxidative stress, and other immune-imposed stresses [3, 4].

About 90% of people who are infected with *Mtb* never go on to develop active disease, but instead have latent TB, in which the immune system is able to control infection and prevent it from progressing [2]. Individuals with latent TB do not have clinical symptoms and cannot spread *Mtb* to others. The main risk factor for progression to active disease is a weakened immune system. In fact, co-infection with Human Immunodeficiency Virus (HIV) has led to a resurgence of active TB in recent decades, and TB remains a leading cause of death in people with Acquired Immune Deficiency Syndrome (AIDS) [2, 5].

A persistent disease requires a persistent response. The 2021 Global Tuberculosis Report published by the World Health Organization (WHO) estimates that 1.5 million people died of TB in 2020, and that recent progress in reducing TB incidence has stalled globally during the COVID-19 pandemic [2]. Access to treatment for drug-resistant TB has fallen by 15%, with only one in three people with MDR TB receiving needed therapy [2]. Access to preventive treatment has dropped by

21%, and global spending on TB diagnostics, treatment, and prevention has plummeted to less than half of what the WHO estimates is needed to achieve milestones in its End TB Strategy [2]. The social, political, and economic challenges of TB control are exacerbated by the months-long regimens currently required to treat *Mycobacterium tuberculosis* (*Mtb*). Strengthening research programs to improve TB therapy will synergize with global health efforts to increase access to, as well as success of, treatment.

Overview of antibiotic use in TB

The first anti-tuberculous agent, streptomycin, was discovered by Selman Waksman, Elizabeth Bugie, and Albert Schatz in 1943. Patients who received streptomycin saw initial clinical improvement but eventually developed resistance; single-drug treatment did not significantly improve TB mortality in the long term [6-8]. These discoveries ushered in an era of small molecule discovery against *Mtb* and the development of a multidrug therapy against this disease. Standard treatment of drug susceptible TB currently takes 4-9 months and combines rifapentine-moxifloxacin or rifampin-ethambutol with isoniazid and pyrazinamide. Relapse is estimated to occur in about 5% of patients with drug-susceptible after 6 months of first-line treatment, and in about 20% of patients after a 4-month course [9]. The lengthy duration of treatment and its associated side effects (including nausea, malaise, neuropathy, and temporary deafness), as well as acquired drug resistance, have been major barriers to eliminating TB worldwide.

TB requires multidrug therapy to minimize rates of acquired genetic resistance. The use of multiple drugs reduces the probability of survival of a strain that is already resistant to a single drug [10]. Multidrug therapy is administered for long periods of time to circumvent *Mtb*'s ability to develop phenotypic resistance, in which a subpopulation of metabolically altered cells tolerates antibiotic exposure and requires a longer time to eradicate [10, 11]. *Mtb* is also intrinsically resistant to most of

the antibiotics used to treat other bacterial infections. As a result, TB-specific drug discovery programs have been carried out and identified more potent – and thus less well-tolerated – small molecules.

Drug resistant TB

The emergence and spread of multidrug resistant (MDR) TB pose a massive medical and economic burden. MDR TB is defined by *Mtb* that is resistant to at least one first-line TB drug in addition to isoniazid or rifampicin [2]. Extensively drug resistant (XDR) TB is resistant to multiple first-line TB drugs and is even more complicated to treat. Recent advances in MDR and XDR TB therapy have significantly improved treatment outcomes and reflect ongoing progress in anti-tubercular drug discovery. The drug pretomanid was approved in late 2019 for use in combination with bedaquiline and linezolid in a 26–39-week regimen in patients with XDR TB and non-responsive MDR TB. Pretomanid was first discovered in 2000 when it was found to have potent bactericidal activity against both growing and nongrowing drug susceptible and MDR *Mtb.* This drug has a unique mechanism of action with no cross-resistance to existing TB drugs [12]. Follow-on studies in murine TB models found that combining pretomanid with moxifloxacin and pyrazinamide cleared infections more rapidly than the current first-line regimen [13].

Long-term relapse-based experiments in mice established shorter and more effective regimens by combining pretomanid and bedaquiline with linezolid or moxifloxacin and pyrazinamide [14-16]. The Nix-TB trial (ClinicalTrials.gov #NCT02333799) found that combining bedaquiline, pretomanid, and linezolid could treat patients with highly drug-resistant TB in 6 months (compared to traditional 20-month regimens), though not without significant adverse events [17]. The shift to an all-oral, more effective, and shorter regimen for drug-resistant TB was a major success. Nonetheless, its duration and side effects warrant continued research, as access to simpler therapies remains a priority for drug susceptible, MDR, and XDR TB.

Designing new regimens to reduce treatment failure

Treatment failure occurs when a patient is not cured or relapses after therapy from drug resistance. Treatment failure could arise from a variety of factors, both host and bacterial. Differing drug metabolism or inability to complete prescribed therapy can lead to inadequate antibiotic exposure on the host side. Inflammatory lesions, such as granulomas, can also change *Mtb*'s microenvironment and lead to altered drug susceptibility because of local bacterial adaptations. From the pathogen's standpoint, additional factors may come into play. Treatment failure may occur because of both acquired and intrinsic drug resistance, which arise from distinct mechanisms. Bacterial subpopulations with altered susceptibility might produce pathogens that survive even extended antibiotic treatment.

Treatment failure in TB can be combated by examining the tools available to identify new antibiotic targets, as well as to use existing drugs in new ways to maximize bacterial killing. While the scope of this thesis is limited to bacterial factors, synergy with host interventions would also be a successful and noteworthy strategy for shortening treatment and decreasing failure rates. In the lab, identifying new antibiotic targets can be accomplished through high-throughput small molecule screens as well as target-based discovery born out of genetic methods. Researchers can also apply these strategies to lend efficacy to existing drugs and quantify synergies between different experimental treatments. Historically, synergy was not a priority when establishing TB regimens. We propose a synergy-focused framework for designing new treatment courses that focuses on well-tolerated combination antibiotics that maximize bacterial killing at all stages of growth while minimizing treatment length. Strengthening research programs to improve TB therapy will synergize with global health efforts to increase access to, as well as success of, treatment.

Identifying new antibiotic targets using chemical screens

Systematic screens of soil, bacterial, or fungal extracts as well as synthetic chemical libraries have seen the most translational success so far in antibiotic discovery [18]. A benefit to a chemical screen approach is the convenience of starting with small molecules with promising physiochemical properties that can be further modified. A major barrier to TB drug development is cell wall penetration, and chemical screens select for compounds that can already enter *Mtb* cells. Many first- and second-line TB drugs are derived from natural products including rifampicin and aminoglycosides such as streptomycin [19]. The recent advances in MDR and XDR TB regimens with pretomanid and bedaquiline are also outcomes of whole-cell library screens [19]. These approaches work by testing compound libraries for their ability to block bacterial growth *in vitro*, usually under standardized aerobic growth conditions, and has enabled the identification of particularly accessible bacterial targets and pathways that are susceptible to existing compounds.

While historically effective, chemical library screening has now led to recurring targets (such as MmpL3) and redundancies in hits, with similar small molecules repeatedly being discovered in different libraries. At a time when more diverse drugs and targets are needed, this is a significant challenge with current drug discovery efforts. In fact, the most-used antibiotics across bacterial infections block the same small subset of targets [20]. This is also a reflection of library screen design: the same approaches to identifying anti-TB compounds will yield the same results. In the era of antibiotic resistance, diversity of mechanism is crucial to bypass existing resistance mechanisms.

Despite substantial efforts in systematic chemical library screens, treatment of drug-susceptible TB has remained largely unchanged since the mid-twentieth century, highlighting the need for creative new approaches. These are ongoing. Library screens using specialized strains and other growth conditions such as macrophage screens, hypoxic media, or granuloma and caseum-like environments are likely to improve translation from *in vitro* hits to *in vivo* success (reviewed in [21]). In 2009, Christophe, et al., published a cell-based assay that used confocal fluorescence microscopy to

screen for compounds that blocked *Mtb* replication within macrophages. Through this screen, they identified dinitrobenzamide derivatives with potent anti-tubercular activity and showed that these compounds inhibited the essential cell wall synthesis enzyme DprE1 [22]. At the same time, a study was published on the synthesis of benzothiazinones with anti-TB activity that used reverse genetics also to show DprE1 as the target of inhibition [23]. Since these findings, DprE1 inhibitors with different types of chemical scaffolds have been developed and are being investigated as potential TB therapeutics (reviewed in [24]).

Pyrazinamide is a breakthrough TB drug that underscores the value of testing multiple growth conditions and mimicking the host environment. In a standard broth microdilution assay, pyrazinamide does not have appreciable growth-inhibiting effects on *Mtb*. However, when added under hypoxic conditions, pyrazinamide becomes highly sterilizing and has been critical to reducing TB treatment times from multiple years to several months [25]. This example shows the importance of evolving chemical screens to identify critical compounds that may not otherwise be uncovered using standard laboratory growth conditions. In subsequent sections of this dissertation, we will highlight advances in maximizing the utility of compounds identified in chemical screens.

Identifying new antibiotics using genetic tools

Starting with a small molecule and identifying the target for promising hits is the empirical, top-down approach to drug discovery. Recent progress in bacterial genetics, high-throughput sequencing, and medicinal chemistry offer a new promise to dedicating increased efforts to the bottom-up approach of target-based drug development, which thus far has not yielded much success in bacteriology. In this strategy, a single gene product or mechanism is identified as an effective drug target based on biological studies. Inhibition of this target is shown *in vitro* to be sufficient to confer a meaningful therapeutic effect. The identification of new targets and mechanisms of bacterial killing

will also likely circumvent pre-existing resistance mechanisms and thus be applicable to drug susceptible, MDR, and XDR-TB.

In the past, functional deletions such as genetic knockouts have been used to validate hits but with two major drawbacks. First, targets that are essential for bacterial viability cannot be knocked out; second, antibiotics do not always fully inhibit their targets. Instead, genetic knockdowns – titrating levels of gene expression or gene products – offer a more realistic simulation for potential inhibitors of essential and non-essential genes and offer insight on the "vulnerability" of a target: how much (or how little) target inhibition is required for a therapeutic effect. Three primary genetic approaches have been used in TB research to study individual targets and their vulnerability: transposon sequencing (TnSeq), proteolytic degradation systems, and CRISPR-interference (CRISPRi).

Transposon sequencing

Transposon sequencing (TnSeq) works by mapping random transposon integration sites in saturated mutant libraries: the ability or inability of a locus to sustain transposon insertion is indicative of that gene's requirement for growth in the condition tested. The predecessor to TnSeq, transposon site hybridization (TraSH), first identified the complete set of *Mtb* genes required for growth under different conditions. This tool combined high-density insertional mutagenesis using phage containing a *mariner*-based transposon with microarrays to map pools of mutants [26]. It has since been replaced with TnSeq, which uses next generation sequencing to quantify marked transposon insertions across the genome [27-29].

In addition to providing insight on gene essentiality, TnSeq has been a powerful tool to identify so-called "conditional essentiality." While some genes may not be required for growth in standard laboratory media, they may no longer sustain transposon insertions in other conditions. Recent work has shed light on genes required for host-relevant conditions such as cholesterol catabolism [30] and

different genetic backgrounds *in vivo* using collaborative cross mouse panels [31]. TnSeq has also been used to investigate phenotypic variation in clinical *Mtb* strains: certain genes are differentially required across clinical strains, including *katG*, which activates the pro-drug isoniazid, a first-line TB drug [32]. This finding shows the ability for TnSeq to predict resistance mechanisms to antibiotics: a loss of function mutation in *katG* would confer isoniazid resistance by failing to activate this drug in cells.

Studies on the conditional essentiality of *Mtb* genes across strains and growth conditions have produced extensive amounts of data on the "druggable" genome in *Mtb*: genes that could be further explored as putative drug targets because they are indispensable for growth or confer increased susceptibility to antibiotics when inactivated. Following up on hits of interest and transforming findings into phenotypic assays for both chemical screening and medicinal chemistry can help establish more productive strategies for TB drug discovery.

Genetic knockdowns

Proteolytic degradation systems and CRISPR-interference (CRISPRi) allow us to study essential genes by providing titratable ways – much like drug screens, since compounds hit their targets with varying strength – to reduce their abundance in the bacterial cell. Proteolytic degradation works by tagging a gene of interest with a degradation signal – here, a DAS tag – causing inducible expression of an accessory molecule – stringent starvation protein B (SspB) that shuttles tagged proteins for degradation using the endogenous protease ClpXP [33]. Different intracellular levels of SspB allow for a range of protein knockdown. CRISPRi instead uses targeted transcriptional repression. An inducible nuclease deactivated Cas9 (dCas9) is guided to a target gene by a single guide RNA molecule (sgRNA) with complementarity to the target DNA sequence [34]. The sgRNA molecule also contains a short protospacer-adjacent motif (PAM) for initial dCas9 recognition, which disrupts the target DNA and facilitates binding of sgRNA to its complement [34]. This interaction physically blocks RNA

polymerase from being able to initiate transcription or fully elongate mRNA. Different PAM sequences confer a range of dCas9 binding, which in turn modulates the level of knockdown [34].

Both tools facilitate target-based drug discovery by allowing researchers to define the vulnerability of specific genes or pathways. Proteolytic degradation systems were recently used in a large chemical-genetic screen to combine small molecules with a pool of *Mtb* strains depleted in essential genes [35]. Because these hypomorphs are hypersensitive, this approach was found to yield more hit compounds of interest than whole cell chemical screens alone, and their effects on different strains shed light on compound mechanisms of action. Over new 40 compounds were found to target previously established *Mtb* targets including DNA gyrase, cell wall biosynthesis, and RNA polymerase. An inhibitor of a new target which interfered with the essential *Mtb* efflux pump EfpA was also identified. This inhibitor, which was effective against an EfpA hypomorph, was then chemically modified for increased potency against a wild type *Mtb* strain [35]. This example shows the utility of combining genetic knockdowns with whole cell chemical screens to identify small molecules that would not be unearthed by exclusively screening wild type cells.

Genetic tools have also been used on their own to prioritize putative drug targets for future drug development. Recently, a large-scale CRISPRi screen quantified the vulnerability of essential genes and pathways to predict *Mtb*'s susceptibility to an antibiotic targeting that gene or pathway [36]. A considerable challenge in target-based drug discovery is the development of a selective drug from scratch with suitable pharmacokinetic and toxicological profiles. Identifying highly vulnerable targets that require only small levels of inhibition for a clinically relevant phenotype would maximize the likelihood of success, since lower levels of target engagement would need to be achieved for compound efficacy. Recent advances in medicinal chemistry such as fragment-based drug design and dynamic combinatorial chemistry have the potential to further increase the likelihood of success for compound development [37] (reviewed in [38]).

Multiple highly vulnerable targets have been identified that do not yet have inhibitors against them. Several promising pathways emerged from this screen that were even more vulnerable than the targets of current TB antibiotics such as protein folding and secretion, metabolism, DNA replication, cell division, and tRNA synthetases [36]. The latter group – aminoacyl tRNA synthetases (aaRS) – were found to be highly vulnerable regardless of the *Mtb* strain tested. Because aaRS have conserved active sites, compounds designed to target them could target multiple synthetases and reduce rates of antibiotic resistance [39]. Efforts are already underway to develop aaRS inhibitors against *Mtb* [39-42] (reviewed in [43], and discussed in Chapter 3 of this dissertation). These enzymes are already the targets of the anti-malarial halofuginone and the antibiotic mupirocin.

These approaches have two other uses. One is that they can be used for validating chemical-genetic interactions. For compounds whose targets require validation, strains with depletions of hypothesized targets or potential activators can be constructed using the genetic tools described above. This permits mapping to the true target in whole cells, as discussed above. Conversely, specifically constructed strains can aid in targeted drug discovery using a whole cell approach. For example, Evans, et al. used a complementary genetic approach to transcriptionally silence multiple genes in the panthothenate and coenzyme A biosynthesis pathways [44]. These strains were then used with chemical screening to discover whole cell-active inhibitors.

Antibiotic synergy

Target-based discovery has already offered new and promising insights to help simplify TB therapy and reduce treatment duration. By studying the interplay of drugs and specific targets, we can design more deliberate regimens with a focus on synergistic interactions. Synergy refers to a combined effect of multiple drugs that is greater than the sum of their individual effects. While TB combination therapy was developed for several important reasons, synergy was not front of mind when designing

current regimens. How can we apply a synergy-focused framework in the design of new TB treatments?

One way to do this is by screening genetic libraries against existing antibiotics to find genes whose depletion hypersensitizes *Mtb* to existing drugs that are either already used or currently ineffective against TB. Both deletion and depletion mutants can phenocopy antibiotics targeting the mutated protein, allowing us to screen for synergistic "drugs" without yet having a molecule in hand. In a recent TnSeq screen, transposon mutant libraries were screened in the presence of different antibiotics with diverse mechanisms of action [45]. Multiple genetic determinants of antibiotic susceptibility were involved in synthesis and maintenance of *Mtb*'s cell envelope. For instance, deletion of the gene *fecB*, which mediates cell wall integrity, conferred susceptibility to every antibiotic tested. Findings like this suggest that efforts directed toward increasing permeability of *Mtb* cells would expand the arsenal of antibiotics that could potentially be used to treat TB by exploiting synergy between cell wall inhibitors and intracellular antibiotics. Similarly, another TnSeq screen performed in mice treated with the first-line TB drugs rifampicin, isoniazid, ethambutol, and pyrazinamide found that the bottleneck for rifampicin efficacy is permeability to the drug, while isoniazid susceptibility is predominantly affected by replication rates [46]. These findings were also recently corroborated by observations that growth on cholesterol – a host-relevant carbon source – decreased susceptibility to rifampicin by causing lipid composition changes on *Mtb*'s cell envelope. Efforts targeting cell wall synthesis pathways would likely then enhance killing by rifampicin during infection [47].

Another chemical-genetic screen was recently performed using CRISPRi libraries. Expression levels of most *Mtb* genes were titrated and bacterial fitness quantified in the presence of different antibiotics [48]. A putative aminoglycoside transporter was identified when decreased levels of Rv1819c (*bacA,* an ABC importer of hydrophilic solutes) conferred resistance to streptomycin,

showing once again the importance of understanding determinants of drug resistance and the promise of increasing cell wall permeability to improving *Mtb* susceptibility to antibiotics.

Combining existing drugs in new ways

In addition to chemical-genetic screens to identify mechanisms of synergy between putative drug targets and existing antibiotics, combinatorial drug screening offers an approach to quantify synergy and prioritize drug combinations to test *in vivo*. New experimental and analytical methodologies have strengthened our ability to measure drug interactions. Checkerboard assays have historically been the gold standard for measuring pairwise drug interactions. These assays test antibiotics in double serial dilutions and compare their combined effect with each drug's individual effect in a microtiter plate. The recent development of the more efficient and less expensive DiaMOND (Diagonal Measurement Of N-way Drug interactions) offers a relatively simple way to measure interactions between any number of drugs [49]. This technique compares dose responses for mixtures of drugs with dose responses of each individual drug using mathematical modeling. DiaMOND's efficiency comes from applying geometric models to factor high-order drug interactions into lower-order components, creating a framework to predict higher-order interactions.

Synergy studies *in vitro* have been extended to prioritize experimental drug combinations *in vivo*. Recent work by Larkins-Ford et al. identified signatures of drug potency and interactions in *in vitro* models that were predictive of efficacy in preclinical mouse models of TB [50]. The ability to identify synergy and antagonism between different drugs *in vitro* will be extremely helpful in designing future combination drug regimens against TB, especially as more drug targets enter the discovery pipeline. Drugs that bolster each other in combination will likely be more effective in clearing infections and have fewer side effects in patients due to reducing both dosage and treatment time.

Prioritizing new antibiotic regimens

An obvious challenge to the design of new combination therapies is the financial and time cost of large-scale clinical trials to assess their efficacy. Thus, preclinical testing of TB therapies will need to address multiple important factors to prioritize regimens for clinical assessment: (1) *in vitro* efficacy on total killing in different bacterial subpopulations and growth conditions, and (2) their efficacy in animal models of TB relapse.

A major challenge to TB treatment is the heterogeneity of bacterial populations within a host as well as host environments. As described above, TB therapy is administered for several months because *Mtb* creates phenotypically diverse subpopulations with varying levels of drug tolerance. This is a result both of *Mtb*'s metabolic adaptation to different microenvironments within a host such as different carbon sources and other changes between granulomas, as well as *Mtb*'s asymmetric growth and division pattern (reviewed in [51]). For instance, genetic knockdown of *lamA*, which influences cell size variation in mycobacteria, increases *Mtb* susceptibility to rifampicin and vancomycin [52]. Assays that measure total bacterial killing or the rate of bacterial killing – as opposed to minimal inhibitory concentrations, the concentration at which >90% of bacterial growth is inhibited in a broth microdilution assay – might be more informative about the bactericidal dynamics of small molecules. Recent progress with animal models has also increased our ability to assess applicability of *in vitro* findings to *in vivo* models. Infection relapse models, in which mice are monitored for culturable bacteria after stopping drug treatment, are an important way to test the total sterilizing activity of a potential therapy [50]. Work on understanding the metabolic changes *Mtb* undergoes in different microenvironments demonstrates the importance of testing compounds in different growth conditions including various carbon sources, pH, and hypoxia [11, 53]. Future work continuing to understand how these subpopulations form will facilitate the discovery of putative drug targets that synergize to fully sterilize all diseased microenvironments.

Conclusion

In this chapter, we have outlined challenges of current multidrug regimens against tuberculosis and lay out a synergy-focused framework for ongoing and future drug discovery efforts. The rational design of regimens that sterilize diverse phenotypic subpopulations will maximize bacterial killing while minimizing both treatment duration and infection relapse. A deeper understanding of the fundamental molecular biology of *Mtb* is critical in the re-design of more effective anti-TB strategies. Importantly, the TB field currently has all the necessary tools to screen for and prioritize drug targets *in vitro* based on the vulnerability of essential and non-essential genes in the *Mtb* genome, and to translate these findings in *in vivo* models. Combining genetic methods with chemical screens offers a formidable strategy to redefine and accelerate the preclinical design of TB therapy by identifying powerful new targets altogether, as well as targets that lend new efficacy to existing drugs.

Overview of findings

In the following three chapters, we apply the genetic tools described above to identify and characterize promising candidates for target-based drug discovery against *Mtb*. The bulk of our work focuses on a specific enzyme, peptidyl tRNA hydrolase (Pth), described in detail in Chapter Two and Chapter Three. We find that while Pth could be investigated as a new antibiotic target on its own, its added appeal is as an enzyme whose inhibition would lend efficacy to existing drugs when combined in a synergy-focused regimen.

In Chapter Two, we identify two distinct biological roles for Pth in *Mtb*. We demonstrate that while one is required for bacterial survival, the other is not. Understanding the essential function of a protein is critical for assessing the ease with which cells could develop resistance against an inhibitor of that protein simply by reducing the need for it. Work from this chapter justifies our continued research into Pth as a viable anti-*Mtb* drug target.

In Chapter Three, we dive deeper into the essential role Pth plays in *Mtb* and probe the vulnerability of protein synthesis in this pathogen by assessing how Pth interacts with tRNA in cells. We develop new experimental strategies to study tRNA in *Mtb* and lay a groundwork for future studies of tRNA dynamics. tRNA turnover is a critical and tightly regulated process in all domains of life, but it is an under-studied aspect of mycobacterial physiology.

We next examine Pth through a therapeutic lens. We discover that drugs targeting this enzyme in *Mtb* would synergize with two existing classes of antibiotics that are not currently used to treat TB: macrolides and aminoacyl tRNA synthetase inhibitors. Macrolides are inexpensive, well-tolerated drugs used to treat other bacterial infections but are not effective on their own against TB. Aminoacyl tRNA synthetase inhibitors have seen success in malaria treatment as well as certain types of skin infections and are currently being developed to target *Mtb*.

In the final chapter of this thesis, we discuss the implications of our work and lingering questions that would further improve our understanding of *Mtb* biology. We also discuss ongoing work that builds on the findings presented in this dissertation. Altogether, our goal is to contribute to a growing body of knowledge of *Mtb* physiology and the development of new strategies against an age-old disease.

References

1. Kapur, V., T.S. Whittam, and J.M. Musser, *Is Mycobacterium tuberculosis 15,000 years old?* J Infect Dis, 1994. **170**(5): p. 1348-9.
2. W.H.O., *Global tuberculosis report 2021*. 2021.
3. Ehlers, S. and U.E. Schaible, *The granuloma in tuberculosis: dynamics of a host-pathogen collusion.* Front Immunol, 2012. **3**: p. 411.
4. Martin, C.J., A.F. Carey, and S.M. Fortune, *A bug's life in the granuloma.* Semin Immunopathol, 2016. **38**(2): p. 213-20.
5. Bruchfeld, J., M. Correia-Neves, and G. Kallenius, *Tuberculosis and HIV Coinfection.* Cold Spring Harb Perspect Med, 2015. **5**(7): p. a017871.
6. Gernez, R., Breton, and et al., *[Treatment of pulmonary tuberculosis in children with streptomycin].* Sem Hop, 1948. **24**(89): p. 2916.
7. Regniers, P., J. Beerens, and B. De Landsheere, *Streptomycin treatment of pulmonary tuberculosis in adults.* Belg Tijdschr Geneesk, 1949. **5**(1): p. 2-20.
8. Tempel, C.W., *The place of streptomycin in the treatment of pulmonary tuberculosis.* Bull U S Army Med Dep, 1949. **9**(1): p. 25-34.
9. Colangeli, R., et al., *Bacterial Factors That Predict Relapse after Tuberculosis Therapy.* N Engl J Med, 2018. **379**(9): p. 823-833.
10. Connolly, L.E., P.H. Edelstein, and L. Ramakrishnan, *Why is long-term therapy required to cure tuberculosis?* PLoS Med, 2007. **4**(3): p. e120.
11. Hicks, N.D., et al., *Clinically prevalent mutations in Mycobacterium tuberculosis alter propionate metabolism and mediate multidrug tolerance.* Nat Microbiol, 2018. **3**(9): p. 1032-1042.
12. Stover, C.K., et al., *A small-molecule nitroimidazopyran drug candidate for the treatment of tuberculosis.* Nature, 2000. **405**(6789): p. 962-6.
13. Nuermberger, E., et al., *Powerful bactericidal and sterilizing activity of a regimen containing PA-824, moxifloxacin, and pyrazinamide in a murine model of tuberculosis.* Antimicrob Agents Chemother, 2008. **52**(4): p. 1522-4.
14. Tasneen, R., et al., *Sterilizing activity of novel TMC207- and PA-824-containing regimens in a murine model of tuberculosis.* Antimicrob Agents Chemother, 2011. **55**(12): p. 5485-92.
15. Li, S.Y., et al., *Bactericidal and Sterilizing Activity of a Novel Regimen with Bedaquiline, Pretomanid, Moxifloxacin, and Pyrazinamide in a Murine Model of Tuberculosis.* Antimicrob Agents Chemother, 2017. **61**(9).
16. Xu, J., et al., *Contribution of Pretomanid to Novel Regimens Containing Bedaquiline with either Linezolid or Moxifloxacin and Pyrazinamide in Murine Models of Tuberculosis.* Antimicrob Agents Chemother, 2019. **63**(5).
17. Conradie, F., et al., *Treatment of Highly Drug-Resistant Pulmonary Tuberculosis.* N Engl J Med, 2020. **382**(10): p. 893-902.
18. Tommasi, R., et al., *ESKAPEing the labyrinth of antibacterial discovery.* Nat Rev Drug Discov, 2015. **14**(8): p. 529-42.
19. Mdluli, K., T. Kaneko, and A. Upton, *The tuberculosis drug discovery and development pipeline and emerging drug targets.* Cold Spring Harb Perspect Med, 2015. **5**(6).
20. Payne, D.J., et al., *Drugs for bad bugs: confronting the challenges of antibacterial discovery.* Nat Rev Drug Discov, 2007. **6**(1): p. 29-40.
21. Dartois, V. and C.E. Barry, 3rd, *A medicinal chemists' guide to the unique difficulties of lead optimization for tuberculosis.* Bioorg Med Chem Lett, 2013. **23**(17): p. 4741-50.

22. Christophe, T., et al., *High content screening identifies decaprenyl-phosphoribose 2' epimerase as a target for intracellular antimycobacterial inhibitors.* PLoS Pathog, 2009. **5**(10): p. e1000645.
23. Makarov, V., et al., *Benzothiazinones kill Mycobacterium tuberculosis by blocking arabinan synthesis.* Science, 2009. **324**(5928): p. 801-4.
24. Chikhale, R.V., et al., *Overview of the Development of DprE1 Inhibitors for Combating the Menace of Tuberculosis.* J Med Chem, 2018. **61**(19): p. 8563-8593.
25. Wade, M.M. and Y. Zhang, *Anaerobic incubation conditions enhance pyrazinamide activity against Mycobacterium tuberculosis.* J Med Microbiol, 2004. **53**(Pt 8): p. 769-773.
26. Sassetti, C.M., D.H. Boyd, and E.J. Rubin, *Comprehensive identification of conditionally essential genes in mycobacteria.* Proc Natl Acad Sci U S A, 2001. **98**(22): p. 12712-7.
27. Zhang, Y.J., et al., *Global assessment of genomic regions required for growth in Mycobacterium tuberculosis.* PLoS Pathog, 2012. **8**(9): p. e1002946.
28. van Opijnen, T. and A. Camilli, *Transposon insertion sequencing: a new tool for systems-level analysis of microorganisms.* Nat Rev Microbiol, 2013. **11**(7): p. 435-42.
29. DeJesus, M.A., et al., *Comprehensive Essentiality Analysis of the Mycobacterium tuberculosis Genome via Saturating Transposon Mutagenesis.* mBio, 2017. **8**(1).
30. Griffin, J.E., et al., *High-resolution phenotypic profiling defines genes essential for mycobacterial growth and cholesterol catabolism.* PLoS Pathog, 2011. **7**(9): p. e1002251.
31. Smith, C.M., et al., *Host-pathogen genetic interactions underlie tuberculosis susceptibility in genetically diverse mice.* Elife, 2022. **11**.
32. Carey, A.F., et al., *TnSeq of Mycobacterium tuberculosis clinical isolates reveals strain-specific antibiotic liabilities.* PLoS Pathog, 2018. **14**(3): p. e1006939.
33. Kim, J.H., et al., *Protein inactivation in mycobacteria by controlled proteolysis and its application to deplete the beta subunit of RNA polymerase.* Nucleic Acids Res, 2011. **39**(6): p. 2210-20.
34. Rock, J.M., et al., *Programmable transcriptional repression in mycobacteria using an orthogonal CRISPR interference platform.* Nat Microbiol, 2017. **2**: p. 16274.
35. Johnson, E.O., et al., *Large-Scale Chemical-Genetic Strategy Enables the Design of Antimicrobial Combination Chemotherapy in Mycobacteria.* ACS Infect Dis, 2020. **6**(1): p. 56-63.
36. Bosch, B., et al., *Genome-wide gene expression tuning reveals diverse vulnerabilities of M. tuberculosis.* Cell, 2021. **184**(17): p. 4579-4592 e24.
37. Scott, D.E., et al., *A fragment-based approach to probing adenosine recognition sites by using dynamic combinatorial chemistry.* Chembiochem, 2009. **10**(17): p. 2772-9.
38. Ladame, S., *Dynamic combinatorial chemistry: on the road to fulfilling the promise.* Org Biomol Chem, 2008. **6**(2): p. 219-26.
39. Kovalenko, O.P., et al., *Dual-target inhibitors of mycobacterial aminoacyl-tRNA synthetases among N-benzylidene-N'-thiazol-2-yl-hydrazines.* Medchemcomm, 2019. **10**(12): p. 2161-2169.
40. Gudzera, O.I., et al., *Identification of Mycobacterium tuberculosis leucyl-tRNA synthetase (LeuRS) inhibitors among the derivatives of 5-phenylamino-2H-[1,2,4]triazin-3-one.* J Enzyme Inhib Med Chem, 2016. **31**(sup2): p. 201-207.
41. Li, X., et al., *Discovery of a Potent and Specific M. tuberculosis Leucyl-tRNA Synthetase Inhibitor: (S)-3-(Aminomethyl)-4-chloro-7-(2-hydroxyethoxy)benzo[c][1,2]oxaborol-1(3H)-ol (GSK656).* J Med Chem, 2017. **60**(19): p. 8011-8026.
42. Soto, R., et al., *Identification and characterization of aspartyl-tRNA synthetase inhibitors against Mycobacterium tuberculosis by an integrated whole-cell target-based approach.* Sci Rep, 2018. **8**(1): p. 12664.
43. Kim, S.H., S. Bae, and M. Song, *Recent Development of Aminoacyl-tRNA Synthetase Inhibitors for Human Diseases: A Future Perspective.* Biomolecules, 2020. **10**(12).

44. Evans, J.C., et al., *Validation of CoaBC as a Bactericidal Target in the Coenzyme A Pathway of Mycobacterium tuberculosis.* ACS Infect Dis, 2016. **2**(12): p. 958-968.
45. Xu, W., et al., *Chemical Genetic Interaction Profiling Reveals Determinants of Intrinsic Antibiotic Resistance in Mycobacterium tuberculosis.* Antimicrob Agents Chemother, 2017. **61**(12).
46. Bellerose, M.M., et al., *Distinct Bacterial Pathways Influence the Efficacy of Antibiotics against Mycobacterium tuberculosis.* mSystems, 2020. **5**(4).
47. Koh, E.I., et al., *Chemical-genetic interaction mapping links carbon metabolism and cell wall structure to tuberculosis drug efficacy.* Proc Natl Acad Sci U S A, 2022. **119**(15): p. e2201632119.
48. Li, S., et al., *A chemical-genetic map of the pathways controlling drug potency in Mycobacterium tuberculosis.* bioRxiv, 2021: p. 2021.11.27.469863.
49. Cokol, M., et al., *Efficient measurement and factorization of high-order drug interactions in Mycobacterium tuberculosis.* Sci Adv, 2017. **3**(10): p. e1701881.
50. Larkins-Ford, J., et al., *Systematic measurement of combination-drug landscapes to predict in vivo treatment outcomes for tuberculosis.* Cell Syst, 2021. **12**(11): p. 1046-1063 e7.
51. Chung, E.S., W.C. Johnson, and B.B. Aldridge, *Types and functions of heterogeneity in mycobacteria.* Nat Rev Microbiol, 2022.
52. Rego, E.H., R.E. Audette, and E.J. Rubin, *Deletion of a mycobacterial divisome factor collapses single-cell phenotypic heterogeneity.* Nature, 2017. **546**(7656): p. 153-157.
53. Gouzy, A., et al., *Growth of Mycobacterium tuberculosis at acidic pH depends on lipid assimilation and is accompanied by reduced GAPDH activity.* Proc Natl Acad Sci U S A, 2021. **118**(32).

Chapter Two: A tRNA-acetylating toxin and detoxifying enzyme in *Mycobacterium tuberculosis*

Authors: Francesca G. Tomasi[1], Alexander M. J. Hall[2], Jessica T. P. Schweber[1], Charles L. Dulberger[1], Kerry McGowen[1], Qingyun Liu[1], Sarah M. Fortune[1], Sophie Helaine[2], Eric J. Rubin[1]

Affiliations: [1]Department of Immunology and Infectious Diseases Harvard T. H. Chan School of Public Health, Boston, MA USA; [2]Department of Microbiology, Harvard Medical School, Boston, MA, USA

Author Contributions: Conceptualization: F.G.T., J.T.P.S., E.J.R.; Methodology: F.G.T, A.M.J.H. (mass spectrometry), C.L.D. (protein purification); Investigation: F.G.T., A.M. J.H., J.T.P.S., C.L.D., K.M.; Data Curation: F.G.T., A.M. J.H. (mass spectrometry), Q.L. (clinical isolate analysis) Writing – Original Draft: F.G.T.; Writing – Review & Editing: F.G.T., A.M.J.H., J.T.P.S., C.L.D., K.M., Q.L., S.H., E.J.R.

Publication: This chapter appears as "A tRNA-acetylating toxin and detoxifying enzyme in *Mycobacterium tuberculosis*" in *Microbiology Spectrum*, Volume 10, Number 3, May 2022.

Abstract

Toxin-antitoxin (TA) systems allow bacteria to adapt to changing environments without altering gene expression. Despite being overrepresented in *Mycobacterium tuberculosis* (*Mtb*), their individual physiological roles remain elusive. We describe a TA system in *Mtb* which we have named TacAT due to its homology to previously discovered systems in Salmonella. The toxin, TacT, blocks growth by acetylating glycyl-tRNAs and inhibiting translation. Its effects are reversed by the enzyme peptidyl tRNA hydrolase (Pth), which also cleaves peptidyl tRNAs that are prematurely released from stalled ribosomes. Pth is essential in most bacteria and thereby has been proposed as a promising drug target for complex pathogens like *Mtb*. Transposon sequencing data suggest that the *tacAT* operon is nonessential for *Mtb* growth *in vitro*, and premature stop mutations in this TA system present in some clinical isolates suggest that it is also dispensable *in vivo*. We assessed whether TacT modulates *pth* essentiality in *Mtb*, as drugs targeting Pth might prompt resistance if TacAT is disrupted. We find that *pth* essentiality is unaffected by the absence of *tacAT*. These results highlight a fundamental aspect of mycobacterial biology and indicate that Pth's essential role hinges on its peptidyl-tRNA hydrolase activity. Our work underscores Pth's potential as a viable target for new antibiotics.

Introduction

Mycobacterium tuberculosis (*Mtb*), which causes tuberculosis (TB), is a leading cause of global infectious disease mortality [1]. *Mtb*'s ability to regulate its growth in different stressful conditions *in vitro* is thought to be an important part of its success *in vivo*. One of this pathogen's tools for growth regulation is an expansive network of toxin antitoxin (TA) systems, with at least 100 putative modules that encompass nearly 4% of *Mtb*'s coding capacity [2, 3]. Most of these systems in *Mtb* can be grouped into five main families based on sequence homology: VapBC, MazEF, RelBE, HigBA, and ParDE [4,

5].Toxins of TAs are characterized by their general intracellular targets and mechanisms of activity with most known *Mtb* toxins being RNases that cleave rRNA, mRNA, or tRNA.

In type II TA systems, the most widespread and heavily-studied type, a protein antitoxin is bound tightly to its cognate protein toxin and acts to neutralize it[6]. If the antitoxin is degraded, the toxin assumes its active form and blocks an essential process such as DNA replication or protein synthesis until antitoxin production resumes [6]. Despite being widespread in bacteria, the physiological roles of TA systems are just emerging, with some having been linked to plasmid maintenance, bacteriophage immunity, and the formation of dormant, antibiotic-tolerant persisters [7, 8]. TA systems might play a role in *Mtb*'s ability to withstand host and antibiotic pressures by controlling growth under different stress conditions [4, 9, 10]. However, it remains to be determined whether or to what extent they play a role in pathogenesis. A significant barrier to understanding TA systems is the challenge of directly measuring native toxin activity in cells, and therefore understanding when they are active and how they interact with other enzymes. Because of the nature of TA system autoregulation and post-translational control, transcription upregulation data alone do not necessarily indicate toxin activation [11]. So far, studies investigating TA systems in bacteria often measure activity in cells using ectopic overexpression constructs [4, 5, 12]. These studies offer fascinating mechanistic insights but do so in isolation from other intracellular systems, and it has been difficult to link the molecular mechanisms of TA systems to their biological roles.

Recently, a new class of TA systems called TacAT was discovered in Salmonella and homologs have since been identified in other species including *Escherichia coli* and *Klebsiella pneumoniae*[13-17]. The toxins in this family are GCN5-related N-acetyltransferases that acetylate aminoacyl tRNA and block incorporation of an amino acid into a growing peptide chain. TacT's unique mechanism of action – which can be detected using liquid chromatography-coupled mass spectrometry – makes it an appealing TA system to study in the context of bacterial physiology [13, 14, 18, 19]. An unusual aspect

of TacAT systems is that, while the antitoxin can block toxin activity as seen with other TA systems, the effect can also be reversed via the ubiquitous and essential bacterial enzyme peptidyl tRNA hydrolase (Pth) [13, 14]. This enzyme cleaves acetylated amino acids from tRNA molecules, effectively unblocking protein synthesis. TacT's mechanistic connection to an essential enzyme makes it an appealing TA system to study in the context of gene essentiality.

Here we describe an *Mtb* homologue of the TacAT TA system, the first of its kind to be identified in this organism. We show that this TA system is encoded by the Rv0918-0919 operon and confirm that Rv0919 encodes a tRNA-acetylating toxin whose activity can be reversed by *Mtb* Pth (Rv1014c). While *pth* is required for growth in *Mtb*, transposon sequencing data suggest that the *Mtb* TacAT operon is dispensable for growth *in vitro*, and we have identified premature stop mutations in this TA system in clinical isolates[20]. If TacT activity modulates *pth* essentiality in *Mtb*, then drugs targeting Pth might prompt resistance if TacAT activity is disrupted as has already happened in clinical isolates. However, we find that while the *tacAT* operon is indeed dispensable, *pth* essentiality is unaffected by the absence of this TA system. Our results indicate that Pth's essential role in *Mtb* hinges on its function in cleaving peptidyl-tRNA and not acetylated aminoacyl tRNA. Our work underscores Pth's potential as a viable target for new antibiotics, while also highlighting multiple angles from which to study TA systems in *Mtb*.

Results

Rv0918-0919 encodes a toxin-antitoxin system that inhibits growth by acetylating glycyl-tRNAs

Previous studies have identified over 100 putative TA systems in *Mtb*, based on genetic architecture and homology to known TA systems [5]. The *Mtb* operon Rv0918-0919 has been computationally flagged as a possible TA system due to its polycistronic organization and the presence

of a conserved, DNA-binding RHH domain in the putative antitoxin gene, Rv0918 (Figure 2.1A) [5, 21]. Rv0919 contains a conserved GNAT domain, and protein BLAST results show >50% sequence identity to the N-acetyltransferase TacAT toxins in Salmonella (Figure 2.1A) [22].

We hypothesized that Rv0919 encodes a TacT-like toxin that inhibits growth by blocking translation. The closely related but faster-growing, non-pathogenic model organism *Mycobacterium smegmatis* (*Msmeg*) does not encode any putative TacAT-like systems [21, 22]. Therefore, to study *Mtb* TacT in isolation from other potential interacting genes we built an integrating vector carrying Rv0919 under the control of an anhydrous tetracycline (aTC)-inducible promoter. Induced overexpression of Rv0919 in *Msmeg* inhibited growth (Figure 2.1B), while constitutive expression of the entire Rv0918-0919 operon did not (Figure 2.1C), showing that Rv0919 encodes a growth-inhibiting enzyme that is not active in the presence of Rv0918.

We next assessed Rv0919 activity *in vitro* using a cell-free protein synthesis kit. We found that, while GFP could be efficiently expressed in this system, adding a DNA construct encoding Rv0919 blocked synthesis, though only when acetyl co-enzyme A was added (Figure 2.1D). This suggests that Rv0919 uses acetyl co-enzyme A as an acetyl group donor, as has been seen with other TacAT systems[14]. A construct encoding Rv0919 with an active site mutation homologous to one identified in Salmonella (Y138F in *Mtb*) partially abrogated protein synthesis (Figure 2.1E) [13]. These results suggest that Rv0919 inhibits growth by acetylating a component of the protein synthesis apparatus.

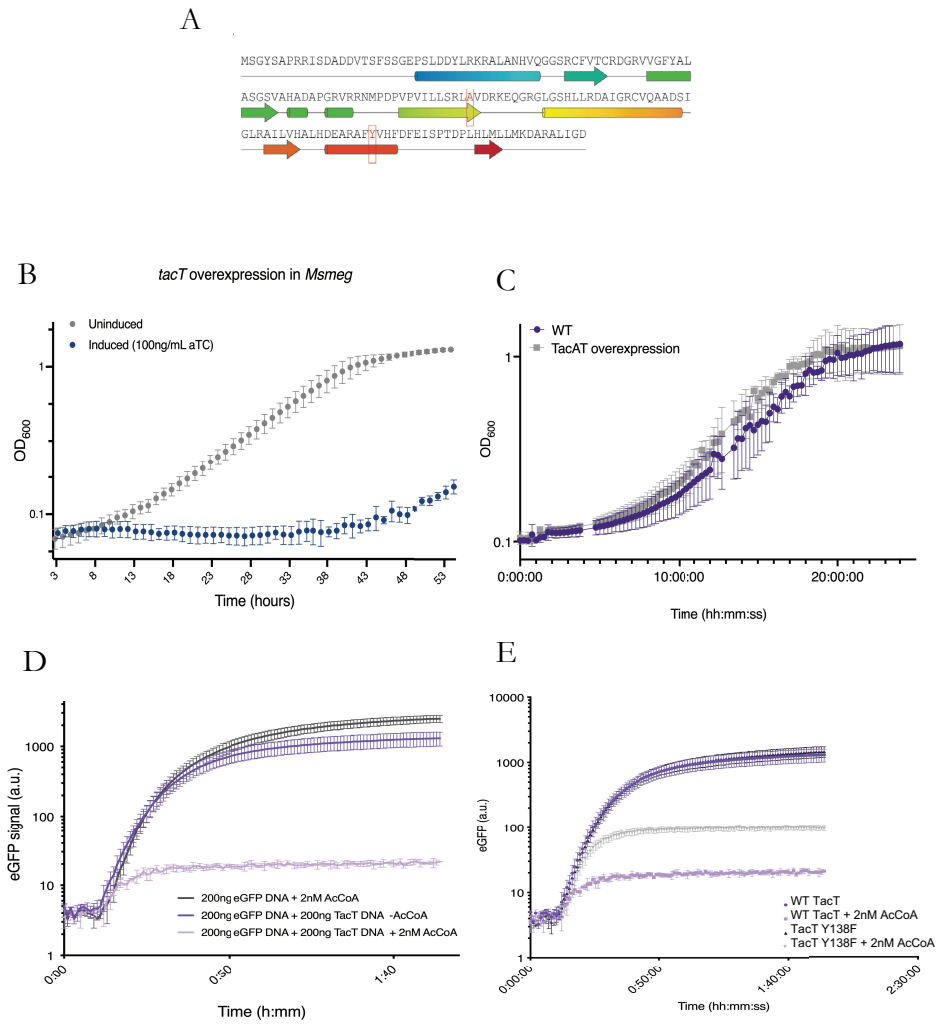

Figure 2.1: TacT is a toxin that inhibits protein synthesis. (A) Amino acid sequence and high-confidence model of *Mtb* TacT (Rv0919) generated using the PHYRE2 protein fold recognition server [23], with the final output modelled on the structure of TacT1 from Salmonella Typhimurium (PDB: 5fvj) [14]. Active side residues in red were mutated for catalytically inactive TacT for subsequent experiments. **(B)** Heterologous overexpression of TacT (Rv0919) blocks growth of *Msmeg*. *Mtb tacT* was cloned under a tetracycline-inducible promoter and integrated into the *Msmeg* genome. Addition of anhydrous tetracycline (aTC; 100ng/mL) leads to overexpression of *tacT*. Strains were diluted to an OD of 0.003 and growth was measured by optical density at 600nm (OD_{600}). Results are from 3 biological replicates. **(C)** Exogenous expression of *Mtb* TacAT (Rv0918-0919) does not block growth of *Mycobacterium smegmatis (Msmeg)*. The *Mtb tacAT* operon was cloned under a constitutive promoter and integrated into the *Msmeg* genome. Strains were diluted to an OD of 0.05 and growth was measured as in (C). Results are from three biological replicates. **(D)** *Mtb* TacT blocks translation in the presence of acetyl coenzyme A. A TacT expression construct was added to the PURExpress in vitro Protein Synthesis Kit with an eGFP expression construct. Protein synthesis was read out as eGFP synthesis and monitored spectrophotometrically at excitation of 488nm and emission of 509nm. Results are from technical triplicates. **(E)** The active site mutation Y138F reduces *Mtb* TacT toxicity. Cell-free protein synthesis reactions were carried out as in (D). Attenuated TacT was made using an Rv0919 expression construct containing the mutation Y138F. Results are from technical triplicates.

All other described TacAT-like systems encode a toxin that acetylates the amino acid on charged tRNA. Different organism toxins acetylate different tRNAs. For instance, in *Salmonella*, three different TacT-like toxins have been described. These block elongation by acetylating glycyl, isoleucyl, leucyl, and, to a lesser extent, other aminoacyl tRNAs *in vitro* [13] but solely glycyl-tRNA *in vivo* (in preparation). Meanwhile, in *E. coli*, the GNAT toxin AtaT was initially thought to block initiation of protein synthesis by acetylating methionine on initiator fMet-tRNA [17] but was more recently reported to acetylate preferentially glycyl-tRNA alongside others [19]. We hypothesized that *Mtb* TacT also acetylates charged tRNAs. To identify if any and which tRNA species might be affected by this enzyme, we purified total RNA from *Msmeg* overexpressing *Mtb* TacT and used liquid chromatography-coupled mass spectrometry to analyze tRNAs (Figure 2.2A). A strong acetylation peak was detected for glycyl-tRNA (Figure 2.2B; Dataset D2.1), but not for any other tRNAs, indicating that *Mtb* TacT specifically acetylates glycyl-tRNAs.

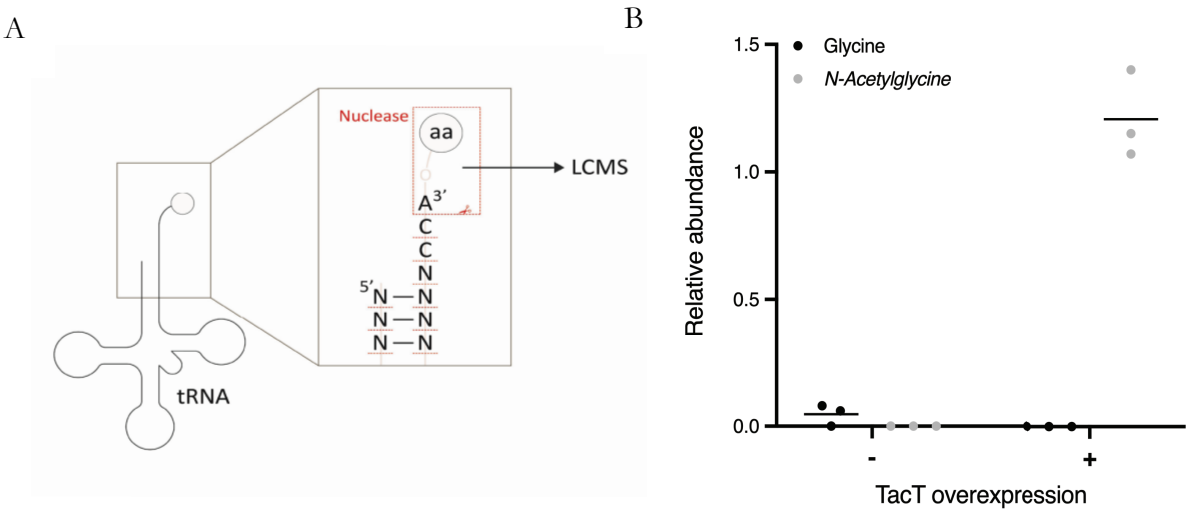

Figure 2.2 : TacT acetylates glycyl-tRNA. TacT acetylates glycyl-tRNA. *Msmeg* overexpressing *Mtb tacT* was grown to mid-log phase and induced for *tacT* overexpression for 3 hours. **(A)** Total RNA from triplicate cultures was collected along with an uninduced control for liquid chromatography-mass spectrometry analysis as described. **(B)** The relative abundance of unacetylated and *N*-acetylated glycyl-tRNA fragments are shown.

Peptidyl tRNA hydrolase (Pth) reverses TacT-induced translation inhibition

Previous work has shown that the enzyme peptidyl tRNA hydrolase (Pth) detoxifies the effects of TacT acetylation by cleaving acetylated amino acids from corrupted tRNAs [14]. To test whether *Mtb* Pth reverses TacT activity, we purified recombinant *Mtb* Pth and added it to our cell-free protein synthesis assay (Figure A2.1). Indeed, purified Pth was sufficient to rescue GFP expression in the presence of active *Mtb* TacT and acetyl coenzyme A (Figure 2.3B) but had no effects on translation in the presence of catalytically inactive TacT (Figure 2.3A, B). Thus, *Mtb* Pth also cleaves N-acetylated aminoacyl-tRNA thereby counteracting the effect of the toxin.

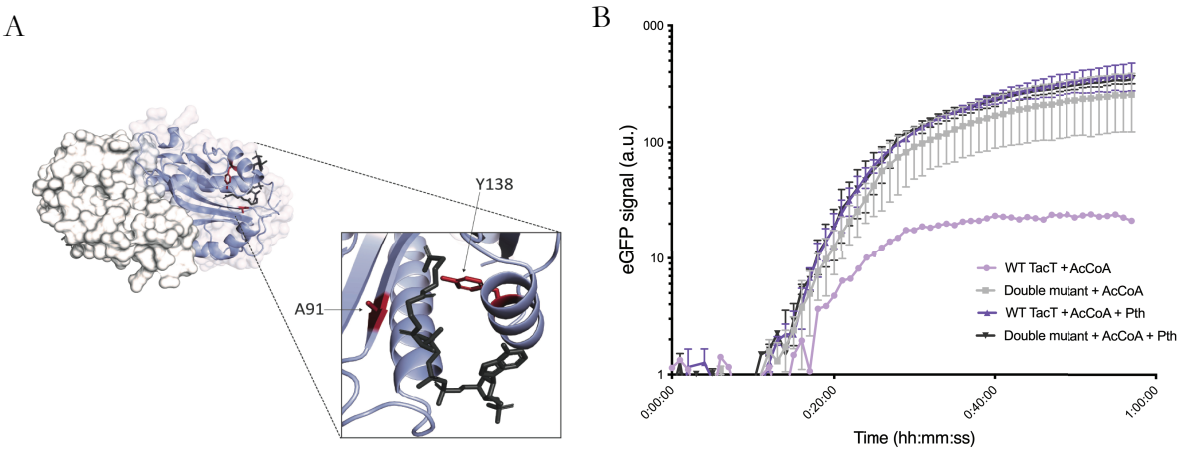

Figure 2.3: *Mtb* Pth detoxifies TacT. (A) Model of *Mtb* TacT dimer generated as described in Figure 1, with one monomer showing mutations for catalytic inactivation (Y138F and A91P; red). Acetyl coenzyme A is shown in the TacT binding pocket and colored by element. **(B)** Cell-free protein synthesis reactions were set up as described in Figure 2.1. Inactive TacT ("Double Mutant") was made using an Rv0919 expression construct containing both active side residue mutations Y138F and A91P. Purified *Mtb* peptidyl tRNA hydrolase (Pth) was added where indicated (8μM), as was acetyl co-enzyme A (AcCoA; 2nM). In reactions without Pth, an equal volume of storage buffer was added. Protein synthesis was read out as eGFP synthesis and monitored spectrophotometrically at excitation of 488nm and emission of 509nm. Results are from technical duplicates.

tacAT* does not affect *pth* essentiality in *Mtb

In addition to reversing the effects of TacT-like toxins, Pth's primary known function is to cleave short peptides from peptidyl-tRNAs that are prematurely released from stalled ribosomes [24,

25]. As with other bacteria, transposon sequencing (TnSeq) data suggest that *pth* is essential in *Mtb* [20]. We built *Mtb pth* transcriptional knockdowns using CRISPR interference (CRISPRi)[26]. Cells induced for *pth* depletion show a marked growth defect, confirming that Pth is required for normal growth (Figure 2.4). Given TacAT's connection to this essential enzyme, we assessed whether it contributes to *pth* essentiality in *Mtb*.

Transposon sequencing data indicate that the TacAT operon Rv0918-0919 is nonessential for *Mtb* growth *in vitro*, and we have identified premature stop mutations in this TA system in clinical isolates, suggesting it is also dispensable *in vivo* (Table A2.1) [20]. We built in-frame deletions of the *tacAT* operon in *Mtb* and used CRISPRi to deplete *pth* in this strain. In the absence of *tacAT*, *pth* knockdowns still failed to grow normally *in vitro*, suggesting that while the *tacAT* operon is dispensable, *pth* essentiality is unaffected by the absence of this TA system (Figure 2.4).

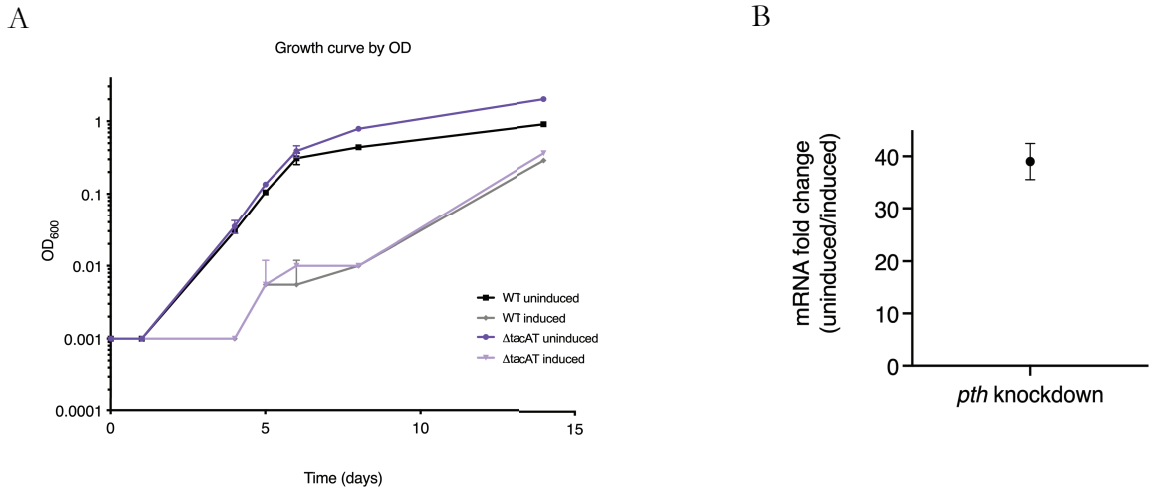

Figure 2.4: *pth* is still required for normal growth of a *Mtb tacAT* knockout. (A) *Mtb⊥tacAT* and WT *Mtb* (H37Rv; parental strain) were transformed with *pth* knockdown constructs using mycobacterial CRISPR-interference (CRISPRi). Strains were diluted to an OD600 of 0.001 and either induced for *pth* knockdown (100ng/mL aTC) or uninduced. Growth was measured by optical density at 600nm (OD_{600}). Results are from biological duplicates. **(B)** Changes in *pth* transcript levels during knockdown, as measured by RT-qPCR. Relative fold change of each mRNA was quantified by normalization to levels of *Mtb sigA* transcript. Points represent the mean of three biological replicates, with error bars depicting standard deviation.

We also performed LCMS on *Mtb* induced or uninduced for *pth* knockdown and were unable to detect glycyl-tRNA acetylation in either strain grown (Figure A2.2). Thus, growth defects of a *pth* knockdown *in vitro* are not a result of the accumulation of acetylated glycyl-tRNAs.

Discussion

Toxin-antitoxin (TA) systems have been identified in most bacterial genomes and have been implicated in a variety of physiological functions ranging from phage protection and plasmid maintenance to pathogenesis and the general stress response. Interestingly, *Mycobacterium tuberculosis* (*Mtb*) encodes one of the largest repertoires of TA systems in bacteria, yet plasmids are absent from this organism [27]. Furthermore, the role of TA systems in *Mtb* against bacteriophages is still under study [28]. It is tempting to speculate that *Mtb*'s broad TA system toolkit serves as a growth regulator during human infection. However, experimental evidence for this is lacking, largely due to the difficulties of systematically deleting many genes simultaneously in *Mtb* and overlapping mechanisms of action that make it difficult to directly measure the activity of individual toxins. Some studies have examined the roles of individual TA systems in *Mtb* using genetic deletions and overexpression systems, and linked activity of some toxins to pathogenesis [10, 29, 30]. Nonetheless, the level and spectrum of TA system involvement during *Mtb* infection remains unresolved.

Here, we have identified and characterized a TA system in *Mtb* whose mechanism of action is distinct from the other known TA systems in this organism. While most toxins in *Mtb* are ribonucleases, TacT instead blocks growth by acetylating charged tRNAs. This activity can be detected using liquid chromatography-coupled mass spectrometry, making it an appealing TA system to study in its native form. We have shown that *Mtb* TacT acetylates glycyl tRNAs using an overexpression construct in *Msmeg* but have been unable to detect this modification in wild type *Mtb*. Future work

that increases the sensitivity and throughput of LCMS-based or other forms of detection for tRNA acetylation will allow researchers to probe the effects of various physiological conditions on this tRNA modification and identify conditions during which TacT is activated in *Mtb* and in other bacteria containing homologous TA systems.

Recent work using genome sequence from clinical isolates of *Mtb* has shed light on the selective pressures imposed on *Mtb*'s genome during human infection [31, 32]. The essentiality of a gene is correlated with its level of tolerance for nonsynonymous mutations [33]. We have found that the TacAT operon in *Mtb* is dispensable *in vitro*, and clinical genomic data support that this operon is also dispensable *in vivo*, given many nonsynonymous mutations – including premature stop codons – that have accumulated in clinical strains.

The other unique aspect of TacAT is its mechanistic connection to the essential enzyme peptidyl tRNA hydrolase (Pth), which reverses TacT-induced aminoacyl tRNA acetylation. Pth is ubiquitous and thought to be essential across bacteria; in fact, the three critical active site residues His22, Asp95 and Asn116 are universally conserved [34]. Archaea, meanwhile, encode a conserved functional homolog, *pth2*, which does not share significant sequence similarity to bacterial *pth* [34]. Most eukaryotes contain both *pth* and *pth2* genes, though these enzymes are individually nonessential. Interestingly, structural studies have found that mycobacterial Pth is divergent from other bacterial Pth in several regions [35, 36]. Because of its essentiality in bacteria and unique structure in mycobacteria, in addition to the vulnerability of translation rescue systems in *Mtb,* Pth has been proposed as an intriguing drug target in difficult-to-treat organisms like *Mtb* [35, 37, 38]. Understanding the critical functions of Pth is important from a drug development perspective, especially when considering potential sources for antibiotic resistance. For instance, if TacT activity were a significant source for *pth* essentiality in *Mtb*, then inhibitors targeting Pth would lose efficacy in clinical isolates with a disrupted *tacAT* operon. Our work has shown that *Mtb* TacT's connection

to Pth is not the source of *pth* essentiality. This bodes well for studies of Pth as an antibiotic target since mutations inactivating *tacAT* have already been identified in clinical isolates. Finally, biochemical assays to assess Pth inhibitors can exploit the relationship between Pth and TacT using *in vitro* protein synthesis kits by screening for loss of Pth-mediated detoxification.

Materials and Methods

Bacterial strains and growth conditions: *Mtb* and *Msmeg* strains were grown from frozen stocks into Middlebrook 7H9 medium supplemented with 0.2% glycerol, 0.05% Tween-80, and ADC (5g/L bovine serum albumin, 2g/L dextrose, 3 μg/ml catalase). Cultures were incubated at 37 °C. Antibiotics or inducing agents were used when needed at the following concentrations in both Mtb and Msmeg: kanamycin (25μg/ml), anhydrous tetracycline (aTC; 100ng/mL), hygromycin (50μg/ml), and nourseothricin (20μg/ml). Transformed Mtb and Msmeg strains were plated onto 7H10 agar plates with the appropriate antibiotic(s). Strains were grown to mid log-phase for all experiments unless otherwise specified (OD_{600} 0.4-0.6). *E. coli* strains for cloning or protein purification were grown in LB broth or on LB agar with appropriate antibiotics at the following concentrations: kanamycin (50 μg/ml), zeocin (50μg/ml), and nourseothricin (40 μg/ml). Induction time for *pth* depletion in *Mtb* was 4 days. Induction for *tacT* overexpression in *Msmeg* was 3 hours.

Bacterial strain construction: Table A2.2 depicts the strains, plasmids, primers, and recombinant DNA used for this study. Plasmids were built by restriction digest of a parental vector and inserts were prepared either by restriction enzyme cloning or Gibson assembly [39] using 40bp overhangs, as specified in Table A2.2. Plasmids were isolated from *E. coli* and confirmed via Sanger sequencing carried out by Genewiz, LLC (Massachusetts, USA).

Deletion mutants: The knockout strain Δ*tacAT*::zeo (zeocin) was built using double-stranded recombineering in the parental *Mtb* strain H37Rv. A linear dsDNA fragment was constructed using stitch PCR with the primers listed in Table A2.2 which consisted of a 500bp region upstream of the *tacAT* operon (Rv0918-019), 500bp downstream region, and a *lox*-zeo-*lox* fragment. This cassette was

transformed into an H37Rv recombineering strain as described [40] and plated on 7H10 + zeocin plates.

tacAT, tacT alleles*:* Plasmid FT2, used for inducible *tact* overexpression in *Msmeg*, was generated using a parental vector (CT16) that integrates into the L5 mycobacterial phage site. This plasmid also encodes for kanamycin resistance and contains both the tet promoter (directly upstream of *tacT*) and the tet repressor. CT16 was digested with ClaI and XbaI (New England Biolabs). *tacT* (Rv0919) was PCR-amplified and ligated into the plasmid using restriction cloning. Plasmid FT3, used for *tacAT* overexpression, was generated by placing *tacAT* together under the constitutive UV15 promoter in a parental vector (CT250) which was digested with NdeI and HindIII (New England Biolabs). The *tacAT* operon Rv0918-0919 was ligated to the plasmid using Gibson cloning.

Pth knockdown constructs*:* Transcriptional knockdown of *pth* was accomplished using mycobacterial CRISPRi-interference (CRISPRi). Knockdown constructs were built as previously described [26] by annealing oligos for *pth* and ligating them into a linearized BsmBI-digested plasmid (CT 296; gift of Jeremy Rock) that contains mycobacterial CRISPRi. The knockdown vector FT110 was transformed in both H37Rv wild type (WT) and ΔtacAT::ZeoR.

Purification of *Mtb* Pth: *Mtb pth* (Rv1014c) was cloned with a C-terminal 6x His-tag and expressed from pET28a in BL21-CodonPlus (DE3)-RP *E. coli* under conditions like those previously described[41]. 1 L of log-phase culture (OD600 ~ 0.7) was induced with 1 mM isopropyl β-D-1-thiogalactopyranoside (IPTG) for 4 hours at 37°C. Cells were harvested at 6,000g for 15 minutes, and the resulting pellet was frozen at -80°C. The pellet was thawed with a stir-bar at 4°C in lysis buffer containing 50 mM Tris HCl pH 7.5, 300 mM NaCl, 10% glycerol, DNase powder, 1 tablet complete

EDTA-free protease inhibitor and 2 mM 2-mercaptoethanol (BME), and cells were lysed using a French press. Lysate was clarified by spinning at 30,000g for 30 minutes and brought up to 20 mM imidazole pH 7.5. His-tagged Pth was then extracted via batch binding 2.5 mL equilibrated Ni-NTA beads incubated with lysate for 1 hour at 4°C. Beads were collected and washed with 20 mL lysis buffer containing 2 mM BME. A second wash included 20 mL lysis buffer with 20 mM imidazole and 2 mM BME, followed by 5 mL of lysis buffer with 30 mM imidazole, and a final wash with 5 mL lysis buffer containing 40 mM imidazole and 2 mM BME. Samples were eluted with lysis buffer containing 200 mM imidazole pH 7.5 in 750µL fractions and analyzed via SDS-PAGE (Figure A2.1, left). The cleanest elution fractions (4-6 and 7-9) were desalted into lysis buffer containing BME, concentrated with a 10 KDa MWCO Amicon ultra 4 spin column to 1 mL and further purified by FPLC via gel filtration chromatography with a Superdex 75 Increase 10/300 GL column in buffer containing (25 mM Tris-HCl pH 7.5, 150 mM NaCl, 2 mM BME). Fractions were analyzed via SDS-PAGE (Figure A2.1, right) and fractions 2d2-2d3 (at an elution volume ~13 mL) were pooled and brought up to 5% glycerol with 2 mM fresh BME. Nanodrop readings suggested that other fractions containing what appeared to be pure Pth were contaminated by unknown nucleic acid species. Nucleic acid-free protein (fractions 2d2-2d3) was aliquoted into 10 uL aliquots, flash frozen with liquid nitrogen, and stored at -80°C. Pth protein concentration was calculated using a Coomassie Plus (Bradford) Assay (Pierce).

***In vitro* translation:** To assess the effect of TacT on translation, *in vitro* translation reactions were prepared with purified *tacT* DNA (WT, Y138F, or Y138F/A91P), 2nM acetyl coenzyme A, and purified Pth. A master mix of purified eGFP DNA (200ng per reaction), *tact* DNA (180ng per reaction) and PURExpress (New England Biolabs) components were prepared in triplicate reactions with 8µM of Pth and 2nM acetyl coenzyme A. When no Pth was added, an equal volume of storage buffer was used in place of protein. When no acetyl coenzyme A was added, an equal volume of water was added.

Reactions were carried out in 12μL in a black Co-star 384-well plate for 2 hours at 37°C, and eGFP fluorescence (excitation = 488 nm and emission = 509 nm) was measured over time on a SpectraMax M2 microplate reader.

mRNA quantification: 10mL *Mtb* cultures were harvested at 4,000rpm for 10 minutes and pellets were resuspended in 1mL TriZol reagent (ThermoFisher Scientific). Samples were lysed by bead beating. Purified DNase-treated RNA was used as template for cDNA synthesis, following manufacturer's instructions with Superscript IV (Life Technologies). RNA was removed using RNase A (ThermoFisher Scientific) and cDNA cleaned up by column purification (Zymo Research). qPCR was performed using iTaq Universal SYBR Green Supermix (BioRad). mRNA fold-change was calculated using the ΔΔCt method, where *pth* transcript level was normalized by *sigA* level in each condition.

Liquid chromatography-coupled mass spectrometry: Purified RNA (30 – 50 μg) was spiked with 1 μM ^{15}N-AMP and incubated with 1U Nuclease P1 in 10mM ammonium acetate for 30 minutes at 25 °C (Figure 2.2 and Figure A2.2). Alternatively, purified RNA was incubated with 25 μg purified Pth in buffer (10 mM Tris acetate, 10mM magnesium acetate, 20mM ammonium acetate pH 8) for 1 hour at 37 °C. Processed RNA samples were diluted 1:3 with acetonitrile + 0.2% v/v acetic acid, centrifuged for 10 minutes at 21,000 *g*, room temperature to remove any precipitate, and transferred to glass microvials. Samples were analyzed on a Thermo Ultimate 3000 LC coupled with a Q-Exactive Plus mass spectrometer in both positive and negative ion modes. Five microliters of each sample were injected on a Zic-pHILIC Column (150x2.1 mm, 5-micron particles, EMD Millipore). The mobile phases are (A) 20 mM ammonium carbonate in 0.1 % ammonium hydroxide and (B) acetonitrile 97% in water. The gradient conditions were as follows: 100% B at 0 min, 40% B at 20 min, 0% B at 30 min

for 5 min, then back to 100% B in 5 min, followed by 10 min of re-equilibration. A constant flow rate of 0.200 L/minute was used. The mass spectrometer was calibrated immediately prior to use. Data were analyzed using Thermo Xcalibur 3.0 with ICIS automated peak integration (Default settings: Smoothing Points = 9; Baseline Window = 40; Area Noise Factor = 2; Peak Noise Factor = 10) followed by manual data curation. In analysis of NP1 treated samples (Figure 2 and Figure A2.2), peak areas were normalized relative to the peak area of the ^{15}N-AMP spike-in. To distinguish between isobaric tRNA fragments derived from *N*-acetylserine and glutamic acid ([M+H]+ ion m/z = 476.1057), RNA samples instead treated with Pth (to cleave *N*-acetyl amino acids from tRNAs) were compared by LC/MS to purified standards of each amino acid, allowing for identification of peaks discriminated by retention time (Figure A2.3). These data indicate that glutamic acid, and not *N*-acetylserine, contributes the entirety of the MS signal detected for ions with an m/z of 147.0532, and that TacT does not acetylate seryl-tRNA.

Whole genome sequencing analysis of clinical isolates: Whole genome sequences of 55778 Mtb isolates were obtained from 211 BioProjects under the following accession codes: ERP001037, ERP002611, ERP008770, PRJDB10607, PRJDB3875, PRJDB6149, PRJDB7006, PRJDB8544, PRJDB8553, PRJEB10385, PRJEB10533, PRJEB10577, PRJEB10950, PRJEB11460, PRJEB11653, PRJEB11778, PRJEB12011, PRJEB12179, PRJEB12184, PRJEB12764, PRJEB13325, PRJEB13764, PRJEB13960, PRJEB14199, PRJEB15076, PRJEB15382, PRJEB15857, PRJEB18529, PRJEB20214, PRJEB21685, PRJEB21888, PRJEB21922, PRJEB23245, PRJEB23495, PRJEB2358, PRJEB23648, PRJEB23664, PRJEB23996, PRJEB24463, PRJEB25506, PRJEB25543, PRJEB25592, PRJEB25814, PRJEB25968, PRJEB25971, PRJEB25972, PRJEB25991, PRJEB25997, PRJEB25998, PRJEB25999, PRJEB26000, PRJEB26001, PRJEB26002, PRJEB27244, PRJEB27354, PRJEB27366, PRJEB27446, PRJEB27847, PRJEB2794, PRJEB28497, PRJEB28842, PRJEB29199, PRJEB29276, PRJEB29408,

PRJEB29435, PRJEB29446, PRJEB29604, PRJEB30463, PRJEB30782, PRJEB30933, PRJEB31023, PRJEB31905, PRJEB32037, PRJEB32234, PRJEB32341, PRJEB32589, PRJEB32684, PRJEB32773, PRJEB33896, PRJEB35201, PRJEB39699, PRJEB40777, PRJEB5162, PRJEB5280, PRJEB5899, PRJEB5925, PRJEB6273, PRJEB6717, PRJEB6945, PRJEB7056, PRJEB7281, PRJEB7669, PRJEB7727, PRJEB7798, PRJEB8311, PRJEB8432, PRJEB8689, PRJEB9003, PRJEB9201, PRJEB9206, PRJEB9308, PRJEB9545, PRJEB9680, PRJEB9709, PRJEB9976, PRJNA200335, PRJNA217391, PRJNA219826, PRJNA220218, PRJNA229360, PRJNA233386, PRJNA235852, PRJNA237443, PRJNA244659, PRJNA254678, PRJNA259657, PRJNA268900, PRJNA270137, PRJNA282721, PRJNA287858, PRJNA295328, PRJNA300846, PRJNA302362, PRJNA305488, PRJNA306588, PRJNA308536, PRJNA318002, PRJNA352769, PRJNA353873, PRJNA354716, PRJNA355614, PRJNA356104, PRJNA361483, PRJNA369219, PRJNA376471, PRJNA377769, PRJNA379070, PRJNA384604, PRJNA384765, PRJNA384815, PRJNA385247, PRJNA388806, PRJNA390065, PRJNA390291, PRJNA390471, PRJNA393378, PRJNA393923, PRJNA393924, PRJNA401368, PRJNA401515, PRJNA407704, PRJNA413593, PRJNA414758, PRJNA419964, PRJNA421323, PRJNA421446, PRJNA428596, PRJNA429460, PRJNA430531, PRJNA431049, PRJNA436223, PRJNA436997, PRJNA438921, PRJNA448595, PRJNA453687, PRJNA454477, PRJNA475130, PRJNA475771, PRJNA480117, PRJNA480888, PRJNA481625, PRJNA481638, PRJNA482095, PRJNA482716, PRJNA482865, PRJNA486713, PRJNA488343, PRJNA488426, PRJNA492975, PRJNA506272, PRJNA509547, PRJNA512266, PRJNA522942, PRJNA523164, PRJNA523499, PRJNA524863, PRJNA526078, PRJNA528965, PRJNA533314, PRJNA540911, PRJNA549270, PRJNA559678, PRJNA566379, PRJNA573497, PRJNA578162, PRJNA586859, PRJNA587747, PRJNA589048, PRJNA591498, PRJNA595834, PRJNA598949, PRJNA598981, PRJNA608715, PRJNA632617, PRJNA663350, PRJNA678116, PRJNA679443, PRJNA683067, PRJNA684613, PRJNA688213, SRA065095. The Sickle tool was used for trimming whole-genome

sequencing data [42]. Sequencing reads with Phred base quality scores above 20 and read lengths longer than 30 were kept for analysis. The inferred ancestral genome of the most recent common ancestor of the MTBC was used as the reference template for read mapping [43]. Sequencing reads were mapped to the reference genome using Bowtie 2 (version 2.2.9) [44] . SAMtools (v1.3.1) was used for SNP calling with mapping quality greater than 30. Fixed mutations (frequency ≥ 75%) were identified using VarScan (v2.3.9) with at least 10 supporting reads and the strand bias filter option on. SNPs in repetitive regions of the genome (e.g., PPE/PE-PGRS family genes, phage sequences, insertion, or mobile genetic elements) were excluded [45, 46].

References

1. W.H.O., *Global tuberculosis report 2021*. 2021.
2. Fernandez-Garcia, L., et al., *Toxin-Antitoxin Systems in Clinical Pathogens*. Toxins (Basel), 2016. **8**(7).
3. Gupta, A., et al., *Co-expression network analysis of toxin-antitoxin loci in Mycobacterium tuberculosis reveals key modulators of cellular stress*. Sci Rep, 2017. **7**(1): p. 5868.
4. Slayden, R.A., C.C. Dawson, and J.E. Cummings, *Toxin-antitoxin systems and regulatory mechanisms in Mycobacterium tuberculosis*. Pathog Dis, 2018. **76**(4).
5. Sala, A., P. Bordes, and P. Genevaux, *Multiple toxin-antitoxin systems in Mycobacterium tuberculosis*. Toxins (Basel), 2014. **6**(3): p. 1002-20.
6. Fraikin, N., F. Goormaghtigh, and L. Van Melderen, *Type II Toxin-Antitoxin Systems: Evolution and Revolutions*. J Bacteriol, 2020. **202**(7).
7. Helaine, S. and E. Kugelberg, *Bacterial persisters: formation, eradication, and experimental systems*. Trends Microbiol, 2014. **22**(7): p. 417-24.
8. Page, R. and W. Peti, *Toxin-antitoxin systems in bacterial growth arrest and persistence*. Nat Chem Biol, 2016. **12**(4): p. 208-14.
9. Ramage, H.R., L.E. Connolly, and J.S. Cox, *Comprehensive functional analysis of Mycobacterium tuberculosis toxin-antitoxin systems: implications for pathogenesis, stress responses, and evolution*. PLoS Genet, 2009. **5**(12): p. e1000767.
10. Tiwari, P., et al., *MazF ribonucleases promote Mycobacterium tuberculosis drug tolerance and virulence in guinea pigs*. Nat Commun, 2015. **6**: p. 6059.
11. LeRoux, M., et al., *Stress Can Induce Transcription of Toxin-Antitoxin Systems without Activating Toxin*. Mol Cell, 2020. **79**(2): p. 280-292 e8.
12. Ramirez, M.V., et al., *MazF6 toxin of Mycobacterium tuberculosis demonstrates antitoxin specificity and is coupled to regulation of cell growth by a Soj-like protein*. BMC Microbiol, 2013. **13**: p. 240.
13. Rycroft, J.A., et al., *Activity of acetyltransferase toxins involved in Salmonella persister formation during macrophage infection*. Nat Commun, 2018. **9**(1): p. 1993.
14. Cheverton, A.M., et al., *A Salmonella Toxin Promotes Persister Formation through Acetylation of tRNA*. Mol Cell, 2016. **63**(1): p. 86-96.
15. Wilcox, B., et al., *Escherichia coli ItaT is a type II toxin that inhibits translation by acetylating isoleucyl-tRNAIle*. Nucleic Acids Res, 2018. **46**(15): p. 7873-7885.
16. Qian, H., et al., *Identification and characterization of acetyltransferase-type toxin-antitoxin locus in Klebsiella pneumoniae*. Mol Microbiol, 2018. **108**(4): p. 336-349.
17. Jurenas, D., et al., *AtaT blocks translation initiation by N-acetylation of the initiator tRNA(fMet)*. Nat Chem Biol, 2017. **13**(6): p. 640-646.
18. Zhang, C., et al., *Substrate specificities of Escherichia coli ItaT that acetylates aminoacyl-tRNAs*. Nucleic Acids Res, 2020. **48**(13): p. 7532-7544.
19. Yashiro, Y., et al., *Mechanism of aminoacyl-tRNA acetylation by an aminoacyl-tRNA acetyltransferase AtaT from enterohemorrhagic E. coli*. Nat Commun, 2020. **11**(1): p. 5438.
20. DeJesus, M.A., et al., *Comprehensive Essentiality Analysis of the Mycobacterium tuberculosis Genome via Saturating Transposon Mutagenesis*. mBio, 2017. **8**(1).
21. Kapopoulou, A., J.M. Lew, and S.T. Cole, *The MycoBrowser portal: a comprehensive and manually annotated resource for mycobacterial genomes*. Tuberculosis (Edinb), 2011. **91**(1): p. 8-13.
22. Altschul, S.F., et al., *Basic local alignment search tool*. J Mol Biol, 1990. **215**(3): p. 403-10.
23. Kelley, L.A., et al., *The Phyre2 web portal for protein modeling, prediction and analysis*. Nat Protoc, 2015. **10**(6): p. 845-58.

24. Das, G. and U. Varshney, *Peptidyl-tRNA hydrolase and its critical role in protein biosynthesis.* Microbiology (Reading), 2006. **152**(Pt 8): p. 2191-2195.
25. Sharma, S., et al., *Structural and functional insights into peptidyl-tRNA hydrolase.* Biochim Biophys Acta, 2014. **1844**(7): p. 1279-88.
26. Rock, J.M., et al., *Programmable transcriptional repression in mycobacteria using an orthogonal CRISPR interference platform.* Nat Microbiol, 2017. **2**: p. 16274.
27. Zainuddin, Z.F. and J.W. Dale, *Does Mycobacterium tuberculosis have plasmids?* Tubercle, 1990. **71**(1): p. 43-9.
28. Lobato-Marquez, D., R. Diaz-Orejas, and F. Garcia-Del Portillo, *Toxin-antitoxins and bacterial virulence.* FEMS Microbiol Rev, 2016. **40**(5): p. 592-609.
29. Sharma, A., et al., *VapC21 Toxin Contributes to Drug-Tolerance and Interacts With Non-cognate VapB32 Antitoxin in Mycobacterium tuberculosis.* Front Microbiol, 2020. **11**: p. 2037.
30. Talwar, S., et al., *Role of VapBC12 Toxin-Antitoxin Locus in Cholesterol-Induced Mycobacterial Persistence.* mSystems, 2020. **5**(6).
31. Meehan, C.J., et al., *Whole genome sequencing of Mycobacterium tuberculosis: current standards and open issues.* Nat Rev Microbiol, 2019. **17**(9): p. 533-545.
32. Stucki, D., et al., *Mycobacterium tuberculosis lineage 4 comprises globally distributed and geographically restricted sublineages.* Nat Genet, 2016. **48**(12): p. 1535-1543.
33. Liu, Q., et al., *Mycobacterium tuberculosis clinical isolates carry mutational signatures of host immune environments.* Sci Adv, 2020. **6**(22): p. eaba4901.
34. Rosas-Sandoval, G., et al., *Orthologs of a novel archaeal and of the bacterial peptidyl-tRNA hydrolase are nonessential in yeast.* Proc Natl Acad Sci U S A, 2002. **99**(26): p. 16707-12.
35. Kabra, A., et al., *Structural characterization of peptidyl-tRNA hydrolase from Mycobacterium smegmatis by NMR spectroscopy.* Biochim Biophys Acta, 2016. **1864**(10): p. 1304-14.
36. Selvaraj, M., et al., *Structures of new crystal forms of Mycobacterium tuberculosis peptidyl-tRNA hydrolase and functionally important plasticity of the molecule.* Acta Crystallogr Sect F Struct Biol Cryst Commun, 2012. **68**(Pt 2): p. 124-8.
37. Alumasa, J.N., et al., *Ribosome Rescue Inhibitors Kill Actively Growing and Nonreplicating Persister Mycobacterium tuberculosis Cells.* ACS Infect Dis, 2017. **3**(9): p. 634-644.
38. Keiler, K.C., *Mechanisms of ribosome rescue in bacteria.* Nat Rev Microbiol, 2015. **13**(5): p. 285-97.
39. Gibson, D.G., et al., *Enzymatic assembly of DNA molecules up to several hundred kilobases.* Nat Methods, 2009. **6**(5): p. 343-5.
40. Murphy, K.C., K. Papavinasasundaram, and C.M. Sassetti, *Mycobacterial recombineering.* Methods Mol Biol, 2015. **1285**: p. 177-99.
41. Bal, N.C., et al., *Characterization of peptidyl-tRNA hydrolase encoded by open reading frame Rv1014c of Mycobacterium tuberculosis H37Rv.* Biol Chem, 2007. **388**(5): p. 467-79.
42. N. A. Joshi, J.N.F. *Sickle: A sliding-window, adaptive, quality-based trimming tool for FastQ files.* [Software] 2011; Available from: Available at https://github.com/najoshi/sickle.
43. Comas, I., et al., *Out-of-Africa migration and Neolithic coexpansion of Mycobacterium tuberculosis with modern humans.* Nat Genet, 2013. **45**(10): p. 1176-82.
44. Langmead, B. and S.L. Salzberg, *Fast gapped-read alignment with Bowtie 2.* Nat Methods, 2012. **9**(4): p. 357-9.
45. Koboldt, D.C., et al., *VarScan 2: somatic mutation and copy number alteration discovery in cancer by exome sequencing.* Genome Res, 2012. **22**(3): p. 568-76.
46. Li, H., et al., *The Sequence Alignment/Map format and SAMtools.* Bioinformatics, 2009. **25**(16): p. 2078-9.

Chapter Three: Peptidyl tRNA hydrolase is required for maintaining tRNA pools in *Mycobacterium tuberculosis*

Authors: Francesca G. Tomasi*[1], Jessica T. P. Schweber*[1], Satoshi Kimura[2,3,4], Junhao Zhu[1], Laura A. T. Cleghorn[5], Susan Davis[5], Simon R. Green[5], Matthew K. Waldor[2,3,4], Eric J. Rubin[1]

Affiliations: [1]Department of Immunology and Infectious Diseases Harvard T. H. Chan School of Public Health, Boston, MA USA; [2]Division of Infectious Diseases, Brigham and Women's Hospital, Boston, MA, USA; [3]Department of Microbiology, Harvard Medical School, Boston, MA, USA; [4] Howard Hughes Medical Institute, Boston, MA, USA; [5]Drug Discovery Unit, School of Life Sciences, University of Dundee, Dundee, UK

Author Contributions: Conceptualization: F.G.T., J.T.P.S., S.K., M.K.W., E.J.R.; Methodology: F.G.T, J.T.P.S. (all proteolytic degradation strain work), S.K., J.Z.; Investigation: F.G.T., J.T.P.S., S.K.; Data Curation: F.G.T., S.K., J.Z. (proteomics data analysis); Design and synthesis of lysine tRNA synthetase inhibitors: L.A.T.C., S.D., S.R.G.; Writing –F.G.T.; Editing – in progress with all listed authors prior to submission for publication

Acknowledgements: Thank you to Renée Robinson at the Harvard University HCMS-Proteomics Core for quantitative TMT proteomic analysis of *Mtb* lysate described in this work.

Abstract

Enzymes involved in rescuing stalled ribosomes and recycling translation machinery are ubiquitous in bacteria. Peptidyl tRNA drop-off is a type of abortive translation that results in the release of a truncated peptide that is still bound to tRNA (peptidyl tRNA) into the cytoplasm. Peptidyl tRNA hydrolase (Pth) recycles the released tRNA by cleaving off the unfinished peptide. While Pth's catalytic mechanism of action is well understood, little is known about peptidyl tRNA drop-off in bacteria from a physiological perspective. Here, we have developed a tRNA sequencing-based strategy called copper sulfate-based tRNA sequencing ($CuSO_4$-tRNAseq) to study Pth in the pathogen *Mycobacterium tuberculosis* (*Mtb*) and find that it modulates tRNA pools and is required for normal growth. While peptidyl tRNA accumulates across all tRNA species in a Pth hypomorph, peptidyl prolyl-tRNA is particularly enriched, suggesting that peptidyl tRNA drop-off occurs most frequently on proline-containing sequences in *Mtb*. A survey of the *Mtb* proteome shows that cells stop synthesizing certain proteins early on in Pth depletion, likely in response to decreased tRNA availability. Applying our findings through a drug development lens, we show that an *Mtb* Pth knockdown is highly susceptible to macrolides, antibiotics that are currently ineffective against TB. Reducing Pth levels also increases *Mtb*'s susceptibility to another antibiotic class – aminoacyl tRNA synthetase inhibitors that are currently being developed against this pathogen. Taken together, our work underscores the importance of Pth in tRNA turnover and provides new biological insights on anti-TB strategies that could exploit synergy between translation inhibition and tRNA turnover.

Introduction

Enzymes involved in ribosome rescue are ubiquitous in bacteria [1]. mRNA truncation, frame-shifting, and readthrough errors can result in unproductive ribosomes that stall on transcripts because the stop codon at the end of mRNA is missing or no longer in-frame [2]. Certain amino acid combinations or codon patterns can also interfere with ribosome efficiency and lead to stalling [3]. Left unaddressed, hiccups in protein synthesis occur frequently enough, even in the absence of cellular stressors, that the accumulation of stalled ribosomes would inhibit a cell's ability to survive [4].

To rescue stalled ribosomes, bacteria use a diverse set of pathways such as trans-translation, drop-off, and – in some lineages – alternative rescue factors and ribosome quality control [5]. In all cases, stalled ribosomes are returned to the free pool of actively translating ribosomes. In trans-translation, a molecule known as transfer-messenger RNA (tmRNA) forms a complex with small protein B (SmpB) to interact with a stalled ribosome. This interaction enables the transfer of an amino acid to the nascent polypeptide and gives it a programmed ending. [1, 6-9]. The ribosomal subunits and tRNA are recycled, the corrupted mRNA degraded, and the incomplete polypeptide is targeted to the proteasome [10]. Trans-translation has been studied extensively and is an active area of antibiotic research given its essentiality and exclusivity to bacteria [11]. Alternative rescue factors A and B (ArfA/B) mediate ribosome rescue – release factor-dependent and independent, respectively – in a variety of bacterial phyla, but unlike trans-translation these processes do not target corrupted mRNA and truncated peptides for degradation. Peptidyl tRNA drop-off, or simply drop-off, is the process by which peptidyl tRNA dissociates from the ribosome either spontaneously or with the help of ribosome recycling factor (RRF), elongation factor G (EF-G), and release factor 3 (RF3) [8, 12, 13]. A key distinction in drop-off is the release of peptidyl tRNA into the cytoplasm; by contrast, rescue systems like trans-translation and ArfA/B hydrolyze peptidyl tRNA that is still bound to the ribosome using different enzymes [1].

The central enzyme in peptidyl tRNA drop-off is peptidyl tRNA hydrolase (Pth), an esterase that recycles tRNA by cleaving the released peptidyl tRNA [8]. While the structure of Pth has been solved in multiple organisms and its catalytic mechanism of action is well understood, little is known about peptidyl tRNA drop-off in bacteria from a physiological perspective [14, 15]. For instance, Pth does not have increased specificity for certain tRNA species *in vitro* [16-18], but it is unclear whether this enzyme preferentially cleaves specific tRNA iso-acceptors *in vivo* perhaps because of potential amino acids that are more susceptible peptidyl tRNA drop-off. tRNA turnover is complex and tightly regulated in cells [19], and Pth's role in tRNA dynamics is not well-understood.

Here, we examine the physiological role of Pth in *Mycobacterium tuberculosis* (*Mtb*), a pathogen that was responsible for over 10.5 million active cases of tuberculosis (TB) and at least 1.5 million deaths in 2020 [20]. *Mtb* has been shown to be highly susceptible to the inhibition of trans-translation during normal growth, suggesting this pathogen has a critical need for ribosome rescue machinery [21]. Work on trans-translation in *Mtb* has opened doors for drug discovery efforts aimed at targeting ribosome rescue in *Mtb* [22]. However, peptidyl tRNA drop-off and the effects of Pth depletion in *Mtb* have not yet been investigated.

We have adapted a tRNA sequencing-based strategy called copper sulfate-based tRNA sequencing ($CuSO_4$-tRNAseq) to study Pth in *Mtb*. Traditional tRNA sequencing allows us to measure both tRNA levels and modification profiles. Supplementing this strategy with chemical treatment of tRNA – like $CuSO_4$ and periodate oxidation – allows us to study additional aspects of tRNA, including aminoacylation [23] and now, N-aminoacylation (N-acetylated aminoacyl-tRNA and peptidyl-tRNA). Using CuSO4-tRNAseq, we find that Pth modulates tRNA turnover during normal growth in *Mtb*. We show that while peptidyl tRNA accumulates across all tRNA species in a Pth hypomorph, peptidyl prolyl-tRNA is particularly enriched, suggesting that peptidyl tRNA drop-off occurs most frequently on proline amino acids in *Mtb*. A study of the *Mtb* proteome shows that cells stop synthesizing several

proteins early on in Pth depletion, likely in response to decreased tRNA availability. We have also applied our findings on Pth's critical role in tRNA turnover through a drug development lens and show that an *Mtb* Pth knockdown is highly susceptible to macrolides, antibiotics that are currently ineffective against TB. Using tRNA sequencing, we show that macrolides add to peptidyl tRNA accumulation in *Mtb*, suggesting that Pth affects intrinsic macrolide resistance by recycling peptidyl-tRNA in the presence of antibiotic. We also show that reducing Pth levels increases *Mtb*'s susceptibility to another antibiotic class – aminoacyl tRNA synthetase inhibitors that are currently being developed against this pathogen. Taken together, our work underscores the importance of Pth in tRNA turnover and provides new biological insights on anti-TB strategies that could exploit synergy between translation errors and tRNA turnover.

Results

pth is required for normal growth of *Mtb*

Transposon sequencing in *Mtb* suggests that, like in *E. coli*, the gene encoding Pth (Rv1014c) is required for survival [24, 25]. We constructed two types of *Mtb* Pth mutants using complementary genetic techniques: proteolytic degradation [26] and CRISPR interference (CRISPRi) [27]. While the first approach depletes intracellular Pth levels by tagging proteins for degradation using a titratable system, the other achieves knockdown through transcriptional repression of varying strengths based on the protospacer-adjacent motif (PAM) used to target catalytically dead Cas9 (dCas9) to *pth* [27]. Both types of strains had growth defects that were proportional to the level of depletion (Figure 3.1), confirming that *pth* is required for normal growth of *Mtb*. Due to the more technical ease of validating *pth* knockdown levels and our use of the tightly-regulated transcriptional repression strain in published work [28], we used the CRISPRi Pth depletion strain for subsequent experiments in this work.

We previously characterized a second function for Pth in *Mtb*. In addition to its peptidyl tRNA hydrolase activity, Pth is a detoxifying enzyme for a tRNA-acetylating toxin TacT that is part of a newly-identified toxin-antitoxin system [28]. We found that this function does not contribute to *pth* essentiality in *Mtb* since TacT was not active during normal laboratory growth conditions and a *tacAT* knockout strain was equally susceptible to *pth* depletion by CRISPRi [28]. Thus, we decided to focus our efforts on studying the effects of Pth depletion in *Mtb* on peptidyl tRNA pools and tRNA turnover following translation errors.

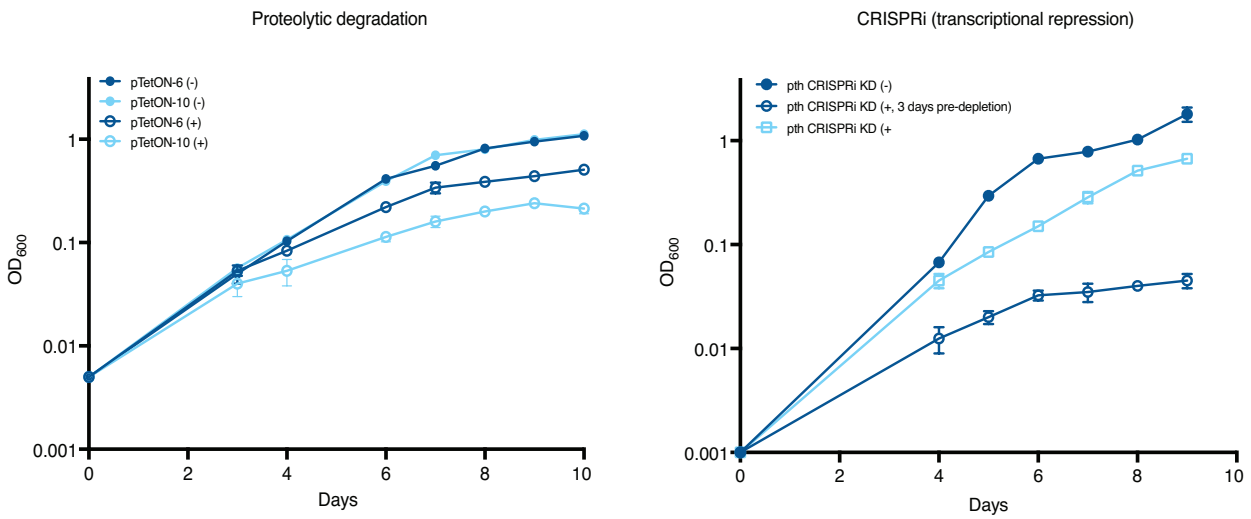

Figure 3.1. Complementary genetic techniques show Pth requirement for normal growth in *Mtb*. Growth curves are shown for different Pth knockdown constructs: proteolytic degradation (left) and transcriptional repression (right). In both panels, (-) = uninduced and (+) = induced for Pth knockdown. Growth was measured spectrophotometrically for each strain by taking OD_{600} measurements over the course of 10 days in the presence or absence of inducer. Prior to taking measurements, strains were diluted to the starting OD_{600} indicated at day 0. Proteolytic degradation strains contain C-terminal DAS-tagged Pth [26]. Briefly, the DAS tag is recognized by the protein SspB, which targets Pth for degradation by the ClpXP protease. In these constructs, SspB levels are modulated by a tetracycline-regulated promoter; removal of anhydrous tetracycline (aTC) in cultures releases TetR to induce SspB expression (pTetON) and subsequently Pth depletion. Numbers next to the plasmid name indicate promoter strength for SspB expression (6 = lower, 10 = higher, corresponding to the expected relative level of protein depletion). For transcriptional repression, CRISPRi strains were built as described [27, 28]. Addition of aTC (50ng/mL) induces site-specific transcriptional repression through steric hindrance of transcription by the presence of a modified nuclease dead Cas9 protein (dCas9). Guide RNA is designed to complement a target DNA sequence (here, the *Mtb* Pth-encoding gene Rv1014c) and protospacer adjacent motif (PAM) within the target sequence, the latter of which modulates the level of knockdown by modulating Cas9 binding to the target sequence. "Pre-depletion" refers to growing cells in the presence of aTC for 3-4 days prior to diluting strains to the indicated starting OD_{600}. Pre-depletion enables a higher level of *pth* knockdown to be achieved before conducting experiments.

tRNA sequencing can be used to measure peptidyl tRNA levels in *Mtb*

Studies of *Escherichia coli* (*E. coli*) Pth have shown that depletion of this enzyme leads to the accumulation of peptidyl tRNA in cells. The identification of peptidyl tRNA has typically been accomplished using Northern blotting [29], making it technically difficult to compare pools across all tRNA species and their respective iso-acceptors. More recent work on other substrates for Pth such

as N-acetylated aminoacyl tRNAs has surveyed tRNA species using mass spectrometry, which substantially increases sensitivity but still poses scalability challenges [28, 30, 31]. To study the effects of *pth* depletion on tRNA pools in *Mtb*, we developed a new tRNA sequencing-based strategy to study changes in a rapid, quantitative, and high-throughput way (Figure 3.2).

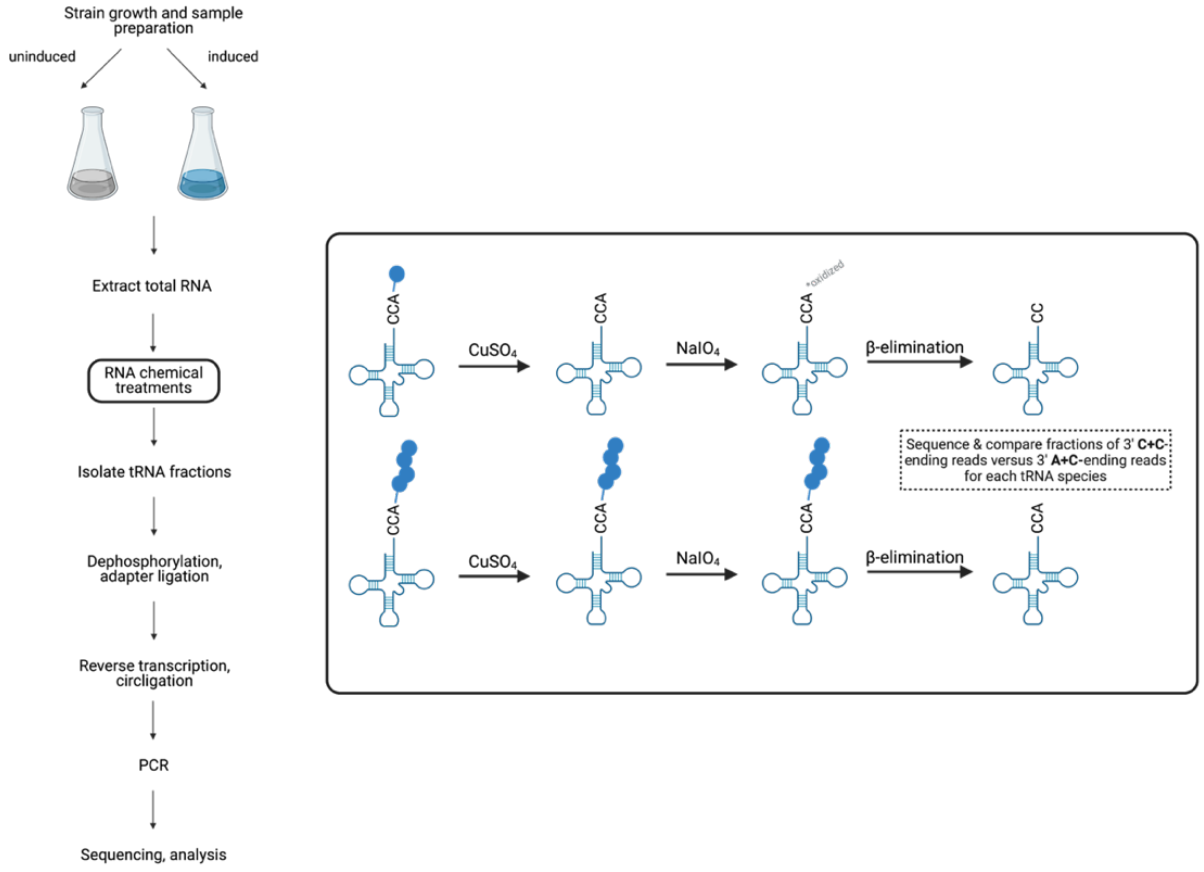

Figure 3.2. Application of tRNA sequencing to measure pools of peptidyl and N-acetylated tRNA. Overview of copper sulfate-based tRNA sequencing ($CuSO_4$-tRNAseq) experiment. Strains are grown and harvested at a normalized cell density. Total RNA is extracted at a low pH to ensure maintenance of the acyl linkage between tRNA and amino acid. Total RNA is subjected to the chemical treatments (boxed) to distinguish between aminoacyl or uncharged tRNA (top) and peptidyl or N-acetylated aminoacyl tRNA (bottom). tRNA fractions are extracted from 1-2µg of total RNA for sequencing library preparation as described in Methods and [32]. The ratio of 3' A+C-ending reads compared to total 3'C+C and 3'A+C ending reads for each tRNA is computed as described [23] to estimate the fraction of peptidyl (or N-acetylated) tRNA in each tRNA species. A higher fraction of A+C-ending reads following $CuSO_4$-tRNAseq suggests a higher proportion of peptidyl or N-acetylated aminoacyl tRNA. Figure created with BioRender.com.

tRNA sequencing has been used to survey tRNA modifications in all domains of life, and recently an application was developed to measure aminoacyl-tRNA fractions at single-base resolution [23]. This method incorporates chemical treatments prior to sequencing that distinguish between charged and uncharged tRNA. All tRNAs share a 3' CCA tail that serves as the aminoacylation site [33]. The first chemical treatment – sodium periodate – has no effect on the 3' end of a charged tRNA, because the bound amino acid protects molecules from oxidation. However, an uncharged tRNA is oxidized at the 3'A. A subsequent β-elimination reaction at high pH then removes an unprotected 3' A residue at the end of uncharged tRNA, or simply deacylates charged tRNA, leaving the 3'A intact on the molecule. Sequencing of tRNA libraries and comparing CC-ending reads to CCA-ending reads for each tRNA isoacceptor provides a global view of tRNA aminoacylation in cells [23].

We adapted this technique to study peptidyl tRNA by adding a chemical treatment prior to periodate oxidation: copper sulfate ($CuSO_4$) deacylates tRNAs charged with a single amino acid, but this treatment leaves N-blocked aminoacyl tRNA (such as N-acetylated aminoacyl tRNA or peptidyl tRNA) untouched [29, 34]. Since *Mtb* TacT acetylates glycyl-tRNA, we used our previously-described *M. smegmatis* (*Msmeg*) strain overexpressing *Mtb* TacT to pilot $CuSO_4$-tRNA sequencing ($CuSO_4$-tRNAseq) [28]. *Msmeg* does not encode its own copy of *tacT*, so we hypothesized that glycyl-tRNA profiles would differ between cultures that were induced or uninduced for *Mtb* TacT overexpression. Indeed, $CuSO_4$-tRNAseq was able to distinguish N-acetylated glycyl-tRNA from regular glycyl-tRNA (Figure 3.3), suggesting that $CuSO_4$-tRNAseq can be used reliably to measure N-blocked aminoacyl tRNA – and thus peptidyl tRNA – levels in *Mtb*.

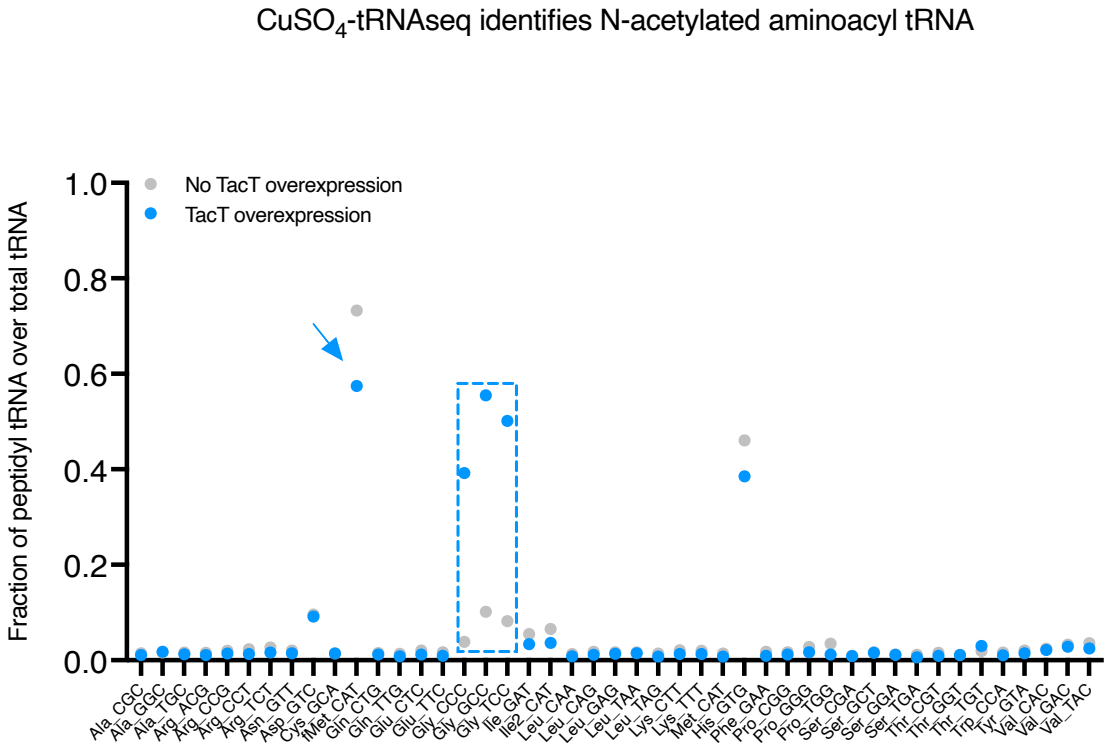

Figure 3.3. $CuSO_4$-tRNA sequencing ($CuSO_4$-tRNAseq) distinguishes N-acetylated aminoacyl tRNA from aminoacyl or uncharged tRNA. $CuSO_4$-tRNAseq was carried out on a previously described *M. smegmatis* (*Msmeg*) strain with inducible *Mtb* TacT overexpression [28]. Pth recognizes and cleaves N-blocked aminoacyl tRNAs including N-acetylated aminoacyl tRNAs and peptidyl tRNA. $CuSO_4$ does not cleave Pth substrates but does cleave individual amino acids off tRNA. *Msmeg* does not naturally encode *tacT*, so acetylated aminoacyl tRNA is not expected in the uninduced *Msmeg* RNA samples, except in the event of any low-level expression from plasmid leakage. *Mtb* TacT (encoded by Rv0919) blocks translation by acetylating glycyl-tRNAs and preventing their incorporation into a growing peptide, thus depleting cells of available glycyl-tRNA pools [28, 30, 31]. The fraction of peptidyl tRNA is plotted as a ratio of the number of 3'CCA-ending reads to the sum of 3'CCA- and 3'CC-ending reads for each tRNA species. $CuSO_4$-tRNAseq identifies N-acetylated glycyl-tRNA in the induced (TacT overexpression) condition (blue dashed box). $CuSO_4$ (and Pth) also do not cleave initiator tRNA (fMet), which contains a formylated methionine. Since TacT expression blocks protein synthesis, the decrease in charged fMet tRNA detected in the overexpression strain (blue arrow) is likely a response to decreased translation and a reduced need for initiator tRNA. Histidyl-tRNA is resistant to $CuSO_4$ deacylation, suggesting that histidine's unique imidazole ring affects the reaction's efficiency. Thus, this tRNA cannot be accurately included in analyses of tRNA pools in subsequent experiments using $CuSO_4$-tRNAseq.

Pth depletion in *Mtb* reduces pools of usable tRNA

We applied $CuSO_4$-tRNAseq to *Mtb* samples to compare tRNA profiles between strains that were induced for *pth* depletion by CRISPRi and uninduced strains with wild-type Pth levels. All three

chemical pre-treatments – $CuSO_4$, $NaIO_4$, and β-elimination – did not significantly affect tRNA counts during sequencing, confirming that any changes we observed between samples are most likely due to biological differences between strains with different intracellular Pth levels (Table A3.1, Figure A3.1).

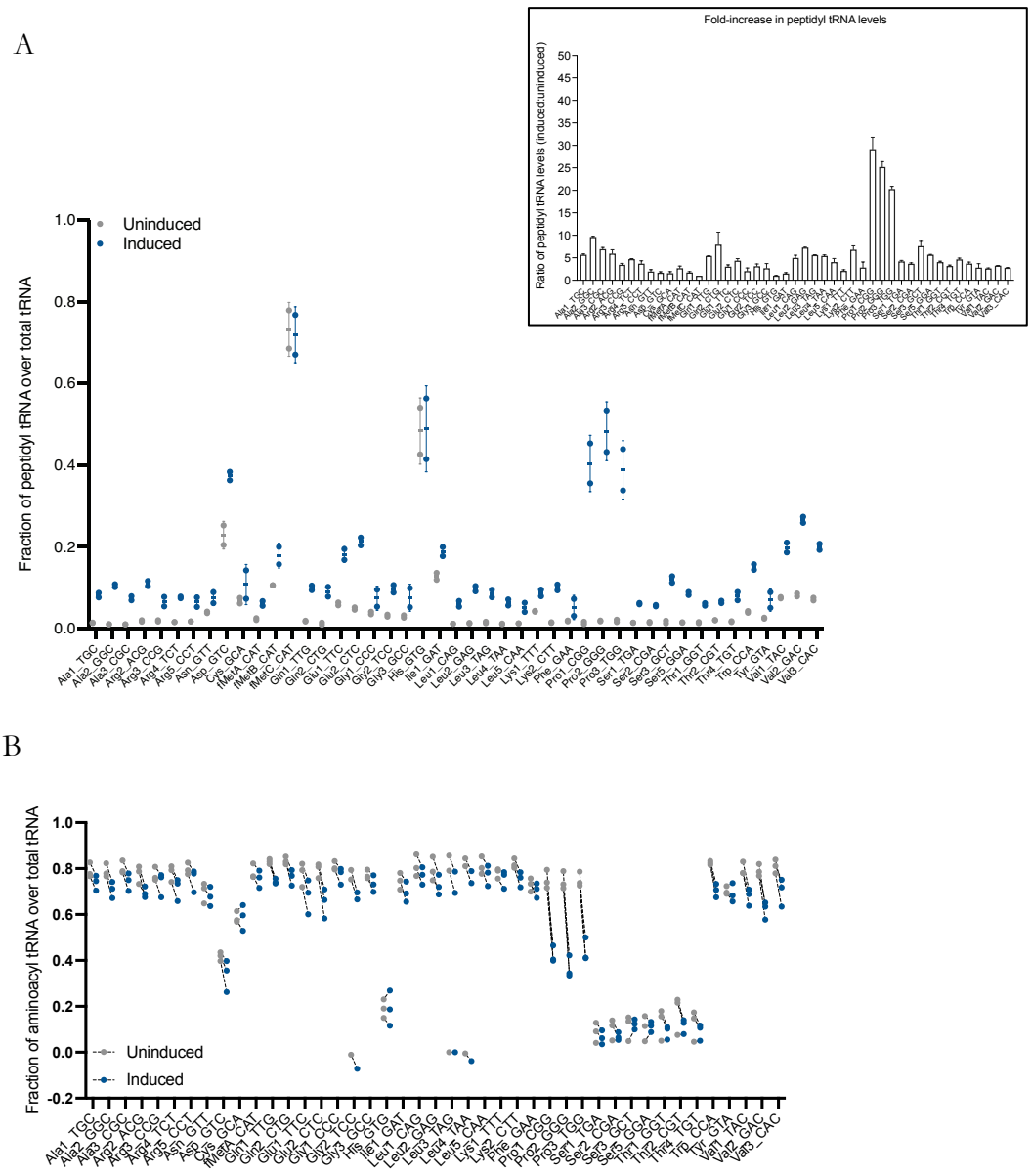

Figure 3.4. Depleting Pth leads to accumulation of peptidyl tRNAs in *Mtb* and a reduction in usable aminoacyl tRNA pools. $CuSO_4$-tRNAseq was carried out in a *Mtb* CRISPRi Pth knockdown. (A) Strains were grown to an OD_{600} of 0.3-0.4 in the presence or absence of inducer (50ng/mL aTC) and total RNA was harvested. The fraction of peptidyl tRNA is plotted as a ratio of the number of 3'CCA-ending reads to the sum of 3'CCA- and 3'CC-ending reads for each tRNA species. The bar plot (top right) displays the ratio of peptidyl tRNA fractions between induced and uninduced strains. (B) RNA samples from (A) were treated with periodate and β-elimination only, without $CuSO_4$ (Dataset 3.2). The aminoacyl (usable) tRNA fraction for each species is the difference between total charged tRNA levels and peptidyl tRNA levels. It is important to note that current methods to extract RNA have been shown to de-acylate serine/threonine tRNAs [23, 35], so absolute total charged levels may be higher than indicated by these data. Serine, threonine, and histidine tRNAs are also typically acylated at lower levels than other tRNAs in bacteria [36].

Peptidyl tRNA accumulation is detected in most tRNAs in an *Mtb pth* knockdown (Figure 3.4A). This suggests that peptidyl tRNA drop-off occurs across amino acids during normal growth and that Pth cleaves all tRNA species *in vivo*. We also observed small but statistically significant decreases in normalized tRNA counts for multiple tRNAs in Pth knockdowns (Pro_GGG, Ile_GAT, Arg_TCT, Arg_ACG, Val_CAC, Cys_CGA, Thr_TGT, Gly_TCC, and Phe_GAA), further underscoring Pth's effects on tRNA availability, though the mechanism of this reduction is unknown (Figure A3.2). Importantly, while the fraction of peptidyl tRNA grew in the absence of wild type Pth levels, the fraction of aminoacyl tRNA decreased, showing a reduction in usable tRNA in *Mtb* upon Pth depletion (Figure 3.4B). Thus, Pth depletion leads to reduced aminoacyl tRNA availability for protein synthesis.

Notably, prolyl-tRNAs made up the most abundant pool of peptidyl tRNA, and this was true across all 3 proline tRNA iso-acceptors. We also detected this change in the same Northern blot (Figure A3.3). Based on our results, while peptidyl tRNA drop-off occurs at all tRNAs to varying degrees during normal growth, peptidyl prolyl-tRNA is the most abundant substrate for Pth in *Mtb*. It is important to note that previous studies investigating the biochemistry of Pth do not see a decrease in enzymatic efficiency on N-blocked proline-tRNAs relative to other tRNAs, suggesting that the increased peptidyl prolyl-tRNA accumulation is not an indicator simply of less efficient Pth catalysis on these substrates [37], though additional studies would have to be performed on peptidyl-tRNA specifically to completely rule this option out.

Pth depletion globally affects protein production

We next assessed the effects of Pth depletion on the *Mtb* proteome. We collected lysate from *pth* knockdown-induced and uninduced cells, as well as from empty guide RNA strains to control for any potential effects of anhydrous tetracycline (CRISPRi inducer). Since knocking down *pth* leads to

growth arrest over time, we collected samples after 2 days of pre-depletion instead of 3 to study the most direct and immediate effects of Pth levels on protein production (Figure 3.1).

Since proline tRNA was the most affected tRNA based on our sequencing results, we hypothesized that Pth knockdowns would be initially depleted in proline-rich proteins due to proline-tRNA starvation. However, while the most depleted protein other than Pth in our induced samples was a proline-rich PE/PPE protein (Figure 3.5, Dataset D3.3), we did not observe a statistically significant relationship between proline enrichment and the likelihood of other proteins being underrepresented in a Pth knockdown. This suggests changes in tRNA availability following Pth depletion have a broader effect on protein synthesis than affecting a single amino acid.

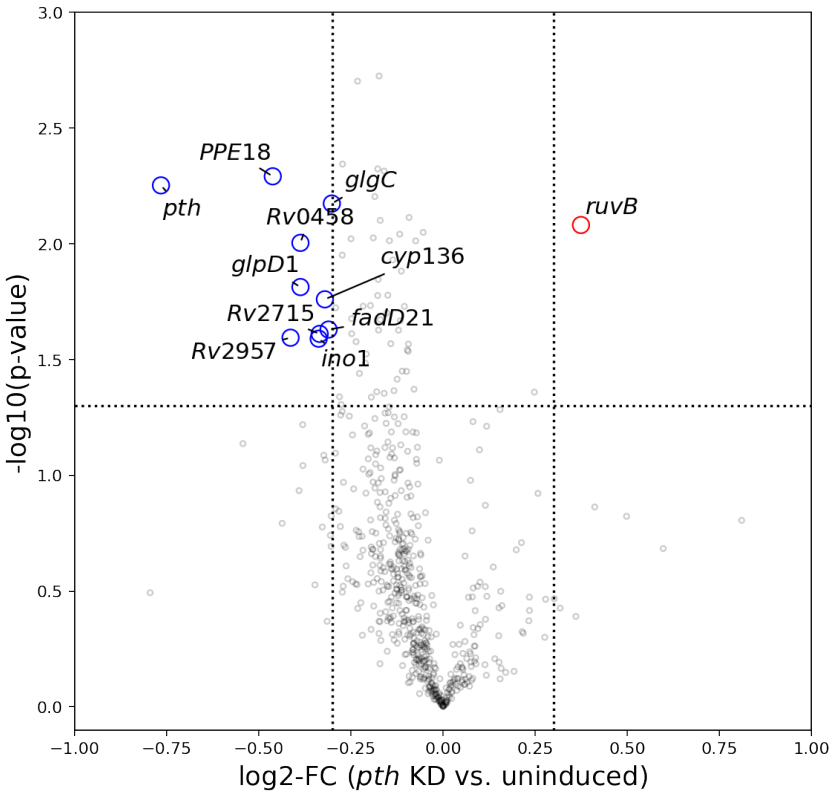

Figure 3.5. Proteins with altered abundance in a Pth depletion strain. 1,824 unique *Mtb* proteins were identified through TMT-labeling and mass spectrometry-based quantitative proteomics described in Methods. 621 proteins (Dataset D3.3) whose average abundance in an uninduced control surpassed 5,000au were analyzed. Proteins with a p-value (unpaired Student's t-test) <0.05 and a $\log_2$-fold change over 0.3 were considered differentially abundant and are highlighted on the volcano plot.

Pth depletion increases *Mtb* sensitivity to candidate aminoacyl tRNA synthetase inhibitors

Our tRNA sequencing and proteomics findings suggest that Pth is broadly required for tRNA turnover in cells. Thus, we wondered whether further targeting a single tRNA species would have a compounded effect on *Mtb* survival in the absence of Pth. In other words, would limiting tRNA availability by some other mechanism synergize with Pth depletion? Efforts are currently underway to develop aminoacyl tRNA synthetase inhibitors for TB, and these types of drugs have seen clinical success against malaria (halofuginone) and certain skin infections (mupirocin). We tested a panel of candidate lysine tRNA synthetase inhibitors (in preparation; compound names have been omitted prior to publication) and found some synergy of these compounds with Pth knockdowns compared to uninduced controls (Figure 3.6). Our results confirm that Pth mediates tRNA turnover in *Mtb*, and that orthogonally targeting cells' ability to maintain normal available aminoacyl tRNA levels can be a powerful anti-TB strategy.

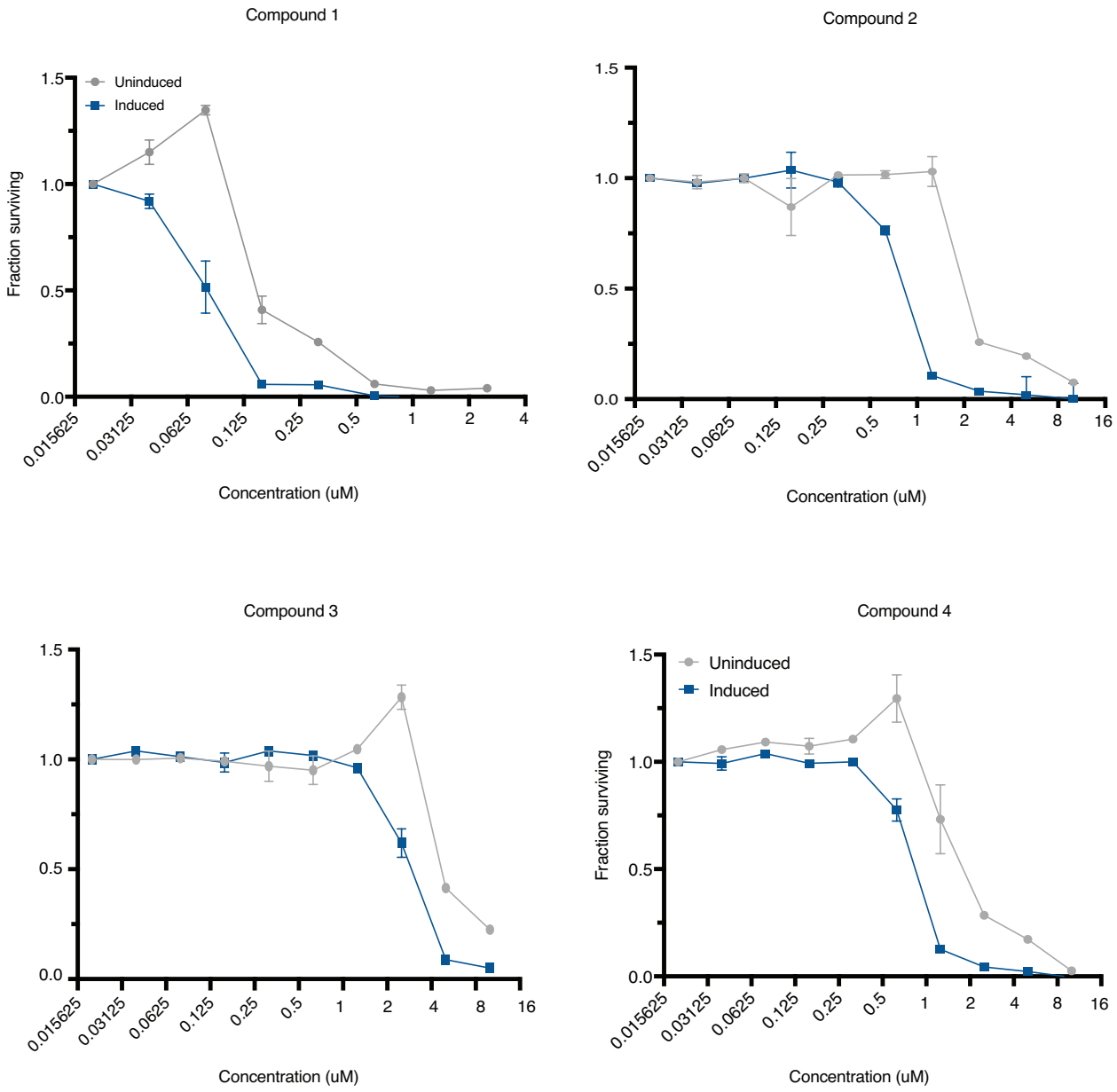

Figure 3.6. Pth depletion increases *Mtb* sensitivity to candidate lysine tRNA synthetase inhibitors. *Mtb* growth in the presence of 4 candidate lysine tRNA synthetase inhibitors is plotted across drug concentrations as determined by fluorescence in an Alamar blue assay. Pth CRISPRi strains were grown to mid-log and diluted to an OD_{600} of 0.001 and plated in serial dilutions of antibiotic in 96-well plates. The fraction of *Mtb* cells surviving is plotted by normalizing fluorescence values to control wells with no drug. Results are representative of two biological replicates.

Pth depletion sensitizes *Mtb* to macrolide antibiotics

In *E. coli*, a temperature-sensitive Pth mutant is hypersusceptible to macrolides, a class of antibiotics that target the large 50S ribosomal subunit [38]. Macrolides are thought to increase rates of

peptidyl tRNA drop-off by obstructing the nascent peptide exit tunnel and leading to early ribosome dissociation from a transcript [39, 40]. Macrolides are not currently used to treat tuberculosis but are generally well-tolerated and are used to treat non-tuberculous mycobacterial infections [41-43]. To see whether an inhibitor targeting Pth in *Mtb* would make this pathogen susceptible to macrolides, we tested our collection of Pth knockdown strains against a panel of macrolides. Interestingly, all levels of Pth depletion tested were hypersusceptible to macrolides but not to other ribosome-targeting antibiotics with different mechanisms of action (Figure 3.7A, Table A3.2). Pth hypomorphs were also more susceptible to the lincosamide clindamycin and the aminonucleoside puromycin, both of which also trigger peptidyl tRNA drop-off (Figure A3.4) [38, 44]. These results suggest that inhibitors even partially blocking wild-type Pth activity would render *Mtb* susceptible to treatment with macrolides or other drugs that also increase peptidyl tRNA drop-off.

Indeed, tRNA sequencing shows a slight accumulation in wild type *Mtb* treated with an inhibitory concentration of erythromycin, and a bigger increase in peptidyl tRNA pools across tRNAs in a Pth knockdown treated with erythromycin (Figure 7B). The effect in wild type cells is likely negligible owing to the presence of Pth, but the larger fractions of peptidyl tRNA in the Pth hypomorph suggest that cells are overloaded with Pth substrates upon erythromycin treatment. This effect was not observed on tRNA pools from *Mtb* treated with chloramphenicol (Figure S4). Our findings confirm that macrolides increase peptidyl tRNA drop-off, and that even slightly perturbing tRNA pools in a Pth knockdown leads to significant phenotypic effects.

A

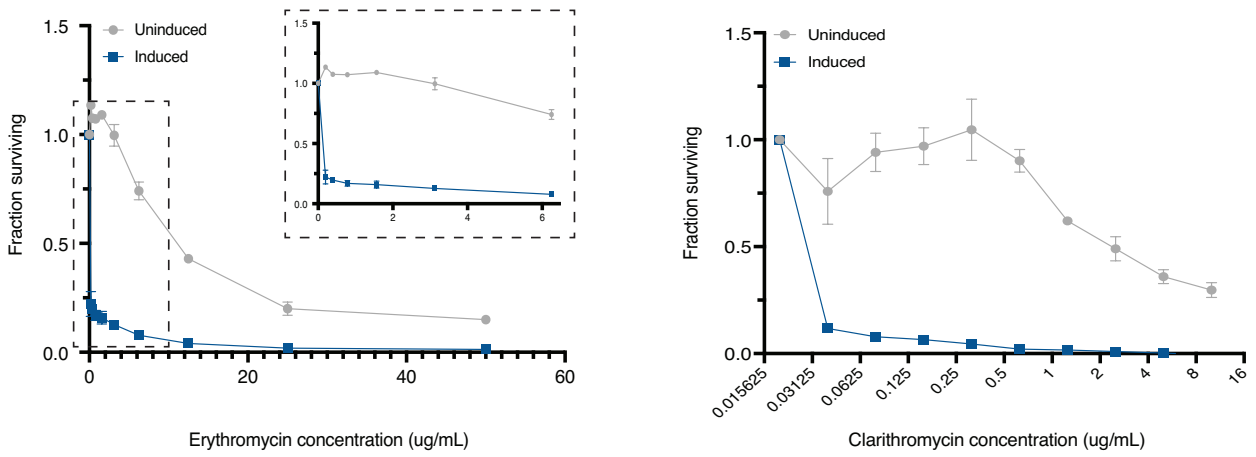

B

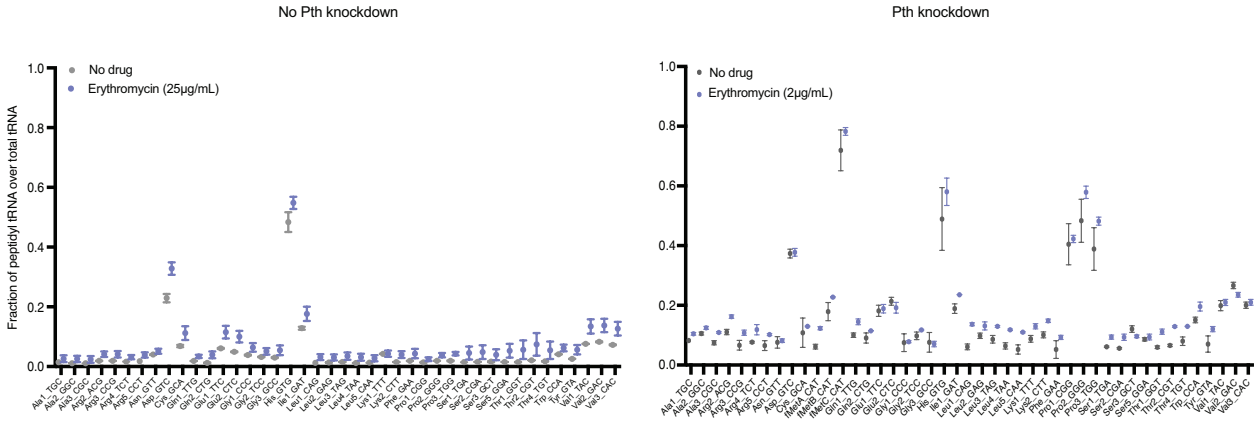

Figure 3.7. Pth depletion sensitizes *Mtb* to macrolides. (A) *Mtb* growth in the presence of two macrolides – erythromycin and clarithromycin – is plotted across drug concentrations as determined by fluorescence in an Alamar blue assay [45]. Pth CRISPRi strains were grown to mid-log and diluted to an OD_{600} of 0.001 and plated in serial dilutions of antibiotic in 96-well plates. The fraction of *Mtb* cells surviving is plotted by normalizing fluorescence values to control wells with no drug. Results are representative of three biological replicates. (B) $CuSO_4$-tRNAseq was performed on Pth CRISPRi strains in the presence and absence of erythromycin. Strains were grown in the presence or absence of inducer as described in Figure 3.3. Uninduced strains were then treated overnight with 25µg/mL of erythromycin, and Pth knockdown-induced strains were treated with 2µg/mL for the same duration. Results are from two independent biological replicates.

Discussion

In this work, we have developed a new application of tRNA sequencing to study peptidyl tRNA in *Mtb*. $CuSO_4$-tRNAseq builds on existing techniques by incorporating copper sulfate treatment to chemically distinguish peptidyl tRNA from aminoacyl or uncharged tRNA. This allows us to study the composition of tRNA pools in a quantitative and high-throughput manner. Previous work studying peptidyl tRNA has relied on Northern blots and mass spectrometry, both of which are extremely valuable but difficult to scale.

We found that depleting Pth leads to a reduction in aminoacyl tRNA availability across most tRNA species in *Mtb*, and that proline tRNA pools are the most substantially impacted. Our findings suggest that while peptidyl tRNA drop-off occurs at all amino acids to some degree during normal growth, this type of ribosome error occurs the most frequently on proline-containing sequences in *Mtb*. Of the 20 amino acids, proline is the only N-alkylamino acid, and its peptide synthesis dynamics are less efficient compared to other amino acids, owing to the alkyl group in proline being directly on the nitrogen used as a nucleophile during peptide bond formation [46].

Our results suggest that Pth is particularly important for recycling peptidyl tRNA that has dropped off during the incorporation of proline to a growing peptide in *Mtb*. Recently, studies have characterized a phenomenon known as intrinsic ribosome destabilization (IRD), in which the nascent chain can trigger premature translation termination [47]. While the mechanism of IRD still requires further study, peptidyl tRNA released into the cytoplasm during abortive IRD can be a substrate for Pth [47]. Interestingly, studies of these truncated peptides have found a relationship between the presence of alternating proline and acidic amino acids and the likelihood that a ribosome will be destabilized [47]. These findings further support our findings that the presence of prolines in a polypeptide predisposes ribosomes to abortive translation.

Mycobacteria are a highly GC-rich genus, and pathogenic mycobacteria are enriched for so-called PE/PPE proteins, outer membrane proteins characterized by their proline-rich N-terminal sequences that make up nearly 10% of the *Mtb* genome [48, 49]. It is tempting to speculate that *Mtb*'s proline richness contributes to a critical need for Pth. Indeed, the PE/PPE protein PPE18 was the second-most depleted protein in a Pth knockdown, second to Pth itself. Despite these proteins taking up a substantial portion of the *Mtb* genome, however, our proteomics work only identified a couple of PE/PPE proteins, suggesting that current lysate extraction methods are not optimized for detecting PE/PPE proteins; future studies of Pth depletion on the effects of PE/PPE production in *Mtb* should incorporate methods focused on optimizing membrane fraction collection and the quantitative identification and differentiation of these proteins.

Beyond PPE18, we were unable to find a pattern in the amino acid composition of other depleted proteins. To identify the most direct effects of Pth depletion, we pre-depleted samples for a shorter time and extracted samples immediately before a growth defect would be seen (Figure 3.1B). As a result, the number of affected proteins and their magnitude of depletion were minimal. Notwithstanding potential shortfalls of our sample preparation, our current data suggest that Pth depletion has a broader effect on protein synthesis; this makes sense in the context of reversibly slowing down translation and growth in the absence of sufficient aminoacyl tRNA, instead of allowing cells to aberrantly translate proteins and risk irreversible damage. Similarly, depletion of a single amino acid triggers the stringent response in bacteria during starvation to stop growth.

Even though proline tRNA turnover was the most impacted by Pth depletion, we also found that *Mtb* Pth hypomorphs were more susceptible to lysine tRNA synthetase inhibitors than uninduced controls. This suggests that the smaller reductions we observed in aminoacyl tRNA availability in other tRNAs (lower rates of peptidyl tRNA drop-off) are also biologically significant, and that Pth broadly mediates tRNA turnover in *Mtb*. *pth* is essential in many other bacterial species including *E. coli* and *B.*

subtilis, neither of which is enriched for polyproline containing proteins. In fact, studies on an *E. coli* temperature-sensitive Pth mutant found suppressor mutations that led to the overproduction of lysine tRNA, suggesting that the growth defect in *E. coli* may be due to lysine-tRNA starvation in this AT-rich organism [50]. Overexpressing other tRNAs individually, meanwhile, did not rescue the growth defect [50]. However, later work found that lysine-tRNA overexpression also led to increased protein synthesis – including Pth synthesis – raising questions on the interpretability of the lysine-tRNA suppressor and potentially pointing to a more global tRNA effect like in *Mtb* [51]. Future work investigating peptidyl tRNA pools in *pth* mutants in other bacteria would shed light on the dynamics of peptidyl tRNA drop-off and Pth's role in other organisms. The tRNA sequencing-based methods outlined in this paper provide a scalable and efficient platform for such efforts.

Tuberculosis (TB) remains a leading infectious disease threat to global health. *Mtb* is intrinsically resistant to most existing antibiotics and current treatment requires a minimum of four months of combination therapy using potent drug regimens which have remained largely unchanged since their discovery in the mid-twentieth century. Success in TB drug discovery so far has stemmed from chemical screening as opposed to a target-based approach. Advances in *Mtb* genetics have reinvigorated target-based discovery efforts by enabling the identification enzymes that are particularly vulnerable even to partial inhibition [52, 53], and innovations in synthetic chemistry promise to improve target-based drug design [54]. A better understanding of the biology of these enzymes and their interactions with existing antibiotics promises to inform the design of synergistic and thus more effective combination therapies that could revolutionize TB treatment.

Protein synthesis is indispensable to any living cell, and in fact many of the antibiotics used to treat other bacterial infectious diseases target some aspect of protein synthesis. Nonetheless, most of these drugs are ineffective against TB, and our current anti-TB arsenal is lacking in protein synthesis inhibitors. Here, we have identified several orthogonal approaches to inhibit protein synthesis in *Mtb*

by impeding an essential mediator of tRNA availability. Our work underscores Pth as a promising candidate for target-based development, given its stand-alone requirement for *Mtb* survival, as well as its ability to potentiate the activity of two classes of translation inhibitors. Despite being ubiquitous in bacteria, the crystal structure of *Mtb* Pth shows structural divergences from other bacteria including its close relative *Msmeg*, suggesting that *Mtb*-specific compounds could be designed for pathogen specificity.

Macrolides are used to treat a variety of clinical pathogens including some non-tuberculous mycobacteria but are currently ineffective against TB. Sensitizing *Mtb* to macrolides by simultaneously targeting Pth offers a new strategy to lend efficacy to an entire class of antibiotics against this devastating disease. Many mycobacteria encode an inducible macrolide resistance mechanism [55, 56]. Exposure to macrolides triggers expression of the so-called *erm* family of genes, whose products methylate ribosomes at the site of macrolide binding. Despite possessing this innate resistance mechanism, macrolides like azithromycin are still used to treat *M. abscessus* infections, suggesting that there could still be success in including macrolides in an anti-TB regimen [41]. Since Pth depletion likely causes global translation arrest, we hypothesize that treating Pth-depleted cells with macrolides will make it difficult – if not impossible – for cells to actively synthesize Erm methyltransferases, whose synthesis is induced by the WhiB7 intrinsic resistance transcription factor, further contributing to their sensitivity to macrolide treatment [57, 58]. Furthermore, *Mtb* clinical isolates lacking *erm* genes have been discovered in an *Mtb* sub-lineage that is endemic to Southeast Asia, and multiple other macrolide-sensitizing genes have been identified in *Mtb* and are worth exploring as additional adjuvants in a macrolide-based anti-TB strategy [57].

A recent survey of gene vulnerability to various levels of depletion using CRISPR interference (CRISPRi) found that even slightly reducing levels of tRNA synthetase expression causes major growth attenuation in *Mtb* [52]. Inhibitors against these enzymes are currently being developed, with

a focus on lysine tRNA synthetases. Our work provides an opportunity to strengthen these already highly potent compounds even further by coupling them with an orthogonal mediator of tRNA availability. While existing proline tRNA synthetase inhibitors like halofuginone unfortunately do not exhibit activity against *Mtb in vitro*, our findings raise the question of whether a Pth inhibitor would synergize more strongly with proline tRNA synthetase inhibitors, given the disproportionate decrease in proline tRNA availability in a Pth knockdown.

Altogether, our work underscores the importance of Pth in tRNA turnover and provides new biological insights on anti-TB strategies that could exploit synergy between translation errors and tRNA turnover. We also lay forth an application of tRNA sequencing that can be used to study peptidyl tRNA and N-acetylated tRNA in other organisms, providing a high-throughput way to shed light on the dynamics of tRNA pools across all kingdoms of life.

Materials and Methods

Bacterial strains and growth conditions: *Mtb* and *Msmeg* strains were grown from frozen stocks into Middlebrook 7H9 medium supplemented with 0.2% glycerol, 0.05% Tween-80, and ADC with or without oleic acid, respectively (5g/L bovine serum albumin, 2g/L dextrose, 3 μg/ml catalase). Cultures were incubated at 37 °C. Antibiotics or inducing agents were used when needed at the following concentrations in both *Mtb* and *Msmeg*: kanamycin (25μg/ml), anhydrous tetracycline (aTC; 100ng/mL), hygromycin (50μg/ml), and nourseothricin (20μg/ml). Transformed *Mtb* and *Msmeg* strains were plated onto 7H10 agar plates with the appropriate antibiotic(s). Strains were grown to mid log-phase for all experiments unless otherwise specified (OD_{600} 0.4-0.6). *E. coli* strains for cloning or protein purification were grown in LB broth or on LB agar with appropriate antibiotics at the following concentrations: kanamycin (50 μg/ml), zeocin (50μg/ml), and nourseothricin (40 μg/ml). Induction time for *pth* depletion in *Mtb* was 3 days.

Bacterial strain construction: Table A3.3 depicts the strains, plasmids, primers, and recombinant DNA used for this study. Plasmids were built by restriction digest of a parental vector and inserts were prepared either by restriction enzyme cloning or Gibson assembly using 40bp overhangs, as specified in Table A3.3. Plasmids were isolated from *E. coli* and confirmed via Sanger sequencing carried out by Genewiz, LLC (Massachusetts, USA).

Pth-knockdown constructs: Transcriptional knockdown of *pth* was accomplished using mycobacterial CRISPRi-interference (CRISPRi) as described with the same strain used in Chapter Two [28]. Proteolytic degradation strains were built using the plasmids and primers listed in Table A3.3. Briefly,

Northern blotting: Acid-PAGE Northern blotting of tRNA was performed as previously described [59]. Briefly, 0.5μg total RNA was electrophoresed on a 6.5% urea gel (7 M urea, 100 mM NaOAc, pH 5.0), transferred to a nitrocellulose membrane by semi-dry blotting, and UV-crosslinked twice (1200μJ). Membranes were incubated with ULTRAhyb-oligo (ThermoFisher Scientific) at 42 °C for 30 min followed by hybridization overnight at 42C with 4pmol probes (Table A3.3) that were radiolabeled using [γ^{-32}P] ATP (PerkinElmer) and T4 Polynucleotide kinase (New England Biolabs). Membranes were washed twice with 2xSSC (3M NaCl, 300mM sodium citrate $2H_2O$) + 0.1% SDS and bound probe was detected using a FLA-5000 PhosphoImager (Fuji).

tRNA sequencing

Extraction of total RNA: Strains were grown to mid-log phase with the appropriate antibiotics and inducing agents described above. RNA was collected at the same OD_{600} for each strain (between 0.4-0.6). Cells were left on ice for 20 minutes, then pelleted by centrifuging at 4,000rpm for 10 minutes at 4C. Pellets were resuspended in 0.5-1mL of TriZol (Life Technologies) and lysed using a BeadBug microtube homogenizer (Millipore Sigma). 200μL of chloroform was added to each tube, after which samples obtained from *Mtb* strains were removed from biosafety level 3 precautions. Samples were centrifuged at 15,000rpm for 15 minutes at 4C and the aqueous layer was collected into a fresh tube. To the original tube, 250μL of sodium acetate buffer (300mM sodium acetate pH 5.2 and 10mM EDTA pH 8.0) was added, and samples were vortexed at 4C for 5 minutes then centrifuged at 15,000g for 15 minutes at 4C. The aqueous layer was added to the fresh sample-containing tubes. 400μL chloroform was added, and tubes were briefly vortexed and then centrifuged at 15,000rpm for 1 minute at 4C. The aqueous phase was collected into a fresh tube and RNA recovered by ethanol precipitation. RNA pellets were resuspended in 10mM sodium acetate pH 5.2 and stored at -80C until processed for sequencing.

Copper sulfate treatment: Copper sulfate treatment of total RNA samples was performed as described [29]. Briefly, 20-30μg of total RNA was added to fresh tubes to a final volume of 54μL in storage buffer (8M urea, 10mM sodium acetate pH 5.2, 1mM EDTA). 6μL of 100mM copper sulfate ($CuSO_4$) were added for a final concentration of 10mM $CuSO_4$ and reactions were incubated at 37C for 1 hour. 1mM EDTA was then added to each tube, along with 3μL of glycogen (2mg/mL). Samples were recovered by ethanol precipitation and stored at -80C between treatments.

Sodium periodate treatment: Sodium periodate ($NaIO_4$) treatment of total RNA samples was performed as described [23]. Briefly, 1μg of total RNA was combined with 100mM sodium acetate pH 5.2 and 50mM $NaIO_4$ in a final volume of 100μL. Reactions were incubated at room temperature in the dark for 30 minutes, and subsequently quenched with 100mM glucose for 5 minutes. Unquenched periodate was removed using Micro Bio-Spin P-6 columns (Bio-Rad Laboratories) according to manufacturer instructions. RNA was recovered by ethanol precipitation.

Beta-elimination treatment: Beta elimination of periodate-oxidized RNA samples was performed as described [23]. Briefly, total RNA collected after periodate oxidation was combined with 60mM sodium borate pH 9.5 (Boston BioProducts) in a final volume of 100μL and incubated for 90 minutes at 45C. Samples were purified with Micro Bio-Spin P-6 columns (Bio-Rad Laboratories) according to manufacturer instructions. RNA was recovered by ethanol precipitation.

Library preparation: Representative gels from each step of tRNAseq library preparation are shown in Figure A3.6.

Isolation of tRNA fraction: 1-2μg of total RNA was run on a 10% TBE-UREA gel (ThermoFisher Scientific) at 250V for 1 hour. Gels were stained with SYBR Gold (ThermoFisher Scientific), and tRNA was excised as shown in Figure A3.6. Excised gels containing tRNA fractions were mashed in RNAse-free tubes, and 300μL elution buffer (300mM NaOAc pH 5.5, 1mM EDTA pH 8.0, 0.10% SDS) was added to each tube. Samples were shaken on a thermoshaker (VWR) for 1-4 hours at 37C and supernatant was collected using an Ultrafree filter column (Millipore Sigma). tRNA was recovered by isopropanol precipitation.

tRNA dephosphorylation: tRNA was dephosphorylated using QuickCIP (New England BioLabs) according to manufacturer instructions, and tRNA was collected by phenol-chloroform extraction followed by isopropanol precipitation.

Adapter ligation: 0.5μL RNase inhibitor was added to 3.5μL dephosphorylated tRNA (200-250ng tRNA) and samples were boiled at 80C for 2 minutes. Boiled tRNA was mixed with 12μL PEG buffer mix (10μL 50% PEG8000, 2μL 10X buffer B0216S; New England Biolabs). 3μL of 5' adenylated linkers (Table A3.3) were added (33pmol/μL) along with 1μL T4 RNA ligase 2 truncated (New England BioLabs) and incubated at 25C for 2.5 hours. Samples were recovered by isopropanol precipitation and run on a 10% TBE-Urea PAGE gel for 40 minutes at 250V (Figure A3.6). Ligated products were recovered by gel excision as described above.

Reverse transcription: Identical quantities of samples with different adapter sequences were pooled for reverse transcription for a total of 200-250ng tRNA. Reverse transcription was performed by combining 2.1μL dephosphorylated tRNA with 100mM Tris-HCl pH 7.5, 0.5mM EDTA, 1.25μM

RT primer (Table A3.3), 450mM NaCl, 5mM $MgCl_2$, 5mM DTT, 500nM TGIRT (InGex), and 15% PEG8000 in a final volume of 9μL. Samples were incubated at 25C for 30 minutes, after which 1μL 10mM dNTPs (New England BioLabs) were added and reactions incubated at 60C for 1 hour. 1.15μL NaOH was added, and samples were boiled for 15 minutes and run on a 10% TBE Urea PAGE gel at 250V for 1 hour. Reverse transcription products were excised from gels as shown in Figure A3.6 and cDNA recovered by isopropanol precipitation. Linear single stranded cDNA was circularized using CircLigase II (Lucigen) in accordance with manufacturer instructions.

PCR of tRNA libraries: PCR reactions were set up using HF Phusion according to the manufacturer's instructions using a universal reverse primer (Table A3.3) and a different index primer for each pool of samples (Figure A3.6). PCR reactions were aliquoted into 4 tubes and collected after 6, 8, 10, and 12 cycles. Samples were run on a Native TBE PAGE gel (ThermoFisher Scientific) at 180V for 50 minutes, and amplified products were cut from the same cycle for each sequencing run. Samples were recovered by gel excision and isopropanol precipitation.

Sequencing: Sequencing was performed on a MiSeq instrument (Illumina) using 75bp single end reads with a version 3, 150 cycle kit.

Analysis: 3' linker sequences and one nucleotide at the 5' end were trimmed using cutadapt and fastx-trimmer. Bowtie v1.2.2 was used with default settings to map reads to reference Mtb or Msmeg tRNA sequences (Datasets D3.1 and D3.2) retrieved from Mycobrowser [60]. Mpileup files were generated using samtools (samtools mpileup -I -A --ff 4 -x -B -q 0 -d 10000000). 3' end termini of mapped reads were piled up using the bedtools genomecov command (-d -3 -ibam). To analyze 3' ends, a cutoff of 500 read counts for each tRNA species was set. The number of 3' termini at any position was divided

by the total number of mapped termini to compute 3' termination frequency. The ratio of peptidyl tRNA for each tRNA species is the 3' termination frequency at the terminal A residue of the 3' CCA tail of each tRNA sequence compared to the sum of the frequencies at the terminal A and at the previous C nucleotide.

Drug susceptibility assays: Drug susceptibility was measured using a minimum inhibitory concentration (MIC) assay as described [45]. Briefly, strains were diluted to an OD_{600} of 0.001 and tested in technical duplicate in serial dilutions of the following antibiotics: erythromycin (GoldBio), clarithromycin (GoldBio), puromycin (GoldBio), clindamycin (GoldBio), chloramphenicol (Sigma Aldrich), isoniazid (Sigma Aldrich), ethambutol (Sigma Aldrich), kanamycin (IBI Scientific), fusidic acid (Sigma Aldrich), linezolid (Sigma Aldrich), and capreomycin (Sigma Aldrich). Lysine tRNA inhibitors were synthesized at the University of Dundee (in preparation) and dissolved in DMSO. When needed (ex. for *pth* knockdown and empty guide RNA controls), strains were pre-induced with aTC as described above. Each MIC assay was conducted in biological triplicates, with each biological replicate conducted in technical duplicate. In plates containing CRISPRi induced cells, aTC was added to each well at a final concentration of 100ng/mL. Here, a technical replicate is considered a single row of drug and bacterial incubation, using bacteria from the same culture. Biological replicates are considered plates set up in the same way using bacteria from a different culture. 96-well plates were agitated at 37°C for 6 days, at which point 0.0002% resazurin was added and plates were agitated at 37°C for an additional 48 hours. Plates were read on a BioTek plate reader at both 24 hours and 48 hours. Resazurin was measured by OD_{570}, and OD_{600} was also measured for each well. Fluorescence was normalized to OD_{600} and to the positive control for each strain (no drug; in CRISPRi induced wells, the positive control still contained aTC), and the fraction of bacteria surviving relative to the no-drug control well was plotted against drug concentration for each well.

Proteomics

Peptide labeling/TMT mass tagging**:** TMT Label Reagents were equilibrated to room temperature prior to use. Anhydrous acetonitrile or ethanol was added to each sample tube and reagent was dissolved for 5 minutes with occasional vortexing. 41uL of TMT Label Reagent were added to each sample (100-200ug provided) and incubated for 1 hour at room temperature. 8uL of 5% hydroxylamine were added to each sample and incubated for 15 minutes to quench each reaction. Equal amounts of samples were pooled and fractionated into 40 fractions for liquid chromatography/mass spectrometry (LC-MS/MS).

Mass spectrometry**:** LC-MS/MS was performed on an Orbitrap Lumos (ThermoFisher, San Jose, CA) equipped with dual pump Ultimate 3000 nanoLC (ThermoFisher, San Jose, CA). Peptides were separated onto a 100μm inner diameter microcapillary trapping column packed with ~5 cm of C18 Reprosil resin (5 μm, 100 Å, Dr. Maisch GmbH, Germany) and an analytical column uPAC Column 50cm by PharmaFluidics (ESI Source Solutions). A separation gradient was created ranging from 5 – 27% ACN in 0.1% formic acid over 90 min at 200 nl min−1. Electrospray ionization was accomplished at a voltage of 1.8 kV using an electrode junction at the end of the microcapillary column and sprayed from fused silica pico tips (New Objective, MA). The LTQ Orbitrap Lumos was operated in a data-dependent mode for mass spectrometry. A mass spectrometry survey scan was performed in the Orbitrap in a range of 395–1,800 m/z at a resolution of 6 × 104, followed by the selection of the 30 most intense ions (TOP30) for CID-MS2 fragmentation in the Ion trap using a precursor isolation width window of 2 m/z, AGC setting of 10,000, and a maximum ion accumulation of 200ms. Singly charged ion species were not subjected to CID fragmentation. Normalized collision energy was set to 35 V and an activation time of 10ms. Ions in a 10ppm m/z window around ions selected for MS2 were excluded from further selection for fragmentation for 60s.

Mass spectrometry**:** Raw data were submitted for analysis in Proteome Discoverer 2.4 (Thermo Scientific). Assignment of MS/MS spectra was performed using the Sequest HT algorithm by searching the data against a protein sequence database including known contaminants such as human keratins and common lab contaminants. Sequest HT searches were performed using a 20ppm precursor ion tolerance and requiring each peptides N-/C termini to adhere with Trypsin protease specificity, while allowing up to two missed cleavages. A MS2 spectra assignment false discovery rate (FDR) of 1% on both protein and peptide level was achieved by applying the target-decoy database search. Filtering was performed using a Percolator. Peptide N termini and lysine residues (+229.162932 Da) were set as static modifications while methionine oxidation (+15.99492 Da) was set as variable modification. A MS2 spectra assignment false discovery rate (FDR) of 1% on both protein and peptide level was achieved by applying the target-decoy database search. Filtering was performed using a Percolator. For quantification, a 0.02 m/z window centered on the theoretical m/z value of each the six reporter ions and the intensity of the signal closest to the theoretical m/z value was recorded. Reporter ion intensities were exported in Proteome Discoverer 2.4 search engine.

Analysis of proteomics data: 1,824 unique *Mtb* proteins were identified through quantitative TMT proteomics (above). A stringent threshold was set to include only proteins whose average abundance in the uninduced control samples surpassed 5,000a.u. 621 proteins passed this threshold (Table A3.2). Proteins with a p-value (unpaired Student's t-test) lower than 0.05 and a $\log_2$-fold change over 0.3 were considered differentially abundant.

References

1. Keiler, K.C., *Mechanisms of ribosome rescue in bacteria.* Nat Rev Microbiol, 2015. **13**(5): p. 285-97.
2. Feaga, H.A., P.H. Viollier, and K.C. Keiler, *Release of nonstop ribosomes is essential.* mBio, 2014. **5**(6): p. e01916.
3. Tanner, D.R., et al., *Genetic identification of nascent peptides that induce ribosome stalling.* J Biol Chem, 2009. **284**(50): p. 34809-18.
4. Keiler, K.C. and H.A. Feaga, *Resolving nonstop translation complexes is a matter of life or death.* J Bacteriol, 2014. **196**(12): p. 2123-30.
5. Muller, C., C. Crowe-McAuliffe, and D.N. Wilson, *Ribosome Rescue Pathways in Bacteria.* Front Microbiol, 2021. **12**: p. 652980.
6. Keiler, K.C., P.R. Waller, and R.T. Sauer, *Role of a peptide tagging system in degradation of proteins synthesized from damaged messenger RNA.* Science, 1996. **271**(5251): p. 990-3.
7. Dulebohn, D., et al., *Trans-translation: the tmRNA-mediated surveillance mechanism for ribosome rescue, directed protein degradation, and nonstop mRNA decay.* Biochemistry, 2007. **46**(16): p. 4681-93.
8. Giudice, E. and R. Gillet, *The task force that rescues stalled ribosomes in bacteria.* Trends Biochem Sci, 2013. **38**(8): p. 403-11.
9. Karzai, A.W., M.M. Susskind, and R.T. Sauer, *SmpB, a unique RNA-binding protein essential for the peptide-tagging activity of SsrA (tmRNA).* EMBO J, 1999. **18**(13): p. 3793-9.
10. Choy, J.S., L.L. Aung, and A.W. Karzai, *Lon protease degrades transfer-messenger RNA-tagged proteins.* J Bacteriol, 2007. **189**(18): p. 6564-71.
11. Ramadoss, N.S., et al., *Small molecule inhibitors of trans-translation have broad-spectrum antibiotic activity.* Proc Natl Acad Sci U S A, 2013. **110**(25): p. 10282-7.
12. Vivanco-Dominguez, S., et al., *Protein synthesis factors (RF1, RF2, RF3, RRF, and tmRNA) and peptidyl-tRNA hydrolase rescue stalled ribosomes at sense codons.* J Mol Biol, 2012. **417**(5): p. 425-39.
13. Rao, A.R. and U. Varshney, *Specific interaction between the ribosome recycling factor and the elongation factor G from Mycobacterium tuberculosis mediates peptidyl-tRNA release and ribosome recycling in Escherichia coli.* EMBO J, 2001. **20**(11): p. 2977-86.
14. Kabra, A., et al., *Unraveling the stereochemical and dynamic aspects of the catalytic site of bacterial peptidyl-tRNA hydrolase.* RNA, 2017. **23**(2): p. 202-216.
15. Sharma, S., et al., *Structural and functional insights into peptidyl-tRNA hydrolase.* Biochim Biophys Acta, 2014. **1844**(7): p. 1279-88.
16. Ito, K., et al., *Structural basis for the substrate recognition and catalysis of peptidyl-tRNA hydrolase.* Nucleic Acids Res, 2012. **40**(20): p. 10521-31.
17. Shiloach, J., Y. Lapidot, and N. de Groot, *The specificity of peptidyl-tRNA hydrolase from E. coli.* FEBS Lett, 1975. **57**(2): p. 130-3.
18. De Groot, N., Y. Groner, and Y. Lapidot, *Peptidyl-tRNA. VII. Substrate specificity of peptidyl-tRNA hydrolase.* Biochim Biophys Acta, 1969. **186**(2): p. 286-96.
19. Sorensen, M.A., A.O. Fehler, and S. Lo Svenningsen, *Transfer RNA instability as a stress response in Escherichia coli: Rapid dynamics of the tRNA pool as a function of demand.* RNA Biol, 2018. **15**(4-5): p. 586-593.
20. W.H.O., *Global tuberculosis report 2021.* 2021.
21. Personne, Y. and T. Parish, *Mycobacterium tuberculosis possesses an unusual tmRNA rescue system.* Tuberculosis (Edinb), 2014. **94**(1): p. 34-42.
22. Alumasa, J.N., et al., *Ribosome Rescue Inhibitors Kill Actively Growing and Nonreplicating Persister Mycobacterium tuberculosis Cells.* ACS Infect Dis, 2017. **3**(9): p. 634-644.

23. Evans, M.E., et al., *Determination of tRNA aminoacylation levels by high-throughput sequencing.* Nucleic Acids Res, 2017. **45**(14): p. e133.
24. DeJesus, M.A., et al., *Comprehensive Essentiality Analysis of the Mycobacterium tuberculosis Genome via Saturating Transposon Mutagenesis.* mBio, 2017. **8**(1).
25. Jinich A, Z.A., DeJesus MA, Flores-Bautista E, Smith CM, Sassetti FCM, Rock CJM, Ehrt S, Schnappinger D, Ioerger GTR, Rhee K, *The Mycobacterium tuberculosis transposon sequencing database (MtbTnDB): a large-scale guide to genetic conditional essentiality.* bioRxiv (preprint), 2021.
26. Kim, J.H., et al., *Protein inactivation in mycobacteria by controlled proteolysis and its application to deplete the beta subunit of RNA polymerase.* Nucleic Acids Res, 2011. **39**(6): p. 2210-20.
27. Rock, J.M., et al., *Programmable transcriptional repression in mycobacteria using an orthogonal CRISPR interference platform.* Nat Microbiol, 2017. **2**: p. 16274.
28. Tomasi, F.G., et al., *A tRNA-Acetylating Toxin and Detoxifying Enzyme in Mycobacterium tuberculosis.* Microbiol Spectr, 2022: p. e0058022.
29. Janssen, B.D., E.J. Diner, and C.S. Hayes, *Analysis of aminoacyl- and peptidyl-tRNAs by gel electrophoresis.* Methods Mol Biol, 2012. **905**: p. 291-309.
30. Cheverton, A.M., et al., *A Salmonella Toxin Promotes Persister Formation through Acetylation of tRNA.* Mol Cell, 2016. **63**(1): p. 86-96.
31. Rycroft, J.A., et al., *Activity of acetyltransferase toxins involved in Salmonella persister formation during macrophage infection.* Nat Commun, 2018. **9**(1): p. 1993.
32. Kimura, S., P.C. Dedon, and M.K. Waldor, *Comparative tRNA sequencing and RNA mass spectrometry for surveying tRNA modifications.* Nat Chem Biol, 2020. **16**(9): p. 964-972.
33. Shepherd, J. and M. Ibba, *Bacterial transfer RNAs.* FEMS Microbiol Rev, 2015. **39**(3): p. 280-300.
34. Schofield, P. and P.C. Zamecnik, *Cupric ion catalysis in hydrolysis of aminoacyl-tRNA.* Biochim Biophys Acta, 1968. **155**(2): p. 410-6.
35. Mohammad, F., R. Green, and A.R. Buskirk, *A systematically-revised ribosome profiling method for bacteria reveals pauses at single-codon resolution.* Elife, 2019. **8**.
36. Avcilar-Kucukgoze, I., et al., *Discharging tRNAs: a tug of war between translation and detoxification in Escherichia coli.* Nucleic Acids Res, 2016. **44**(17): p. 8324-34.
37. Kossel, H., *Purification and properties of peptidyl-tRNA hydrolase from Escherichia coli.* Biochim Biophys Acta, 1970. **204**(1): p. 191-202.
38. Menninger, J.R. and R.A. Coleman, *Lincosamide antibiotics stimulate dissociation of peptidyl-tRNA from ribosomes.* Antimicrob Agents Chemother, 1993. **37**(9): p. 2027-9.
39. Beckert, B., et al., *Structural and mechanistic basis for translation inhibition by macrolide and ketolide antibiotics.* Nat Commun, 2021. **12**(1): p. 4466.
40. Vazquez-Laslop, N. and A.S. Mankin, *How Macrolide Antibiotics Work.* Trends Biochem Sci, 2018. **43**(9): p. 668-684.
41. Choi, G.E., et al., *Macrolide treatment for Mycobacterium abscessus and Mycobacterium massiliense infection and inducible resistance.* Am J Respir Crit Care Med, 2012. **186**(9): p. 917-25.
42. Choi, H., et al., *Treatment outcomes of macrolide-susceptible Mycobacterium abscessus lung disease.* Diagn Microbiol Infect Dis, 2018. **90**(4): p. 293-295.
43. Choi, H., et al., *Clinical Characteristics and Treatment Outcomes of Patients with Acquired Macrolide-Resistant Mycobacterium abscessus Lung Disease.* Antimicrob Agents Chemother, 2017. **61**(10).
44. Aviner, R., *The science of puromycin: From studies of ribosome function to applications in biotechnology.* Comput Struct Biotechnol J, 2020. **18**: p. 1074-1083.
45. Fishbein, S.R.S., et al., *The conserved translation factor LepA is required for optimal synthesis of a porin family in Mycobacterium smegmatis.* J Bacteriol, 2020.

46. Pavlov, M.Y., et al., *Slow peptide bond formation by proline and other N-alkylamino acids in translation.* Proc Natl Acad Sci U S A, 2009. **106**(1): p. 50-4.
47. Chadani, Y., et al., *Intrinsic Ribosome Destabilization Underlies Translation and Provides an Organism with a Strategy of Environmental Sensing.* Mol Cell, 2017. **68**(3): p. 528-539 e5.
48. Cole, S.T., et al., *Deciphering the biology of Mycobacterium tuberculosis from the complete genome sequence.* Nature, 1998. **393**(6685): p. 537-44.
49. Fishbein, S., et al., *Phylogeny to function: PE/PPE protein evolution and impact on Mycobacterium tuberculosis pathogenicity.* Mol Microbiol, 2015. **96**(5): p. 901-16.
50. Heurgue-Hamard, V., et al., *The growth defect in Escherichia coli deficient in peptidyl-tRNA hydrolase is due to starvation for Lys-tRNA(Lys).* EMBO J, 1996. **15**(11): p. 2826-33.
51. Vivanco-Dominguez, S., L.R. Cruz-Vera, and G. Guarneros, *Excess of charged tRNALys maintains low levels of peptidyl-tRNA hydrolase in pth(Ts) mutants at a non-permissive temperature.* Nucleic Acids Res, 2006. **34**(5): p. 1564-70.
52. Bosch, B., et al., *Genome-wide gene expression tuning reveals diverse vulnerabilities of M. tuberculosis.* Cell, 2021. **184**(17): p. 4579-4592 e24.
53. Rock, J., *Tuberculosis drug discovery in the CRISPR era.* PLoS Pathog, 2019. **15**(9): p. e1007975.
54. Scott, D.E., et al., *A fragment-based approach to probing adenosine recognition sites by using dynamic combinatorial chemistry.* Chembiochem, 2009. **10**(17): p. 2772-9.
55. Buriankova, K., et al., *Molecular basis of intrinsic macrolide resistance in the Mycobacterium tuberculosis complex.* Antimicrob Agents Chemother, 2004. **48**(1): p. 143-50.
56. Nash, K.A., et al., *Molecular basis of intrinsic macrolide resistance in clinical isolates of Mycobacterium fortuitum.* J Antimicrob Chemother, 2005. **55**(2): p. 170-7.
57. Li, S., et al., *CRISPRi chemical genetics and comparative genomics identify genes mediating drug potency in Mycobacterium tuberculosis.* Nat Microbiol, 2022. **7**(6): p. 766-779.
58. Madsen, C.T., et al., *Methyltransferase Erm(37) slips on rRNA to confer atypical resistance in Mycobacterium tuberculosis.* J Biol Chem, 2005. **280**(47): p. 38942-7.
59. Kimura, S. and M.K. Waldor, *The RNA degradosome promotes tRNA quality control through clearance of hypomodified tRNA.* Proc Natl Acad Sci U S A, 2019. **116**(4): p. 1394-1403.
60. Kapopoulou, A., J.M. Lew, and S.T. Cole, *The MycoBrowser portal: a comprehensive and manually annotated resource for mycobacterial genomes.* Tuberculosis (Edinb), 2011. **91**(1): p. 8-13.

Chapter Four: Discussion, ongoing work, and future directions

Understanding a protein's essential role in cells

In Chapter Two, we found that in addition to peptidyl tRNA, N-acetylated aminoacyl tRNA is a natural substrate for Pth in *Mtb*. We showed that an *Mtb*-encoded toxin, TacT, blocks protein synthesis by acetylating glycyl-tRNA. This N-blocked tRNA cannot be added to a growing peptide, thus depleting glycyl-tRNA pools and inhibiting protein synthesis. Pth reverses the effects of TacT by hydrolyzing N-glycine to free up the tRNA molecule. We assessed the effects of TacT activity on *pth* essentiality by performing transcriptional repression of *pth* in both a wild-type *Mtb* strain and a *tacAT* knockout, *Mtb*Δ*tacAT*. In the laboratory growth conditions tested, we did not find altered growth or survival following Pth depletion in either strain. Our findings suggest that even though *Mtb* encodes a functional TacT toxin, this enzyme is not active during normal growth and does not contribute significantly to Pth essentiality.

We had several motivations for performing this work. The first was therapeutic: if Pth is required for *Mtb* growth because of TacT activity in cells, then a Pth inhibitor would be a poor choice for drug development. This is because of additional findings we described in Chapter Two. The essentiality of a gene is correlated with its level of tolerance for nonsynonymous mutations [1]. We found that the TacAT operon in *Mtb* is dispensable *in vitro*, and clinical genomic data support that this operon is also dispensable *in vivo*, given many nonsynonymous mutations – including premature stop codons – that have accumulated in clinical isolates. If TacAT mediated *pth* essentiality in *Mtb,* drugs targeting Pth would likely see rapid genetic resistance by a rise in similar mutations inactivating TacAT. Our findings from Chapter Two confirm that during normal growth, Pth is required to cleave peptidyl tRNA that is prematurely released from stalled ribosomes. The biological implications of this are discussed in Chapter Three and summarized in subsequent sections of this chapter.

A TacTful approach to studying toxin-antitoxin (TA) systems

TacT is part of a toxin-antitoxin (TA) system: its cognate antitoxin TacA binds to TacT and sequesters it from activity. Degradation of TacA leads to rapid activation of TacT. TA systems are widespread in bacteria and have been proposed as intriguing mechanisms of stress adaptation. This is because they are fast-acting and reversible. Indeed, TA systems were initially discovered as plasmid maintenance factors: post-segregational killing of plasmid-free cells ensured the survival only of cells encoding both a toxin and an antitoxin [2]. Over time, multiple other roles were proposed for dozens of different TA systems including virulence and pathogenicity, bacterial stress response, phage defense or proliferation, and biofilm production [2].

TA systems are especially abundant in *Mtb* compared to other bacteria, yet plasmids are absent in this organism, and phage infection is uncommon [3]. As discussed in Chapter Two, it is tempting to speculate that *Mtb*'s expansive TA system toolkit serves as a growth regulator during infection. However experimental evidence for this is lacking, largely due to the difficulties of systematically deleting many genes simultaneously in *Mtb* and overlapping mechanisms of action that make it difficult to directly measure the activity of individual toxins. Some studies have examined the roles of individual TA systems in *Mtb* using genetic deletions, overexpression systems, and transcriptional analyses and linked activity of some toxins to pathogenesis [4-6]. It is important to note that overexpression systems typically result in substantially higher expression of a gene of interest than wild type levels [2], and can therefore inflate the physiological effects of an individual gene. Furthermore, simply identifying transcriptional changes in TA system expression does not necessarily correlate to increased toxin activity, as indicated by recent studies that shed light on this phenomenon [7].

Our studies of TacAT in Chapter Two involve two unique approaches that we believe should be adopted in future studies of TA systems. First, we measured toxin activity in its native form using liquid chromatography-coupled mass spectrometry (LCMS). Though we were unable to detect N-

acetylated glycyl tRNA *in vitro* during normal growth, it is still possible that TacT becomes active during infection: applying $CuSO_4$-tRNAseq described in Chapter Three would be a rapid way to survey tRNA pools in host-relevant conditions. Follow-up by Northern blot or LCMS (or deletion of the toxin-encoding gene) would confirm whether changes are specifically due to N-acetylated glycyl tRNA. Applications of this technique can be used across bacterial species to measure the native activity of tRNA acetylating toxins, to determine conditions under which these toxins may be activated.

TacT is a unique toxin, given its defined substrate and the numerous tools available to study it. Most other TA systems are broad-acting RNases. However, we envision the development of additional tRNA or mRNA sequencing-based tools to study the effects of RNA endonuclease toxins by looking at RNA truncation or stability in different growth conditions. Similar approaches have already been developed using RNA sequencing in *E. coli* [8]. From a tRNA perspective, several tRNA-targeting *Mtb* toxins have been identified in addition to TacT. For instance, a family of nucleotidyltransferase toxins called MenT ($MenT_{1-4}$) was recently discovered in *Mtb* [9]. Active MenT blocks protein synthesis by adding pyrimidines to the 3'-CCA tail of uncharged tRNA, making them unable to be aminoacylated. One toxin, $MenT_3$, had preferential activity against serine-tRNA. The physiological role of MenT toxins has not been described, but tRNA sequencing could be used to assess whether any tRNAs under specific growth conditions have extra pyrimidines on their 3' ends.

The second unique approach we took when studying TacAT in *Mtb* was to leverage genomic datasets from clinical samples. If a TA system is found to be activate in certain laboratory growth conditions, the significance of this TA system still needs to be contextualized in human infection. *Mtb* encodes over 100 TA systems: we cannot, with the current tools available to us, feasibly knock out or knock down all of them and test mutants *in vivo*. However, whole genome sequencing of clinical isolates offers a glimpse into the selective pressure different genes face in the real world. We found in Chapter Two that TacAT is not significant in *Mtb* pathogenesis; performing similar analyses on other

TA systems could help narrow down a panel of TA systems that might be important for *Mtb* infection. Follow-on genetic and biochemical analysis of these systems would shed insight on the true physiological roles of TA systems in this complex pathogen.

"tRNAround, bright eyes (every now and then I fall apart)" – ribosomes

In Chapter Three, we learned about peptidyl tRNA drop-off in *Mtb* by studying the effects of knocking down peptidyl tRNA hydrolase (Pth) in cells. We developed a new application of tRNA sequencing, $CuSO_4$-tRNAseq and found that this phenomenon – premature release of peptidyl tRNA from a stalled ribosome – occurs frequently during normal growth. In fact, peptidyl tRNA was detected on virtually all tRNA species in *Mtb*, concurrent to a decrease in aminoacyl tRNA, and we showed that Pth plays a role in maintaining pools of most tRNAs. Interestingly, peptidyl prolyl-tRNA was by far the most abundant substrate for Pth in *Mtb*. Proline's transpeptidation dynamics are less efficient compared to other amino acids, owing to the alkyl group in proline being directly on the nitrogen used as a nucleophile during peptide bond formation [10]. As discussed in Chapter Three, this offers a biochemical explanation for increased peptidyl tRNA drop-off during transpeptidation reactions involving proline.

Mycobacteria are a highly GC-rich genus, and pathogenic mycobacteria are enriched for so-called PE/PPE proteins, outer membrane proteins characterized by their proline-rich N-terminal sequences that make up nearly 10% of the *Mtb* genome [11, 12]. As discussed in Chapter Three, it is tempting to speculate that Pth has a more specific physiological role in *Mtb* that is related to the efficient synthesis of PE/PPE and a heightened demand for proline-tRNA. In fact, the most depleted protein in a Pth knockdown was a PE/PPE protein. Beyond PPE18, however, we did not find a pattern between amino acid sequence and protein abundance, suggesting that Pth depletion (and the reduction of available aminoacyl tRNA) causes a rapid, broader effect on cells' ability to synthesize

proteins. However, as discussed in Chapter Three, there are some limitations to the approach we used for extracting lysate that may have affected our findings. Future work that studies the membrane proteome specifically could identify any effects we may have missed of Pth depletion on the synthesis of PE/PPE proteins. For instance, does the reduced availability of aminoacyl prolyl-tRNA lead to an immediate depletion in other PE/PPE proteins, followed by more global protein synthesis arrest?

Several lingering questions concern the regulation of tRNA dynamics in *Mtb*. Our work suggests that tRNA turnover in *Mtb* is modulated both by tRNA recycling (such as by Pth after ribosome stalling and re-charging by aminoacyl tRNA synthetases after normal translation), and *de novo* synthesis. Understanding the relative contribution of each mode would shed light on how tRNA turnover is broadly regulated in this organism to meet the demand for specific amino acids. In the case of proline tRNA, for instance, our data suggest that Pth-mediated recycling plays a disproportionate role in proline-tRNA dynamics relative to other tRNAs.

What signal(s) upon Pth depletion triggers growth arrest? Based on our findings, we hypothesize that the loss of usable aminoacyl tRNA is a trigger for protein synthesis arrest. Inhibiting translation in this situation is important to prevent the aberrant translation of proteins, which could be lethal. tRNA turnover is tightly regulated, but it has not been studied in *Mtb*. In *E. coli,* tRNA pools are regulated at the transcriptional (synthesis) level and post-transcriptionally via degradation [13, 14]. Studies have found that the fraction of RNA polymerases that transcribe both tRNA and ribosomal RNA (rRNA) in *E. coli* drops from ~80% during logarithmic growth to ~25% upon amino acid starvation [15]. In the case of amino acid starvation, uncharged tRNA at the A-site of the ribosome signals RelA to produce the alarmone ppGpp, which induces the stringent response [16]. In the case of Pth depletion in *Mtb*, however, we did not observe increases in uncharged tRNA pools. Instead, we observed the opposite: an increase in the proportion of tRNAs charged with more than one amino acid (peptidyl tRNA). We also did not observe significant degradation of tRNA. Therefore, we

speculate that a different pathway may be responsible for triggering growth arrest in the presence of increased peptidyl tRNA pools that sequester charged tRNA. Ongoing work to address this question involves sequencing of total RNA samples extracted from Pth depleted strains to study differential gene expression relative to an uninduced control. We hypothesize that genes involved in tRNA turnover and growth arrest will be differentially regulated in a Pth knockdown.

Synergy-based drug discovery and future directions for Pth

Our work provides a concrete example of applying complementary genetic tools with chemical screens to enhance tuberculosis drug discovery. *Mtb* is intrinsically resistant to most existing antibiotics, making it difficult to find effective and well-tolerated drugs to treat cases. Macrolides are used to treat a variety of clinical pathogens but are ineffective against TB. Sensitizing *Mtb* to macrolides by simultaneously targeting Pth as described in Chapter Three offers a new strategy to lend new efficacy to an entire class of existing antibiotics. As discussed in Chapter Three, additional genetic screens identifying modulators of macrolide susceptibility in *Mtb* have shed light on other proteins whose depletion can add to macrolide sensitivity, opening even more doors for refurbishing macrolides in the fight against TB [17].

Lysine tRNA synthetase (KRS) inhibitors are currently being developed against *Mtb*. From a research standpoint, these compounds were a great tool to validate the effects of Pth on tRNA abundance. Since Pth depletion potentiated the effects of KRS inhibitors *in vitro*, we were able to confirm that Pth mediates tRNA dynamics and that orthogonally targeting tRNA turnover is a viable anti-TB strategy. It is possible that other aminoacyl tRNA synthetase (aaRS) inhibitors would be even more effective, given Pth's smaller effects on lysine tRNA pools compared to other species like proline or glutamate (Figure 3.4). In the absence of existing inhibitors against these aaRS, CRISPRi could be adapted to screen genetically for Pth-aaRS synergy, to identify the most effective putative drug

combination. Combinatorial genetic screens are powerful in the absence of existing inhibitors, as they provide insight on interactions between drug targets and information on the degree of inhibition a drug would need to attain to have therapeutic effects.

What is next for a Pth inhibitor?

We do not currently have a working inhibitor against *Mtb* Pth, though some natural products have been described with anti-Pth activity [18, 19]. One of the biggest challenges for screening candidate molecules for anti-Pth activity has been the development of a simple, scalable assay to measure Pth activity and in turn, its inhibition by a candidate molecule. The *in vitro* protein synthesis assay described in Chapter Two offers a potential solution. Since Pth rescues TacT activity *in vitro*, supplementing this system with Pth inhibitors and measuring translation readout in high throughput using a plate reader (e.g., through synthesis of a fluorescent molecule like GFP; Figure 2.3B) could be one potential strategy.

From a drug development perspective, it is also important to consider off-target effects of Pth inhibitors. Pth is ubiquitous in bacteria, and three critical active site residues His22, Asp95 and Asn116 are universally conserved [20]. Archaea encode a conserved functional homolog, *pth2*, which does not share sequence similarity to bacterial *pth* [20]. Most eukaryotic genomes – including human – encode both *pth* and *pth2* genes, though these enzymes are nonessential, suggesting that a bacterial Pth inhibitor would have minimal negative off-target effects on patients [20]. Furthermore, structural studies have found that mycobacterial Pth is structurally divergent from other bacterial Pth, providing additional insight for the design of *Mtb* Pth-specific inhibitors [21, 22].

It will also be important to test Pth essentiality, Pth-macrolide synergy, and Pth-KRS synergy *in vivo*. Ongoing experiments include infecting mice with *Mtb* CRISPRi libraries, including several Pth

CRISPRi knockdowns of varying strength. We eagerly await the results of these experiments as crucial steps in the Pth drug discovery process.

tRNA sequencing: opening doors for tRNA research in *Mtb*

tRNA is very intricate. In addition to its essential function as the adaptor between mRNA and protein, tRNA can act as a signaling molecule, contribute to peptidoglycan formation at the cell wall in bacteria, and modulate the translation of different transcripts [23]. These functions are all accomplished thanks to tRNA's ability to interact with highly diverse structures and enzymes including ribosomes, mRNA, aminoacyl-tRNA synthetases, tRNA modification enzymes, and elongation factors. tRNA's complex and conserved tertiary structure enables this breadth of activity and specificity, and its structure is reinforced with many chemical modifications [23, 24]. The secondary structure of tRNA is shown in Figure 4.1 for simplification.

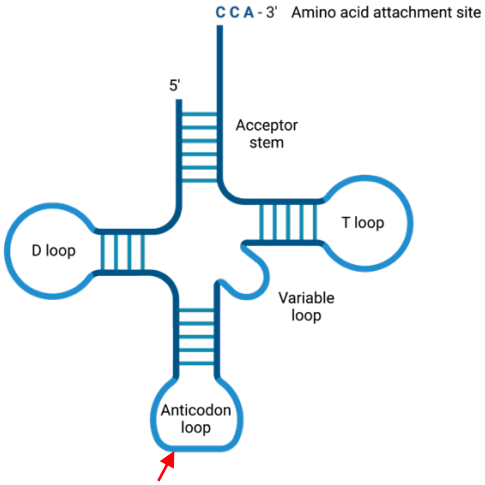

Figure 4.1. Secondary structure of tRNA. tRNA is made up of approximately 76 nucleotides. The acceptor stem is 7-9 nucleotides long. The 3' end of the molecule is the site of amino acid attachment, where aminoacyl tRNA synthetases covalently bond an amino acid to the 3'-OH group on the terminal CCA. The D loop is 4-6 nucleotides long. The anticodon loop contains 5 nucleotides; the 3 nucleotides at the loop contain the anticodon sequence, which is in reverse order of the codon read on mRNA given 3' to 5' directionality when reading mRNA 5' to 3. The first anticodon base (position 34) is called the wobble position (red arrow) and can be modified into nucleotide derivates (ex. adenine to inosine). The T arm is 4-5 nucleotides. Each tRNA loop has chemically modified nucleotides such as methylation and thiolation. tRNA modifications are heavily studied in all domains of life and contribute to the structural and functional integrity of tRNA. Figure created with BioRender.com.

Chemical modifications of tRNA play specific roles in protein recognition, mRNA decoding efficiency, tRNA quality control, and structural stability. For example, modifications at the wobble position in the anticodon loop (Figure 4.1) can expand or restrict the decoding capacity of a specific tRNA. Each tRNA modification is carried out by a specific enzyme, adding to an already large repertoire of cellular factors that interact with tRNA. Advances in mass spectrometry have enabled the identification, localization, and characterization of tRNA modifications in many organisms [24-29]. Within the field of mycobacteriology, extensive research has been conducted to characterize the roles of different tRNA modifications on mycobacterial stress responses, codon bias during adaptation to specific environments, and persistence [30, 31].

Until recently, it was difficult to sequence tRNA molecules because their extensive modifications and stable structure interfere with cDNA synthesis. The discovery and use of a highly processive thermostable group II intron reverse transcriptase allowed researchers to largely overcome this technical challenge, and in 2015 tRNA sequencing was developed as a complement for mass spectrometry [32]. tRNA sequencing allows for the rapid and systematic identification of tRNA modification sites by looking at reverse transcription-derived signatures such as misincorporation and early termination, both of which are likely to happen more frequently at heavily modified sites [32]. Briefly, chemical modifications on tRNA nucleotides disrupt Watson-Crick base pairing and thus increase the frequency of incorporating the wrong nucleotide during reverse transcription. Similarly, modifications can also block reverse transcriptase from being able to interact with template RNA, causing the enzyme to fall off and cause early cDNA synthesis termination at higher rates.

Once these sites are identified and correlated to a specific position on the tRNA molecule, they can be validated by mass spectrometry [26]. Another way to validate predicted modification sites includes genetically knocking out the enzyme responsible for that modification and using tRNA

sequencing to show that the modification signature disappears in a mutant. An example of this approach is described below.

First tRNA sequencing experiment in *Mtb*

At the time of writing this dissertation, tRNA sequencing in *Mtb* has not yet been published. When we were developing $CuSO_4$-tRNAseq described in Chapter Three, we adapted a protocol used on *Vibrio cholerae* and had to assess whether any specific protocol changes would be needed for *Mtb* samples [26, 33]. For this run, we did not perform the chemical treatments – $CuSO_4$, $NaIO_4$, and β-elimination – that we incorporated into CuSO4-tRNAseq, but instead performed a single deacylation reaction on total RNA to free up the 3' end of tRNA for adapter ligation [32]. Fortunately, as discussed in the next section, the entire workflow was successful on our *Mtb* RNA samples, confirming that sequencing library preparation for tRNAseq can be adapted relatively easily across species.

Ongoing work combining tRNAseq and bacterial genetics in *Mtb*

Dataset D4.1 contains the sequencing alignments from our pilot tRNAseq experiment in *Mtb*. The data are also represented in a heatmap in Figure 4.2. While continuing with the development and application of $CuSO_4$-tRNAseq, we decided to use data from this pilot experiment to validate and characterize a putative tRNA modification in *Mtb*. During translation, codon-anticodon interactions at the ribosome A site are mediated by Watson-Crick base pairing. In some tRNAs, the third codon position can form wobble – non-standard – pairs, which allows certain tRNAs to decode multiple codons (Figure 4.1). Interestingly, when the wobble position contains a uridine (U34), this nucleotide is almost always customized by a variety of modifications, and the enzymes responsible for these modifications are universally conserved [34, 35]. While many of these enzymes can be genetically knocked out without affecting tRNA stability or aminoacylation [36], mutants in U34 modifications

are lethal in mouse embryos [37] and reduce yeast adaptability to stressful environments [38]. The actual mechanism of fitness loss is not known. We observed a termination signal corresponding to a putative U34 modification called 5-methylaminomethyl-2-thiouridinylation (mnm^5S^2U; Figure 4.2).

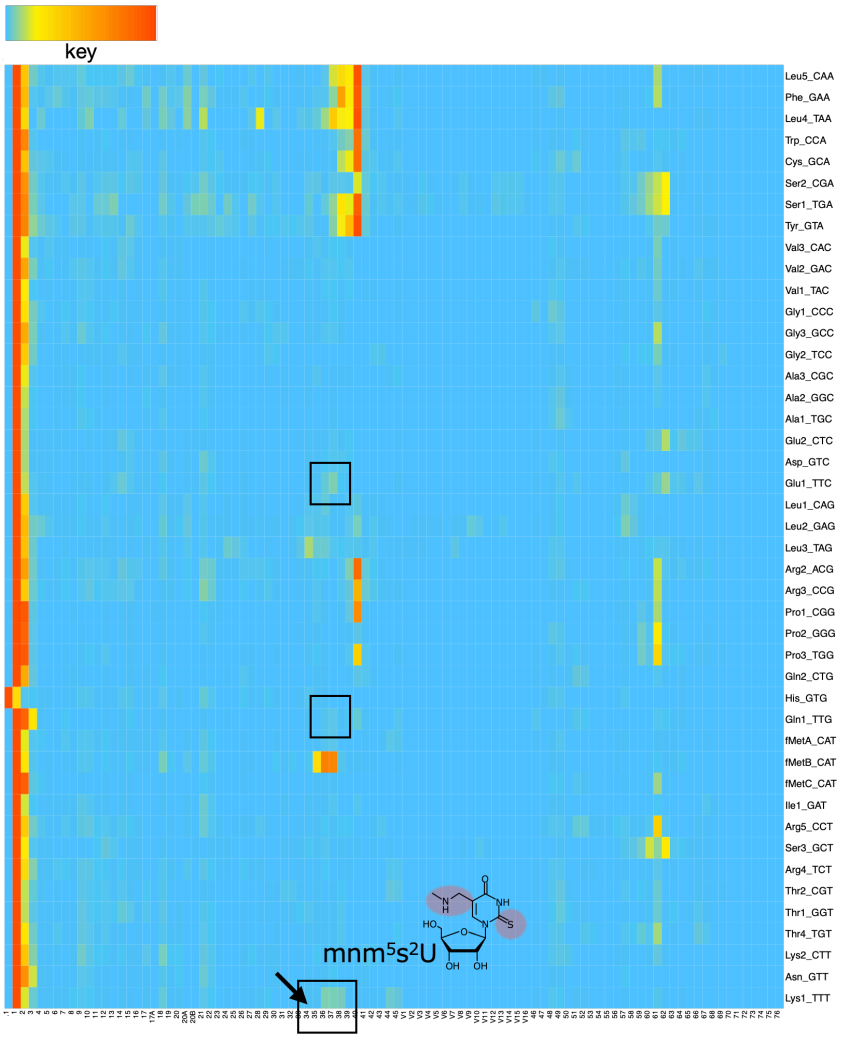

Figure 4.2. Heat map of early termination frequency from tRNA sequencing of wild type *Mtb*. tRNA library preparation, sequencing, and data analysis were performed as described in the Methods for Chapter Three. Total RNA samples were alkali-treated prior to tRNA extraction to deacylate all tRNAs (1 hour at 37C in 100mM Tris-HCl pH 9.0). For analysis of termination frequencies, 5' end termini of mapped reads were piled up using bedtools genomecov (option, -d -5 -ibam). The number of 5' termini at each tRNA position was divided by the total number of mapped termini at that position plus all upstream (5') positions. Heatmap shows termination frequencies at all positions across tRNAs. Locations of termination signals expected from 34U mnm^5S^2U are marked with black boxes, and position 34 of tRNA is indicated with a black arrow. Uridine is shown with mnm^5 (5-methylaminomethyluridine; left) and s^2U (2-thiouridine; right) modifications.

RT termination typically occurs 1-2 nucleotides upstream of the actual modification site. This U34 modification is conserved in lysine (UUU), glutamate (UUG), and glutamine (UUC) tRNA iso-acceptors; the 2-thiouridine modification is performed by a conserved enzyme called MnmA. A BLAST search of the *Mtb* genome against *E. coli* MnmA found that *Mtb* in fact encodes a homolog in the gene Rv3024c. We used double stranded DNA-based recombineering to genetically delete Rv3024c in *Mtb* to build the strain *Mtb⊥mnmA* [39]. Briefly, this method relies on the expression of che9c mycobacteriophage recombinase genes recET regulated by an inducible promoter. The addition of double-stranded DNA encoding an antibiotic resistance cassette flanked with 500bp of homologous sequence upstream and downstream of the target genes allows for the replacement of the target gene with a marker during DNA replication. After building *Mtb⊥mnmA*, we repeated tRNA sequencing (Figure 4.3).

tRNA sequencing on *Mtb⊥mnmA* showed reduced termination signals, suggesting that Rv3024c was in fact involved in the modification responsible for increased termination frequency near position 34 (Figure 4.3A). We also performed iodoacetamide-based derivatization of S^2U modifications (IAA treatment) for better quantification of termination frequency (Figure 4.3B). IAA is a thiol-reactive compound that covalently attaches carboxyamidomethyl to thiolated uridines via nucleophilic substitution [40]. IAA treatment likely increases early termination due to the alkylated products increasing blockage of reverse transcriptase during cDNA synthesis. Together, our results show that the *Mtb* gene Rv3024c encodes an MnmA-like enzyme that modifies position 34 uridines in three tRNA isoacceptors. This represents, to our knowledge, the first application of tRNA sequencing in *Mtb* to study tRNA modifications followed by genetic validation.

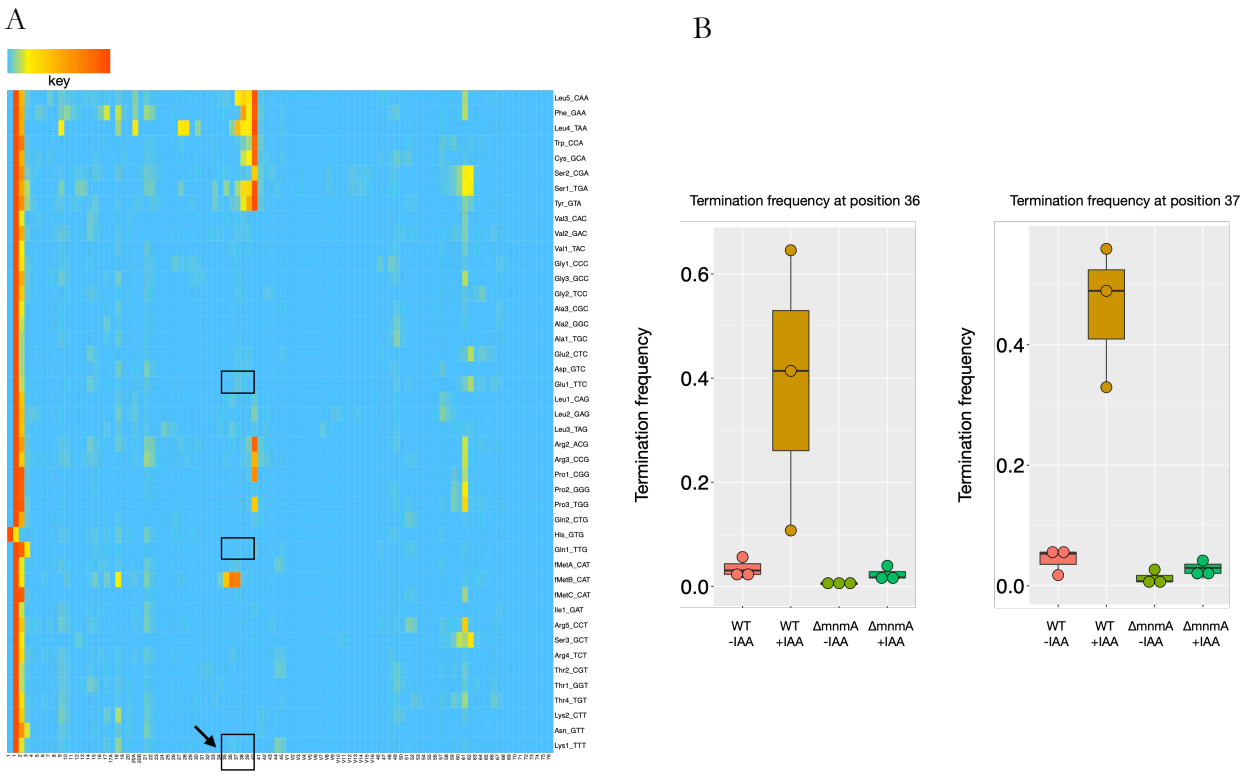

Figure 4.3. Heat map and plot of early termination frequency from tRNA sequencing of *MtbΔmnmA* with and without RNA alkylation. tRNA library preparation, sequencing, and data analysis were performed as described in Figure 4.2. (A) Heat map of early termination frequencies across tRNA molecules and positions for *Mtb⊿mnmA*. (B) Plot of termination frequencies at position 36 and position 37 in wild type (WT) *Mtb* and *Mtb⊿mnmA* for lysine_UUU, glutamate_UUG, and glutamine_UUC isoacceptors. IAA; iodoacetamide. IAA treatment was performed by combining 500ng of total RNA with 10mM of IAA, 50mM NaPO4 pH 8.0, and 50% DMSO in a final volume of 50uL. Reactions were incubated at 50C for 15 minutes and quenched with DTT.

Finally, we tested whether *Mtb⊿mnmA* was attenuated in any specific environmental conditions, since 34U hypomodified strains in other organisms have conditional growth or survival defects [41]. While we were unable to find defects in several *in vitro* media conditions tested, we found that *Mtb⊿mnmA* is significantly attenuated in a macrophage infection model (Figure 4.4). This result is consistent with published transposon-sequencing (TnSeq) experiments that found decreased survival of *mnmA* mutants during mouse infection of *Mtb* transposon libraries [42].

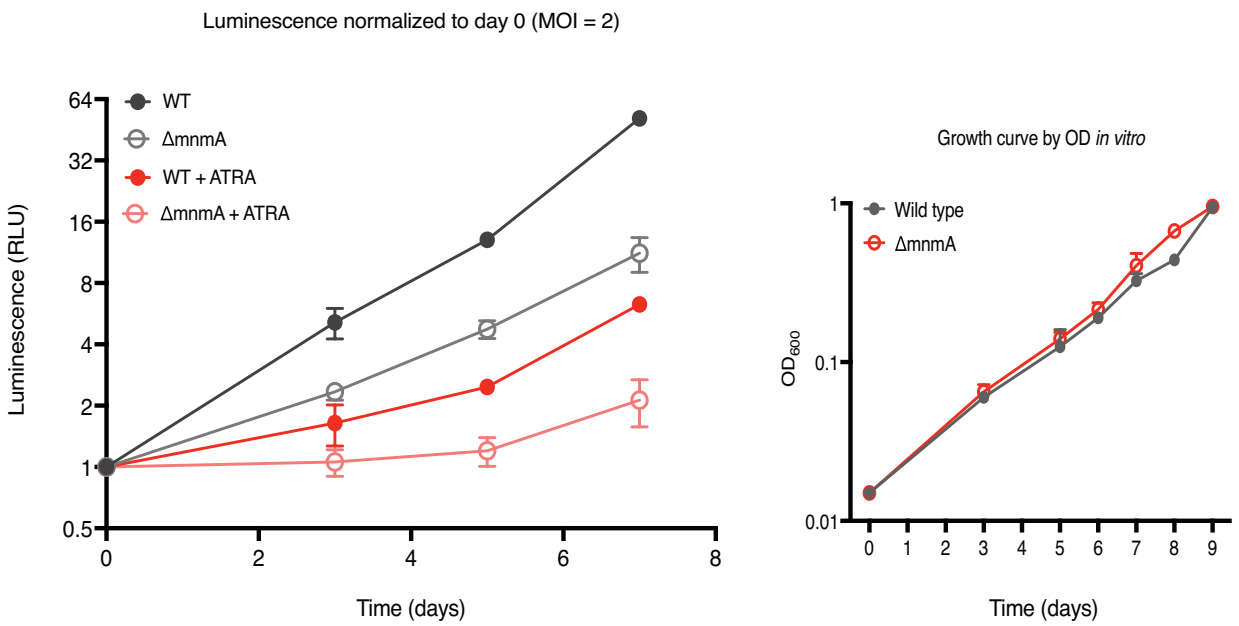

Figure 4.4. *MtbΔmnmA* is attenuated in a macrophage infection model. Left: Auto-luminescent wild type and *⊿mnmA Mtb* strains grown to the same OD_{600} were pelleted by centrifugation and prepared in RPMI media by soft spinning [43]. Briefly, cells were washed, pelleted, resuspended, and centrifuged at 121g, with the top half of the centrifuged supernatant used. Suspensions were diluted to a multiplicity of infection of 2 bacteria per mouse bone marrow-derived macrophage by determining the OD_{600}. Macrophages were infected for 6 hours, followed by a PBS wash and addition of RPMI with or without all-trans retinoic acid (ATRA). ATRA promotes macrophage control of *Mtb* infection [44] and was used to assess strain survival in an increasingly restricted macrophage environment. Survival was measured by luminescence in a BioTek plate reader and normalized to luminescence reads at time 0. Right: Wild type and *Mtb⊿mnmA* do not display differences in growth rate under normal *in vitro* growth conditions.

Our findings underscore the value of studying *Mtb* mutants in disease-relevant models such as macrophage infections, even if growth attenuation is not necessarily observed *in vitro*. They also confirm that tRNA modifications – while nonessential in normal laboratory growth conditions – play critical roles during pathogenesis. Further work understanding the mechanism underlying this infection attenuation would shed light on infection-specific requirements for protein synthesis machinery in *Mtb*. Understanding how the *Mtb* proteome is shaped during macrophage infection – from shifts in codon usage to altered tRNA stability mediated by tRNA modifications like mnm^5S^2U – will be extremely informative from a bacteriology perspective and could have downstream

therapeutic implications. Altogether, by combining tRNA sequencing and genetic tools, we have presented a streamlined genetic and analytical approach for the characterization of many other tRNA modifications predicted in our dataset.

Improving $CuSO_4$-tRNAseq

As mentioned in Chapter Three, current methods to extract RNA including centrifugation and filtration have been suggested to trigger de-acylation of serine/threonine tRNAs [45, 46]. This is probably a result of the hydroxyl group unique to these amino acids, though an exact mechanism remains to be determined. Notably, serine, threonine, and histidine tRNAs have also been reported to generally have lower charging fractions than other tRNAs (as low as <50%), especially in nutrient-rich media, which is supported by our data as well (Figure 3.4) [47]. Nonetheless, the fractions we measured might still be an underestimate though due to our RNA extraction methods. For the purposes of this work, we were still able to compare relative changes in charged fractions between samples that were prepared at the same time in multiple replicates. However, absolute total charged levels may be substantially higher than indicated by these data, since the fraction of aminoacyl tRNA is higher in all other tRNA species.

We observed the opposite issue with histidyl-tRNA, which was resistant to $CuSO_4$ treatment. Copper sulfate acts on the free N terminus of an amino acid, with the nitrogen atom donating its free electron pair [48]. The copper ion then forms a stable complex with the α-amino ester, resulting in de-acylation. Anything bound to the alpha carbon on the amino acid decreases the rate of this reaction [48]; it is therefore likely that the imidazole ring on histidine makes it resistant to copper sulfate de-acylation in the conditions we used. Future optimization of $CuSO_4$ treatment conditions, such as longer incubation, may improve catalysis. Another solution would be to replace $CuSO_4$ treatment with Pth treatment. Unfortunately, we had difficulties optimizing *in vitro* Pth treatment of purified total

RNA while conducting these studies using the *Mtb* protein. One issue included the co-precipitation of tRNA with Pth during purification (Figure A2.1), which could have unintended effects on our sequencing results. Another tougher issue included the stability of purified Pth. When we purified it for use in the cell-free protein synthesis system (Chapter Two), purified Pth lost significant catalytic activity within a day following purification. To make our tRNAseq approach more generalizable, we proceeded with method optimization using a standardized and easily prepared chemical ($CuSO_4$) despite being aware of the improvements of a Pth-based assay. Thus, future work in optimizing Pth purification, storage, and *in vitro* activity outside of a protein synthesis system would improve our ability to study peptidyl-histidyl-tRNA.

Improving the quantitative power of tRNA sequencing

Recently, a more robust method for the absolute quantification of small RNA species in bacteria (including tRNA) was published [49]. This method aims to reduce biases that are likely present in current tRNA sequencing library preparation (outlined in Figure A3.6) due to potential sequence-dependent biases in extraction, ligation, and amplification that lead to inaccurate absolute quantification of tRNA [32, 49, 50]. Absolute Quantification (AQ)-tRNAseq provides a direct correlation between read counts and molecular copy numbers for small RNAs by optimizing the steps in sequencing library preparation that typically introduce the highest amount of bias. This includes changes such as the incorporation of randomized ends on adaptors to reduce ligation bias and the use of more molecular crowding agents like polyethylene glycol (PEG) to increase enzyme efficiency [49].

While we were able to measure relative changes between specific tRNA species across samples in our work (such as differences in proline-tRNA counts with and without Pth depletion), application of AQ-tRNAseq in future work would shed light on absolute tRNA pool quantification and the dynamics of different tRNA species within samples. The method we used, while quantitative when

comparing relative amounts between samples, is not an absolute quantification of tRNA molecules, so there are limitations to the interpretation of Figure A3.2 and our ability to quantify absolute changes in tRNA abundance in *Mtb*.

Some outstanding questions that would contribute to our understanding of tRNA dynamics in *Mtb* include studying the relative abundance of different tRNAs under different growth conditions. For instance, is absolute tRNA abundance correlated to the demand for specific amino acids? How do different cellular stressors such as starvation, hypoxia, or exposure to antibiotics affect absolute tRNA levels? If there are substantial effects on tRNA for instance during infection, then the effects of targeting tRNA pools with a Pth or aminoacyl tRNA synthetase inhibitor could have even larger effects than we observed *in vitro*. Furthermore, being able to quantify absolute numbers of specific iso-acceptors and changes under different growth conditions would be helpful in studying codon bias observed in conditions such as hypoxia in *Mtb* [31].

Concluding remarks

The work contained within this thesis combines genetic tools with analytical techniques to characterize a candidate for target-based drug discovery against TB. It also lays groundwork for future research on the mycobacterial protein synthesis apparatus and raises many new questions about the dynamic role that tRNA plays in mycobacterial physiology. The successful combination of the tools used in this thesis is a result of multiple interdisciplinary collaborations. I hope that this slice of contribution to our understanding of *Mtb* physiology can be used – whether for its concrete findings, methodological descriptions, or general themes – to build upon the way research organizations approach designing innovative and effective ways to combat infectious diseases.

Thanks for reading!

References

1. Liu, Q., et al., *Mycobacterium tuberculosis clinical isolates carry mutational signatures of host immune environments.* Sci Adv, 2020. **6**(22): p. eaba4901.
2. Kamruzzaman, M., A.Y. Wu, and J.R. Iredell, *Biological Functions of Type II Toxin-Antitoxin Systems in Bacteria.* Microorganisms, 2021. **9**(6).
3. Zainuddin, Z.F. and J.W. Dale, *Does Mycobacterium tuberculosis have plasmids?* Tubercle, 1990. **71**(1): p. 43-9.
4. Sharma, A., et al., *VapC21 Toxin Contributes to Drug-Tolerance and Interacts With Non-cognate VapB32 Antitoxin in Mycobacterium tuberculosis.* Front Microbiol, 2020. **11**: p. 2037.
5. Talwar, S., et al., *Role of VapBC12 Toxin-Antitoxin Locus in Cholesterol-Induced Mycobacterial Persistence.* mSystems, 2020. **5**(6).
6. Tiwari, P., et al., *MazF ribonucleases promote Mycobacterium tuberculosis drug tolerance and virulence in guinea pigs.* Nat Commun, 2015. **6**: p. 6059.
7. LeRoux, M., et al., *Stress Can Induce Transcription of Toxin-Antitoxin Systems without Activating Toxin.* Mol Cell, 2020. **79**(2): p. 280-292 e8.
8. Culviner, P.H. and M.T. Laub, *Global Analysis of the E. coli Toxin MazF Reveals Widespread Cleavage of mRNA and the Inhibition of rRNA Maturation and Ribosome Biogenesis.* Mol Cell, 2018. **70**(5): p. 868-880 e10.
9. Cai, Y., et al., *A nucleotidyltransferase toxin inhibits growth of Mycobacterium tuberculosis through inactivation of tRNA acceptor stems.* Sci Adv, 2020. **6**(31): p. eabb6651.
10. Pavlov, M.Y., et al., *Slow peptide bond formation by proline and other N-alkylamino acids in translation.* Proc Natl Acad Sci U S A, 2009. **106**(1): p. 50-4.
11. Cole, S.T., et al., *Deciphering the biology of Mycobacterium tuberculosis from the complete genome sequence.* Nature, 1998. **393**(6685): p. 537-44.
12. Fishbein, S., et al., *Phylogeny to function: PE/PPE protein evolution and impact on Mycobacterium tuberculosis pathogenicity.* Mol Microbiol, 2015. **96**(5): p. 901-16.
13. Svenningsen, S.L., et al., *Transfer RNA is highly unstable during early amino acid starvation in Escherichia coli.* Nucleic Acids Res, 2017. **45**(2): p. 793-804.
14. Zhong, J., et al., *Transfer RNAs Mediate the Rapid Adaptation of Escherichia coli to Oxidative Stress.* PLoS Genet, 2015. **11**(6): p. e1005302.
15. Sorensen, M.A., A.O. Fehler, and S. Lo Svenningsen, *Transfer RNA instability as a stress response in Escherichia coli: Rapid dynamics of the tRNA pool as a function of demand.* RNA Biol, 2018. **15**(4-5): p. 586-593.
16. Haseltine, W.A. and R. Block, *Synthesis of guanosine tetra- and pentaphosphate requires the presence of a codon-specific, uncharged transfer ribonucleic acid in the acceptor site of ribosomes.* Proc Natl Acad Sci U S A, 1973. **70**(5): p. 1564-8.
17. Li, S., et al., *A chemical-genetic map of the pathways controlling drug potency in Mycobacterium tuberculosis*. bioRxiv, 2021: p. 2021.11.27.469863.
18. Harris, S.M., et al., *Peptidyl-tRNA hydrolase screening combined with molecular docking reveals the antibiotic potential of Syzygium johnsonii bark extract.* Nat Prod Commun, 2011. **6**(10): p. 1421-4.
19. Kaushik, S., et al., *The mode of inhibitor binding to peptidyl-tRNA hydrolase: binding studies and structure determination of unbound and bound peptidyl-tRNA hydrolase from Acinetobacter baumannii.* PLoS One, 2013. **8**(7): p. e67547.
20. Rosas-Sandoval, G., et al., *Orthologs of a novel archaeal and of the bacterial peptidyl-tRNA hydrolase are nonessential in yeast.* Proc Natl Acad Sci U S A, 2002. **99**(26): p. 16707-12.
21. Kabra, A., et al., *Structural characterization of peptidyl-tRNA hydrolase from Mycobacterium smegmatis by NMR spectroscopy.* Biochim Biophys Acta, 2016. **1864**(10): p. 1304-14.

22. Selvaraj, M., et al., *Structures of new crystal forms of Mycobacterium tuberculosis peptidyl-tRNA hydrolase and functionally important plasticity of the molecule.* Acta Crystallogr Sect F Struct Biol Cryst Commun, 2012. **68**(Pt 2): p. 124-8.
23. Shepherd, J. and M. Ibba, *Bacterial transfer RNAs.* FEMS Microbiol Rev, 2015. **39**(3): p. 280-300.
24. de Crecy-Lagard, V. and M. Jaroch, *Functions of Bacterial tRNA Modifications: From Ubiquity to Diversity.* Trends Microbiol, 2021. **29**(1): p. 41-53.
25. Grobe, S., et al., *Identification and Quantification of (t)RNA Modifications in Pseudomonas aeruginosa by Liquid Chromatography-Tandem Mass Spectrometry.* Chembiochem, 2019. **20**(11): p. 1430-1437.
26. Kimura, S., P.C. Dedon, and M.K. Waldor, *Comparative tRNA sequencing and RNA mass spectrometry for surveying tRNA modifications.* Nat Chem Biol, 2020. **16**(9): p. 964-972.
27. Ross, R., et al., *Sequence mapping of transfer RNA chemical modifications by liquid chromatography tandem mass spectrometry.* Methods, 2016. **107**: p. 73-8.
28. Su, D., et al., *Quantitative analysis of ribonucleoside modifications in tRNA by HPLC-coupled mass spectrometry.* Nat Protoc, 2014. **9**(4): p. 828-41.
29. Yan, T.M., et al., *Full-Range Profiling of tRNA Modifications Using LC-MS/MS at Single-Base Resolution through a Site-Specific Cleavage Strategy.* Anal Chem, 2021. **93**(3): p. 1423-1432.
30. Chan, C.T., et al., *Identification of N6,N6-dimethyladenosine in transfer RNA from Mycobacterium bovis Bacille Calmette-Guerin.* Molecules, 2011. **16**(6): p. 5168-81.
31. Chionh, Y.H., et al., *tRNA-mediated codon-biased translation in mycobacterial hypoxic persistence.* Nat Commun, 2016. **7**: p. 13302.
32. Zheng, G., et al., *Efficient and quantitative high-throughput tRNA sequencing.* Nat Methods, 2015. **12**(9): p. 835-837.
33. Kimura, S. and M.K. Waldor, *The RNA degradosome promotes tRNA quality control through clearance of hypomodified tRNA.* Proc Natl Acad Sci U S A, 2019. **116**(4): p. 1394-1403.
34. Grosjean, H., V. de Crecy-Lagard, and C. Marck, *Deciphering synonymous codons in the three domains of life: co-evolution with specific tRNA modification enzymes.* FEBS Lett, 2010. **584**(2): p. 252-64.
35. Glatt, S. and C.W. Muller, *Structural insights into Elongator function.* Curr Opin Struct Biol, 2013. **23**(2): p. 235-42.
36. Johansson, M.J., et al., *Eukaryotic wobble uridine modifications promote a functionally redundant decoding system.* Mol Cell Biol, 2008. **28**(10): p. 3301-12.
37. Chen, Y.T., et al., *Loss of mouse Ikbkap, a subunit of elongator, leads to transcriptional deficits and embryonic lethality that can be rescued by human IKBKAP.* Mol Cell Biol, 2009. **29**(3): p. 736-44.
38. Leidel, S., et al., *Ubiquitin-related modifier Urm1 acts as a sulphur carrier in thiolation of eukaryotic transfer RNA.* Nature, 2009. **458**(7235): p. 228-32.
39. van Kessel, J.C. and G.F. Hatfull, *Recombineering in Mycobacterium tuberculosis.* Nat Methods, 2007. **4**(2): p. 147-52.
40. Herzog, V.A., et al., *Thiol-linked alkylation of RNA to assess expression dynamics.* Nat Methods, 2017. **14**(12): p. 1198-1204.
41. Nedialkova, D.D. and S.A. Leidel, *Optimization of Codon Translation Rates via tRNA Modifications Maintains Proteome Integrity.* Cell, 2015. **161**(7): p. 1606-18.
42. Jinich A, Z.A., DeJesus MA, Flores-Bautista E, Smith CM, Sassetti FCM, Rock CJM, Ehrt S, Schnappinger D, Ioerger GTR, Rhee K, *The Mycobacterium tuberculosis transposon sequencing database (MtbTnDB): a large-scale guide to genetic conditional essentiality.* bioRxiv (preprint), 2021.
43. Saito, K., et al., *Rifamycin action on RNA polymerase in antibiotic-tolerant Mycobacterium tuberculosis results in differentially detectable populations.* Proc Natl Acad Sci U S A, 2017. **114**(24): p. E4832-E4840.

44. Babunovic, G.H., et al., *CRISPR Interference Reveals That All-Trans-Retinoic Acid Promotes Macrophage Control of Mycobacterium tuberculosis by Limiting Bacterial Access to Cholesterol and Propionyl Coenzyme A.* mBio, 2022: p. e0368321.
45. Mohammad, F., R. Green, and A.R. Buskirk, *A systematically-revised ribosome profiling method for bacteria reveals pauses at single-codon resolution.* Elife, 2019. **8**.
46. Evans, M.E., et al., *Determination of tRNA aminoacylation levels by high-throughput sequencing.* Nucleic Acids Res, 2017. **45**(14): p. e133.
47. Avcilar-Kucukgoze, I., et al., *Discharging tRNAs: a tug of war between translation and detoxification in Escherichia coli.* Nucleic Acids Res, 2016. **44**(17): p. 8324-34.
48. Schofield, P. and P.C. Zamecnik, *Cupric ion catalysis in hydrolysis of aminoacyl-tRNA.* Biochim Biophys Acta, 1968. **155**(2): p. 410-6.
49. Hu, J.F., et al., *Quantitative mapping of the cellular small RNA landscape with AQRNA-seq.* Nat Biotechnol, 2021. **39**(8): p. 978-988.
50. Zhuang, F., et al., *Structural bias in T4 RNA ligase-mediated 3'-adapter ligation.* Nucleic Acids Res, 2012. **40**(7): p. e54.

Chapter Five: Summary for a general audience

Overview of tuberculosis

Tuberculosis (TB) is a deadly infectious disease that dates back thousands of years. TB has been called many things in different cultures throughout history, from *phthisis* in ancient Greece and *tabes* in ancient Rome, to *the white plague* in the 1700s and *consumption* through the nineteenth century. Despite its many names, this disease is caused by a single bacterial species: *Mycobacterium tuberculosis* (*Mtb*). *Mtb* most commonly infects the lungs and spreads from person to person through aerosols.

Interestingly, about 90% of people who get TB never go on to develop symptoms, but instead have what is called latent TB, in which the immune system can control bacteria to keep them from multiplying and spreading. People with latent TB do not have symptoms and are not contagious. The main risk factor for going from latent TB to active TB is a weakened immune system. For instance, people with HIV/AIDS are much more likely to get severely ill because their immune systems are unable to keep their infection in check. TB is now the leading cause of death for people with AIDS.

Nonetheless, TB is so pervasive that it has been a massive global health burden for as long as it has existed. In 2020 alone, at least 1.5 million people died and another 10.5 million had active TB (you can use these numbers to estimate how many people in the world are likely infected with latent TB). While death and infection rates have been declining over the last century thanks to antibiotics and public health campaigns, progress has stalled globally due to resource reallocation and the strain of COVID-19 on health infrastructure. In 2020, for instance, only 1 in 3 people who needed TB treatment were able to get adequately covered.

Unlike most common bacterial infections that require 1-2 pills daily for a week, someone with TB needs to take a combination of at least 4 different antibiotics for a minimum of 4 months. These antibiotics are very strong and cause a lot of side effects ranging from nausea to neuropathy and temporary deafness, making it particularly challenging to complete months of treatment and be fully

cured. Finding drugs to treat TB has historically been extremely difficult, because *Mtb* has very complicated biology and is naturally resistant to most existing antibiotics used to treat other infections.

The goal of my thesis work is to generate new knowledge on how we can better approach developing drugs to treat TB. I hope this work can contribute to figuring out ways to make *Mtb* more responsive to antibiotics, and to figure out combinations of antibiotics that may work better than the ones we currently have (more quickly, effectively, and with fewer side effects).

What are antibiotics?

Our bodies are made up of trillions of cells, each of which serves as a tiny factory to produce everything we need to stay alive. Bacteria are similar, but instead of being composed of trillions of cells, one bacterium is a single, self-sustaining cell. Antibiotics work by blocking something in bacteria that prevents them from multiplying and spreading, or that immediately kill cells by breaking them apart. There are enough differences between human cells and bacterial cells that scientists develop antibiotics with the goal of targeting things that are unique to bacteria. Side effects often result when a drug affects our own cells in addition to bacterial cells; while this cannot always be 100% avoided, understanding the differences between bacterial cells and human cells helps reduce serious side effects. My thesis work focuses on an enzyme (discussed below) that is unique to bacteria, and I spent five years understanding what it does in *Mtb* and how we can exploit it in drug development.

Humans are not the only species out there trying to kill unwanted bacteria. In fact, the first antibiotics were found in nature. Microbes – tiny organisms including bacteria and fungi – are everywhere on Earth, from the surface of our skin to the bottom of the ocean floor. There are probably a trillion species of microbes out there, each one fighting for a home on this planet. Part of this fight involves the ability to compete with other microorganisms to compete for resources needed

to survive. Thus, over billions of years of evolutionary history, many microbes have developed the ability to produce and release chemicals that kill other species. Many of the antibiotics we use – like penicillin and erythromycin – are chemicals that were discovered in microorganisms as weapons to kill bacteria in nature. Since then, scientists have been able to build on and modify these chemicals to make them work better as medication for humans. While there are many types of antibiotics out there that can target all sorts of things in bacteria, one of the most common drug targets is protein synthesis.

What is protein synthesis?

This section appears in *An Introduction to Ribosomes: Nature's busiest molecular machines*, an article written by the author of this dissertation and published in Harvard's Science in the News blog on October 13, 2020. This article is licensed under a Creative Commons Attribution-Non-Commercial-Share-Alike 4.0 International License and can be found at the original URL: https://sitn.hms.harvard.edu/flash/2020/an-introduction-to-ribosomes-natures-busiest-molecular-machines/.

The "Central Dogma" of biology is based on a cell's ability to read information and turn it into a product: a genome is the complete set of genetic material (DNA) that is stored within a cell. While DNA is analogous to letters of the alphabet, a gene is the word that forms from stringing together these letters in a specific way. Together, genes compose the sentences that make up the genome's instruction manual to build, well, you!

A written instruction manual is not enough to tell a machine how to build a product. Written descriptions are turned into blueprints for manufacturing: a robot can directly interact with a blueprint to piece together an object. The same is true for living cells: our DNA instruction manual is turned into a blueprint called messenger RNA, or mRNA. The biological products made from these blueprints are called proteins, and they perform the structural and functional activities required to keep an organism alive. Just as complex electronics are built from a set of raw materials, the millions of proteins found in nature are made by piecing together different combinations of a set of building blocks known as amino acids. A protein forms when amino acids are linked together and fold into a

specific shape based on chemistry. mRNA tells you which amino acid goes where, to build that protein exactly right. The biological machine that reads mRNA and pieces together amino acids is called a ribosome, and every cell has thousands (bacteria) to millions (some mammalian cells – we're bigger!) of them.

Ribosomes churn out every single protein a cell needs to survive and are incredibly complicated biological machines. In fact, it took decades of research to figure out exactly how they work: the Nobel Prize in Chemistry was awarded in 2009 to three scientists (Venki Ramakrishnan, Thomas Steitz, and Ada Yonath) for their work on understanding the structure and function of the ribosome. While we now know that ribosomes can look different (e.g., bacterial ribosomes look different from human ribosomes despite doing the same thing), all ribosomes perform a universal set of critical functions. They all move along an mRNA blueprint, take an amino acid, and attach it to a growing chain of amino acids that ultimately becomes a protein. How does this work?

mRNA is a chain of chemicals called nucleotides, which a ribosome "reads" in groups of three: every set of 3 nucleotides (called a codon) contains the blueprint for a specific amino acid. A ribosome doing its job looks a bit like a Pacman making its way along a string of cookies: for every set of 3 mRNA nucleotides, the ribosome collects the corresponding amino acid and attaches it to a growing string of amino acids. Ribosomes have essential support workers called transfer RNA (tRNA) that bring them the right amino acid each step of the way: when Pacman opens its mouth over an mRNA codon, tRNA enters the mouth, carrying the right amino acid with it. As the ribosome collects a new amino acid, it attaches this amino acid to the chain it has just pieced together by performing a chemical reaction. As it moves farther along the mRNA, this chain grows. Once a ribosome has finished reading a blueprint, it releases a protein into the cell. That ribosome is then ready to repeat the process.

The ribosome is a very common target for antibiotics because it is necessary for keeping cells alive. For instance, many common antibiotics like azithromycin (used for certain types of pneumonia, ear infections, and skin infections) and tetracyclines (often used to control acne) target the ribosome, and each drug affects ribosomes in slightly different ways. Some drugs bind directly to the ribosome, and physically block it from being able to work properly. Other drugs target the machinery that copies DNA or that builds mRNA or inhibit the ability of a ribosome to start translating mRNA into proteins. And several more drugs target the support workers involved in carrying amino acids and tRNA to the ribosome.

Despite the success of many protein synthesis inhibitors against other bacterial infections, none of these drugs currently make up our first line of TB treatment. This is largely because *Mtb* is naturally resistant to these antibiotics. *Mtb* has all the same machinery as other bacteria for building proteins, so protein synthesis inhibitors *should* work. My thesis work focuses on understanding why these drugs do not work against TB. If we can find enzymes in *Mtb* that affect its susceptibility to existing antibiotics, we could lend efficacy to these drugs by simultaneously targeting those enzymes. And that is exactly what we have done!

Peptidyl tRNA hydrolase: The enzyme I spent half a decade studying

With a great team of scientists, I studied a protein called peptidyl tRNA hydrolase (abbreviated Pth). This enzyme interacts specifically with tRNA, the support workers that bring amino acids to the ribosome during protein synthesis. Using tools we developed in the lab, we learned more about why Pth is important in bacteria, and how it might interact with existing antibiotics to make them more effective against TB. First, what is Pth?

During protein synthesis, the ribosome moves along mRNA and eventually spits out a protein. It turns out that ribosomes can make mistakes, and that these mistakes occur pretty frequently in bacteria for several reasons: they grow very quickly, so ribosomes must work quickly, and bacteria do not really have quality control helpers to make sure everything is going smoothly. There are several types of mistakes that ribosomes can run into: mRNA can be messed up, leading to the production of an incomplete or incorrect protein (many human diseases are caused by this type of mistake in our own cells). Cells could also not have enough amino acids to build a protein, so the ribosome stops because it does not have the raw materials it needs to build a protein (this is called starvation).

And sometimes, the protein being built falls out of the ribosome, still attached to its tRNA helper because it wasn't finished doing its job. We don't fully understand why this last type of error happens, but the main hypothesis is that it has to do with the "bulkiness" of a peptide. In other words, sometimes certain amino acids pieced together can get crowded in the ribosome, affecting its ability to continue Pacman-ing its way across the mRNA blueprint. While some peptides look like snakes and move smoothly through the ribosome, others might look more like globby mess (Figure 5.1). You can imagine that a "bulky"-looking peptide like this would be cramped in a machine like the ribosome and force it to break open to release its contents. When this happens, the ribosome breaks off the mRNA – this process is called peptidyl tRNA drop-off – and releases the unfinished peptide into the cell. Bacteria have different helper enzymes that quickly come and clean up this mess, so that protein synthesis can restart and continue smoothly.

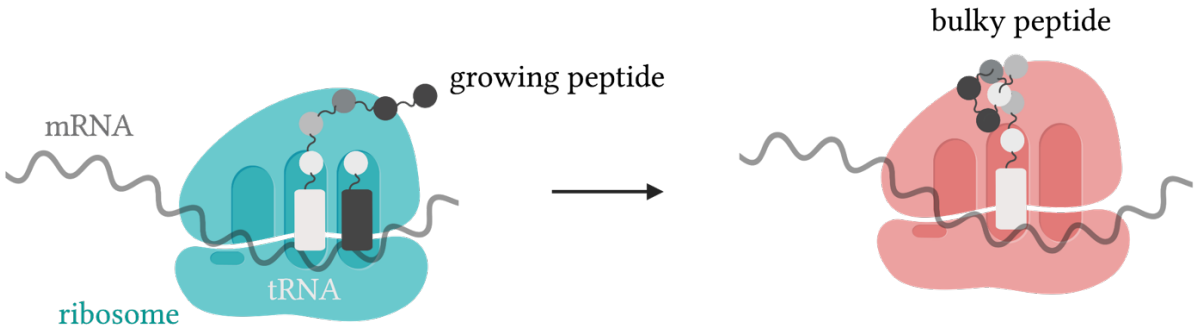

Figure 5.1. Normal protein synthesis vs. synthesis of a bulky protein that causes peptidyl tRNA dropoff. Left: most proteins are built smoothly, and a growing peptide is filed through the ribosome and eventually released as a functional protein. Right: sometimes, different amino acids pieced together can form a bulky shape that makes it very difficult to fit through the ribosome, and this can cause peptidyl tRNA drop-off, release of the bulky unfinished peptide into the cell so the ribosome can start over. Image created with BioRender.com.

The clean-up process is where my favorite enzyme, Pth, comes in. When the ribosome releases the unfinished peptide, it is still connected to a tRNA helper, since the tRNA was in the middle of adding its amino acid to the growing chain. Pth is like a pair of scissors that cuts the unfinished peptide off the tRNA: the tRNA can then go pick up another amino acid for another ribosome, and the peptide gets broken down into individual amino acids again. tRNA supplies aren't infinite in cells, so they need to be recycled constantly.

Something I learned at the beginning of my PhD is that mistakes happen more often than you might imagine during protein synthesis. They happen so frequently, apparently, that Pth is what is called an "essential enzyme" in bacteria – in other words, if you got rid of this enzyme, mistakes would continue to happen during protein synthesis, but they would not be cleaned up. Eventually, there would not be enough tRNA left to continue building proteins because it would all be floating around stuck to a useless peptide instead of being a productive helper, and cells would die.

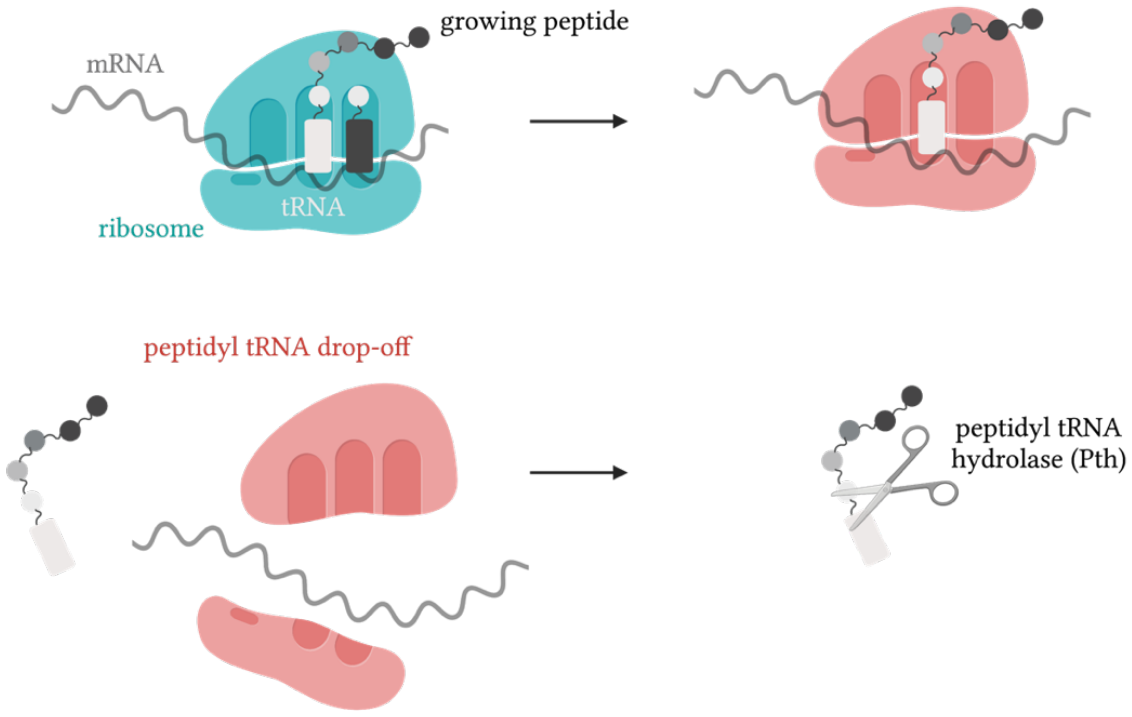

Figure 5.2. Mistakes during protein synthesis require clean-up. A ribosome (blue) reads mRNA (gray) one codon at a time, and tRNA (white and black) brings amino acids together to build a protein (growing peptide). When a mistake happens, the ribosome stops what it's doing (red) and, in some cases, breaks off the mRNA, releasing its contents in a process called peptidyl tRNA drop-off. Peptidyl tRNA hydrolase (Pth; scissor) cuts the unfinished peptide from tRNA, so that all components can be recycled. Image created with BioRender.com.

As mentioned above, many antibiotics target protein synthesis: a few of them even work by messing up ribosomes or tRNA in a way that increases rates of protein synthesis errors so much that bacteria start to go haywire and die. Yet no antibiotics currently target Pth. Our lab wanted to know if it would be worthwhile for someone to develop a drug that blocks Pth activity in TB. Spoiler: we think it would be. The following experiments, taken out of my thesis chapters and repurposed with less jargon-heavy captions, were key for building our case.

The case for a Pth-targeting drug in TB

Unfortunately, there aren't any known chemicals right now that target Pth – otherwise, this would have made our job a lot easier: just test the antibiotic, see if it works, and move on. Instead, we had to create a system in the lab that mimicked an antibiotic targeting Pth. This is accomplished using techniques in the field of "bacterial genetics". Bacterial genetics is exactly what it sounds like: the study of the genetics of bacteria. You have likely heard buzzwords out there like "CRISPR," or "gene editing." We can edit genes in bacteria so that we can reduce the amount of a specific protein that is being made in a cell. Functionally, this mimics an antibiotic, since an antibiotic reduces (or eliminates) the ability of a protein to do what it's supposed to.

We can do this in several different ways – these are discussed at length in Chapter One – but the most common right now involves blocking the cell's ability to make the mRNA encoding a specific protein ("transcriptional repression"). Reducing the amount of mRNA blueprint for your protein of interest reduces the number of ribosomes dedicated to building that protein. This is called a "genetic knockdown," in which the amount of protein being made is reduced. We were able to perform this type of gene editing on *Mtb* to create bacteria with varying levels of Pth expression: cells that made "wild type" (normal; what you expect) amounts of Pth, cells that made a medium amount, and cells that could barely make any.

There are two possible outcomes when building knockdown strains: nothing happens, or something happens. If nothing happens – your bacteria grow just fine and don't suffer from reduced protein levels – this means your protein of interest is not essential. It has some function in the cell, but that function is not critical for survival. If something happens, meanwhile, it suggests that your protein is essential: messing with its normal function makes your cells sick, implying that a drug targeting that protein would kill bacteria. When we knock down Pth in *Mtb*, something happens (Figure 5.3).

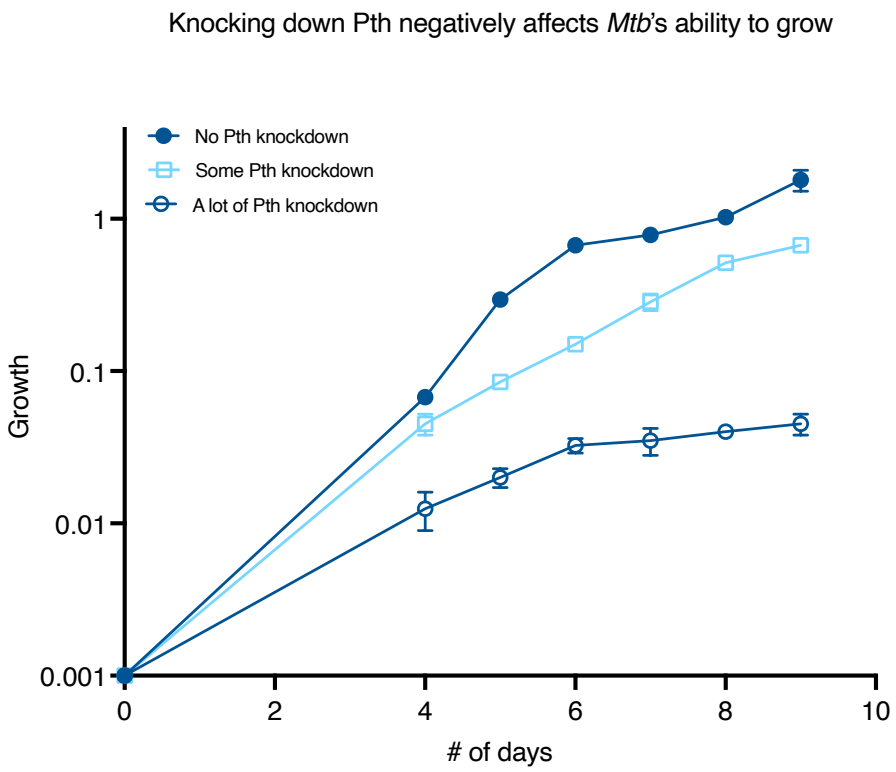

Figure 5.3. Knocking down Pth negatively affects *Mtb*'s ability to grow. We grow bacteria in vials full of liquid, which contains the nutrients bacteria need to grow and multiply. Over time, as more and more bacteria grow, this liquid goes from clear to cloudy. We quantify growth over time by quantifying that cloudiness through a technique called spectrophotometry, which measures light absorption in that liquid. Plotting growth over time tells you how quickly bacteria are growing. The top-most curve in this graph (blue shaded circles; "No Pth knockdown") is what healthy bacteria look like: they grow steadily over time. As you knock down Pth levels (unshaded blue circles) you can see that this growth slows down over time, especially in the strain where a lot of Pth is knocked down.

The results from Figure 5.3 show that Pth is in fact essential, meaning that if we built a drug targeting Pth, we would block *Mtb* from being able to grow. Why is this the case? Recall from Figure 5.2 that Pth is a clean-up crew for ribosomes that make mistakes and can't keep making the protein it was working on. Pth cuts the incomplete peptide from tRNA, so that the tRNA can be reused to build another peptide. You might imagine, then, that getting rid of Pth leads to the accumulation of peptidyl tRNA. Since the tRNA can't be freed up for reuse, if you keep blocking Pth's ability to do its thing, eventually you will not have enough tRNA to continue building proteins, and cells die. This was our

hypothesis: Pth is essential in bacteria because it plays a crucial role in making sure cells have enough tRNA to continue building proteins and growing.

We needed a way to test this hypothesis. There are a lot of tRNA helpers in cells. There are 20 amino acids that can be combined in different ways to make a protein. Each amino acid has its own corresponding tRNA(s). For instance, proline is one amino acid and glutamine is another. For proline to be added to a protein, a proline-specific tRNA picks up and moves proline amino acids. The same goes for glutamine, with a glutamine-specific tRNA. Glutamine-tRNA cannot pick up proline, or vice versa. In most cases, there are a couple of tRNAs that work with the same amino acid; in *Mtb*, then, there are over 40 different types of tRNA. We developed a way to look at all 40 tRNAs in *Mtb* to see how each one is affected in the absence of Pth. Our goal was specifically to measure the amount of peptidyl tRNA in our samples relative to normal tRNA. Peptidyl tRNA cannot be used for protein synthesis, but normal tRNA can. We hypothesized that reducing Pth levels in cells would lead to an accumulation of peptidyl tRNA. We wanted to measure each tRNA individually because we did not know whether Pth would affect all of them in the same way, or if it affected different tRNAs in different ways.

We found that depleting Pth in *Mtb* affects all tRNAs, but to varying levels (Figure 5.4). I won't include the details of this technique, but it took about a year to get up and running and compile these results. Our data suggest that different amino acids are more prone to causing peptidyl tRNA drop-off than others. This is an important finding because it shows that *Mtb* ribosomes can string together many amino acids without any problems, but the use of some other amino acids increases the potential for peptidyl tRNA drop-off to occur (such as via bulkiness as in Figure 5.1). Based on these findings and others described in this thesis, we concluded that Pth is essential in *Mtb* because it plays an important role in making sure that cells have enough tRNA to continue building proteins even when mistakes take place. We also concluded that, while Pth can affect all tRNAs, it is particularly

important for cleaning up peptidyl tRNA drop-of that takes place when specific amino acids are added to a peptide.

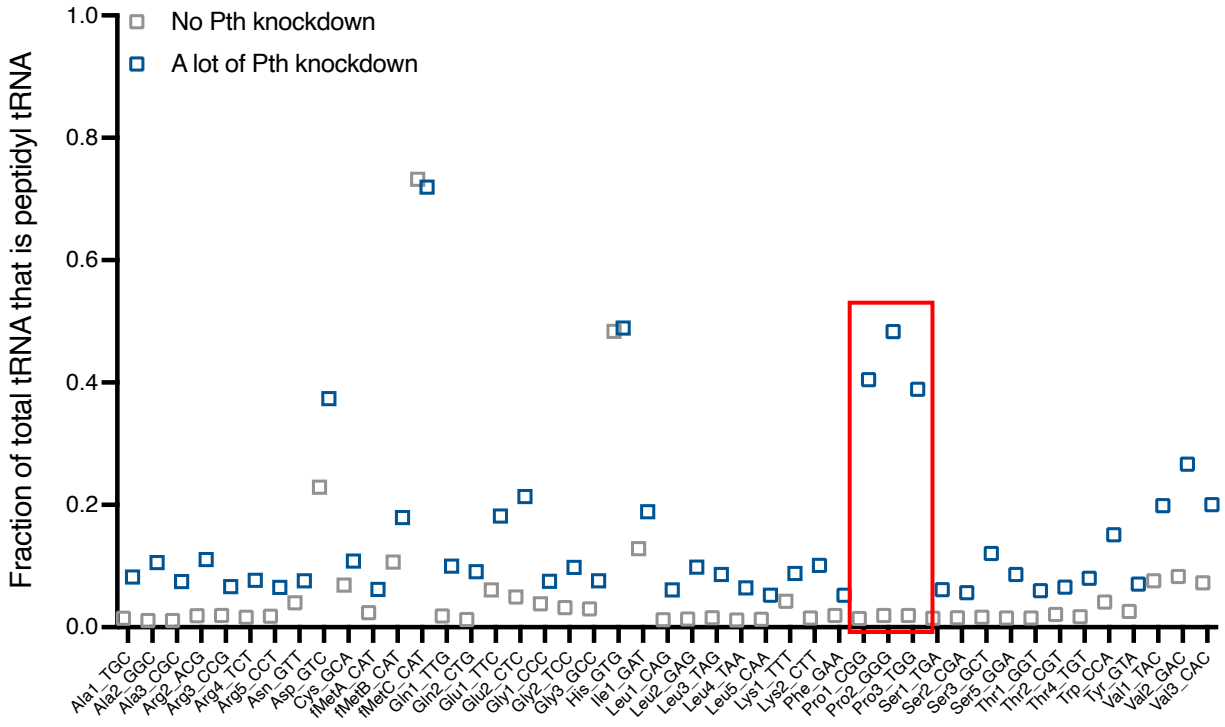

Figure 5.4. Peptidyl tRNA accumulates in cells lacking normal Pth levels. Comparing grey (no Pth knockdown) to blue (a lot of Pth knockdown) shows that there is more peptidyl tRNA in cells lacking normal Pth levels. You can observe this across pretty much every tRNA (each tick on the x-axis is the name of a specific type of tRNA). The tRNAs boxed in red all work with the same amino acid (proline) and were the most substantially affected (the biggest difference between blue and gray) by Pth depletion compared to other tRNAs.

Why is this important or helpful for developing TB drugs? Our work up to this point validates Pth as an important enzyme in *Mtb*, and one that is worth understanding better from a biological perspective. A lot of research goes into the different players in protein synthesis. This is because (1) as scientists we are still trying to understand all the details of how protein synthesis works, and (2) we can use this knowledge to figure out the best antibiotic development strategy. Finding out not only *what* proteins are important, but also *why* they're critical for bacterial survival can help us decide what

to focus drug discovery efforts on. We want to find an enzyme without which *Mtb* would die and build a drug that blocks its ability to keep *Mtb* alive.

Pth affects *Mtb* resistance to some antibiotics

I mentioned earlier in this chapter that TB is hard to cure because *Mtb* is naturally resistant to many antibiotics. This means that taking most antibiotics available to us would not cure someone with TB, even though those same drugs would quickly cure someone with strep throat, a skin infection, or a UTI. We don't know exactly why *Mtb* is naturally resistant to all these antibiotics, and it can be a result of a lot of things unique to this pathogen. For instance, *Mtb* bacteria grow way more slowly than bacteria like *E. coli* or *S. aureus*, which can cause UTIs and skin infections. While the latter two bacteria replicate every 20 minutes, *Mtb* takes 24 hours. Therefore, if you have a UTI, it is important to start taking antibiotics as soon as possible, to prevent the infection from quickly spreading or getting worse. A TB infection, meanwhile, takes a longer time to spread throughout your body and disease lasts for a much longer time. Another reason *Mtb* might be naturally resistant to antibiotics is that it has enzymes that can block drugs from working. For instance, when penicillin is used against TB, enzymes in these bacteria literally cut penicillin up like scissors to paper, making the drug ineffective.

Since our project focuses on protein synthesis in *Mtb*, we wanted to understand why *Mtb* is resistant to a very popular class of protein synthesis-targeting antibiotics called macrolides. You may have heard of azithromycin or erythromycin, which are used often for pneumonia, ear, nose, and throat infections. Macrolides are inexpensive, generally well-tolerated antibiotics with relatively low rates of antibiotic resistance against most infections. It would be great if we could include macrolides in our arsenal against TB for those reasons. Figure 5.5 shows what happens to *Mtb* when you add macrolides to a culture of *Mtb* cells. The gray lines show normal *Mtb* cells, and the blue lines show *Mtb* cells when we knock down Pth.

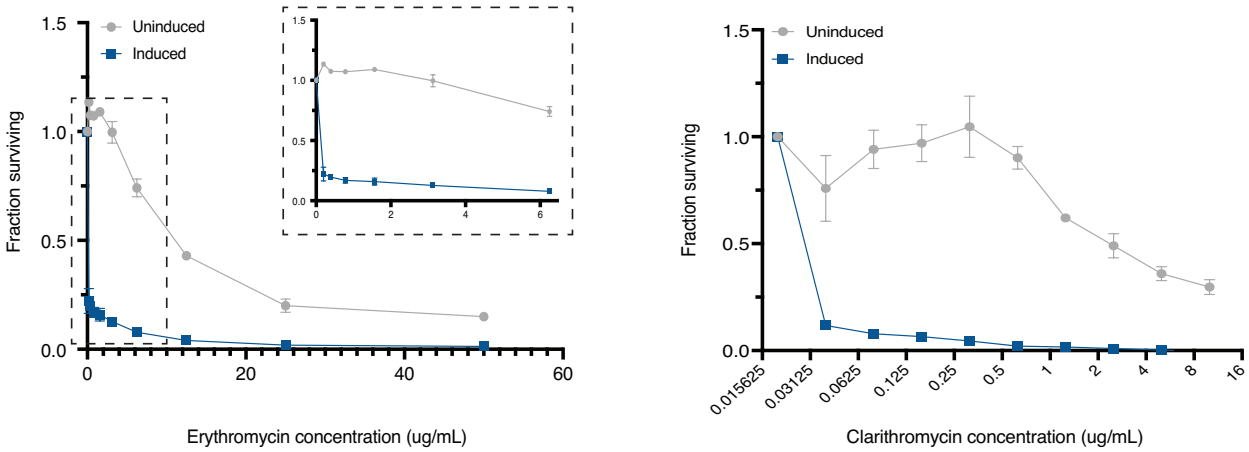

Figure 5.5. Knocking down Pth makes *Mtb* susceptible to macrolides. Each graph shows a different macrolide (left, erythromycin; right, clarithromycin). In gray, wild type (non-manipulated) *Mtb* was exposed to increasing amounts of each drug (x-axis). In blue, the same was done but to *Mtb* Pth knockdowns. On the y-axis, the fraction of bacteria surviving is shown. We measured this by setting up our experiments with the same number of bacteria under each antibiotic concentration. After a week of antibiotic treatment, we compared the number of bacteria in each antibiotic concentration to the number of bacteria in a drug-free well.

Looking at Figure 5.5, you can see a clear difference between the gray line and the blue line for both macrolides. In the gray lines, the highest drug concentration tested still had bacteria growing at the end of the experiment, showing that treating wild type *Mtb* with macrolides fails to kill all bacteria. Meanwhile, in blue, you can see that knocking down Pth levels in *Mtb* led to no bacterial survival. We were very excited to see this because it provides a potential strategy to treat TB with macrolides. We tested other protein synthesis-targeting drugs but did not see this pattern, suggesting that macrolides specifically do something to cells that increases *Mtb*'s need for Pth. In fact, we showed that macrolides cause peptidyl tRNA drop-off, the error that happens at the ribosome that Pth cleans up.

The punchline

The work described in this thesis is the culmination of our efforts to understand one enzyme's purpose in life, and to apply our findings to designing better drugs to treat tuberculosis. Peptidyl tRNA

hydrolase (Pth) is an enzyme that *Mtb* needs to stay alive, because it helps clean up messes made during protein synthesis. By cutting unfinished proteins from tRNA that has fallen out of ribosomes in the middle of protein synthesis, Pth allows tRNA to be recycled. *Mtb* needs Pth to make sure it always has enough tRNA to support its growth. Our work shows that Pth is a promising target for drug development against TB: block Pth activity and cells die. On top of this, we also showed that targeting Pth can be coupled with macrolides to kill *Mtb* even more quickly. Macrolides are inexpensive, generally well-tolerated antibiotics that are used against multiple infectious diseases, but until now we have not been able to use them against TB. We learned that macrolides trigger peptidyl tRNA drop-off in *Mtb* – bacteria have Pth to mitigate this, but if we take away *Mtb*'s sword, we take away its ability to survive exposure to these antibiotics.

We hope that the basic biology we uncovered in this work can be applied to future antibiotic discovery efforts against TB, from testing our observations in animal models of disease, to the eventual development of a drug that targets *Mtb* Pth.

Thanks for reading!

Appendix I: Supplementary figures and tables accompanying Chapter Two

Figures

Tables

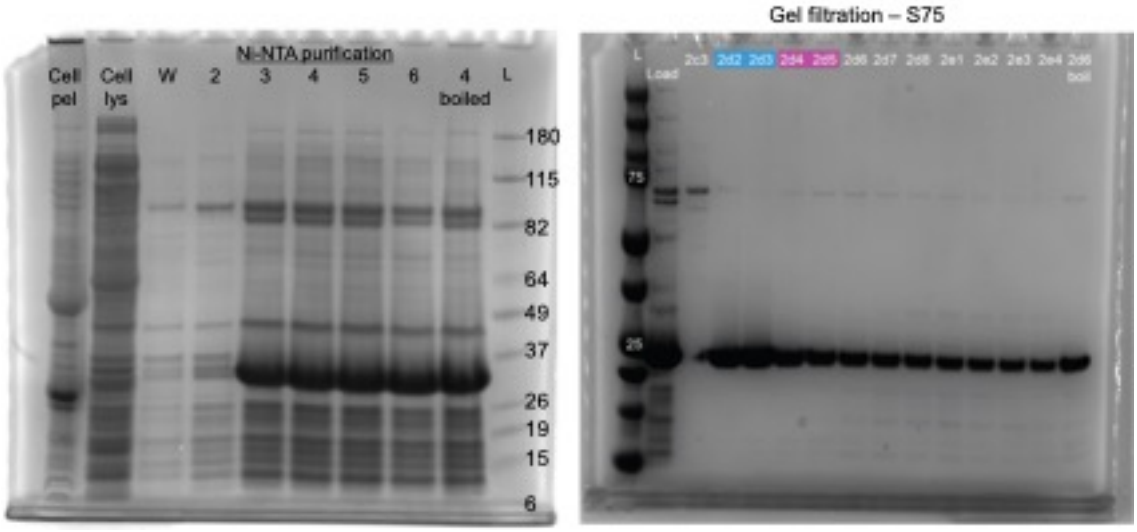

Figure A2.1: *Mtb* Pth purification gels. *Mtb* Pth was purified as described in the Methods in Chapter Two. Briefly, the Pth-encoding gene Rv1014c was cloned with a C' 6x-His tag and expressed from pET28a in BL21 *E. coli*. Following lysate clarification, His-tagged Pth was extracted via batch binding with Ni-NTA beads, and eluted samples were analyzed via SDS-PAGE (left). The cleanest elution fractions (4-6) were desalted and purified further by FPLC via gel filtration chromatography. Fractions were analyzed via SDS-PAGE (right), and nucleic acid-free fractions 2d2-2d3 were pooled for use in biochemistry assays.

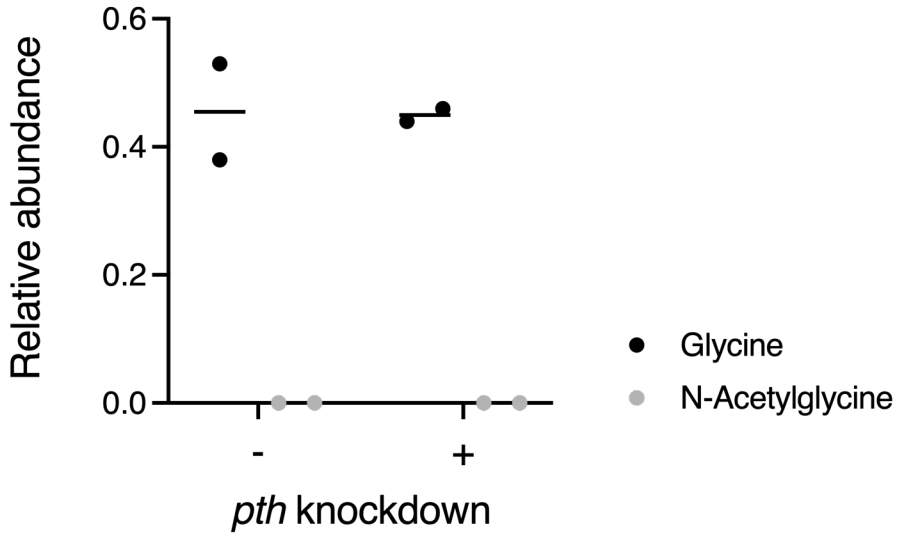

Figure A2.2: TacT is not active in normal *Mtb* laboratory growth conditions. Wild-type *Mtb* was induced for *pth* depletion and incubated for 4 days. Total RNA from duplicate cultures was collected along with an uninduced control for liquid chromatography-mass spectrometry analysis as described in the Methods in Chapter Two. The relative abundance of unacetylated and N-acetylated glycyl-tRNA fragments are shown.

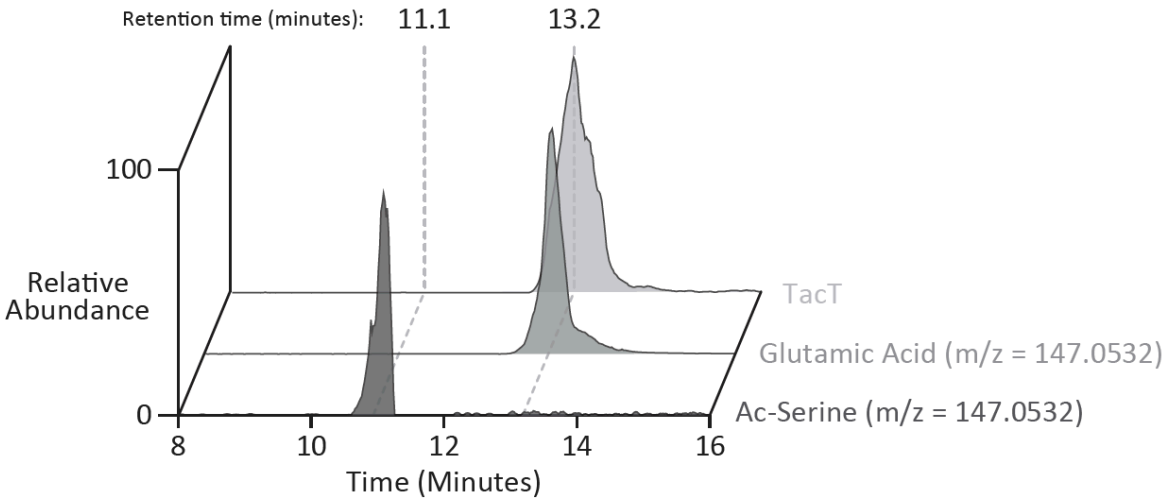

Figure A2.3: Distinction between N-acetylated seryl-tRNA and glutamyl-tRNA. RNA samples treated with Pth were compared to purified standards of each amino acid as described in Methods for Chapter Two.

Table A2.1: Premature stop mutations in the *tacAT* operon have been detected in clinical *Mtb* isolates. 51,229 *Mtb* clinical isolates were screened for premature stop mutations in the *tacAT* operon (Rv0918-0919). Rv0918; antitoxin TacA. Rv0919; toxin TacT.

Strain ID	Genomic location	Ref	Mut	Codon	Codon change	Codons	Gene
ERR2383628	1024217	C	T	3	Nonsynonymous-Arg/R-stop	CGA-TGA	Rv0918
ERR2446182	1024217	C	T	3	Nonsynonymous-Arg/R-stop	CGA-TGA	Rv0918
ERR2446503	1024304	C	T	32	Nonsynonymous-Gln/Q-stop	CAG-TAG	Rv0918
ERR2510816	1024217	C	T	3	Nonsynonymous-Arg/R-stop	CGA-TGA	Rv0918
ERR2512633	1024217	C	T	3	Nonsynonymous-Arg/R-stop	CGA-TGA	Rv0918
ERR2512682	1024217	C	T	3	Nonsynonymous-Arg/R-stop	CGA-TGA	Rv0918
ERR2513326	1024217	C	T	3	Nonsynonymous-Arg/R-stop	CGA-TGA	Rv0918
ERR2514206	1024217	C	T	3	Nonsynonymous-Arg/R-stop	CGA-TGA	Rv0918
ERR2517145	1024304	C	T	32	Nonsynonymous-Gln/Q-stop	CAG-TAG	Rv0918
ERR2517594	1024217	C	T	3	Nonsynonymous-Arg/R-stop	CGA-TGA	Rv0918
ERR2679246	1024217	C	T	3	Nonsynonymous-Arg/R-stop	CGA-TGA	Rv0918
ERR2704811	1024217	C	T	3	Nonsynonymous-Arg/R-stop	CGA-TGA	Rv0918
ERR3170468	1024217	C	T	3	Nonsynonymous-Arg/R-stop	CGA-TGA	Rv0918
ERR3170476	1024590	G	A	127	Nonsynonymous-Trp/W-stop	TGG-TAG	Rv0918
ERR3170479	1024217	C	T	3	Nonsynonymous-Arg/R-stop	CGA-TGA	Rv0918
ERR3275195	1024217	C	T	3	Nonsynonymous-Arg/R-stop	CGA-TGA	Rv0918
ERR3275985	1024217	C	T	3	Nonsynonymous-Arg/R-stop	CGA-TGA	Rv0918
ERR400537	1024217	C	T	3	Nonsynonymous-Arg/R-stop	CGA-TGA	Rv0918
ERR551709	1024217	C	T	3	Nonsynonymous-Arg/R-stop	CGA-TGA	Rv0918
ERR551710	1024217	C	T	3	Nonsynonymous-Arg/R-stop	CGA-TGA	Rv0918

Table A2.1 continued

ERR551711	1024217	C	T	3	Nonsynonymous-Arg/R-stop	CGA-TGA	Rv0918
ERR553341	1024217	C	T	3	Nonsynonymous-Arg/R-stop	CGA-TGA	Rv0918
ERR841431	1024217	C	T	3	Nonsynonymous-Arg/R-stop	CGA-TGA	Rv0918
ERR841466	1024217	C	T	3	Nonsynonymous-Arg/R-stop	CGA-TGA	Rv0918
ERR841467	1024217	C	T	3	Nonsynonymous-Arg/R-stop	CGA-TGA	Rv0918
ERR841468	1024217	C	T	3	Nonsynonymous-Arg/R-stop	CGA-TGA	Rv0918
ERR841471	1024217	C	T	3	Nonsynonymous-Arg/R-stop	CGA-TGA	Rv0918
ERR841472	1024217	C	T	3	Nonsynonymous-Arg/R-stop	CGA-TGA	Rv0918
ERR841473	1024217	C	T	3	Nonsynonymous-Arg/R-stop	CGA-TGA	Rv0918
ERR841475	1024217	C	T	3	Nonsynonymous-Arg/R-stop	CGA-TGA	Rv0918
ERR841476	1024217	C	T	3	Nonsynonymous-Arg/R-stop	CGA-TGA	Rv0918
ERR841477	1024217	C	T	3	Nonsynonymous-Arg/R-stop	CGA-TGA	Rv0918
ERR841478	1024217	C	T	3	Nonsynonymous-Arg/R-stop	CGA-TGA	Rv0918
ERR841480	1024217	C	T	3	Nonsynonymous-Arg/R-stop	CGA-TGA	Rv0918
ERR841481	1024217	C	T	3	Nonsynonymous-Arg/R-stop	CGA-TGA	Rv0918
ERR841483	1024217	C	T	3	Nonsynonymous-Arg/R-stop	CGA-TGA	Rv0918
ERR841484	1024217	C	T	3	Nonsynonymous-Arg/R-stop	CGA-TGA	Rv0918
ERR841485	1024217	C	T	3	Nonsynonymous-Arg/R-stop	CGA-TGA	Rv0918
ERR841486	1024217	C	T	3	Nonsynonymous-Arg/R-stop	CGA-TGA	Rv0918
ERR841487	1024217	C	T	3	Nonsynonymous-Arg/R-stop	CGA-TGA	Rv0918
ERR841488	1024217	C	T	3	Nonsynonymous-Arg/R-stop	CGA-TGA	Rv0918
ERR841489	1024217	C	T	3	Nonsynonymous-Arg/R-stop	CGA-TGA	Rv0918

Table A2.1 continued

SRR2100539	1024217	C	T	3	Nonsynonymous-Arg/R-stop	CGA-TGA	Rv0918
SRR3085279	1024217	C	T	3	Nonsynonymous-Arg/R-stop	CGA-TGA	Rv0918
SRR6045496	1024217	C	T	3	Nonsynonymous-Arg/R-stop	CGA-TGA	Rv0918
SRR6650184	1024454	G	T	82	Nonsynonymous-GlT/E-stop	GAG-TAG	Rv0918
SRR6650210	1024217	C	T	3	Nonsynonymous-Arg/R-stop	CGA-TGA	Rv0918
SRR6650343	1024217	C	T	3	Nonsynonymous-Arg/R-stop	CGA-TGA	Rv0918
SRR7069811	1024217	C	T	3	Nonsynonymous-Arg/R-stop	CGA-TGA	Rv0918
SRR7070126	1024217	C	T	3	Nonsynonymous-Arg/R-stop	CGA-TGA	Rv0918
SRR7070192	1024217	C	T	3	Nonsynonymous-Arg/R-stop	CGA-TGA	Rv0918
SRR7070262	1024217	C	T	3	Nonsynonymous-Arg/R-stop	CGA-TGA	Rv0918
SRR7131039	1024217	C	T	3	Nonsynonymous-Arg/R-stop	CGA-TGA	Rv0918
SRR7131102	1024217	C	T	3	Nonsynonymous-Arg/R-stop	CGA-TGA	Rv0918
SRR7131139	1024217	C	T	3	Nonsynonymous-Arg/R-stop	CGA-TGA	Rv0918
SRR7131190	1024217	C	T	3	Nonsynonymous-Arg/R-stop	CGA-TGA	Rv0918
SRR7131223	1024217	C	T	3	Nonsynonymous-Arg/R-stop	CGA-TGA	Rv0918
SRR7131238	1024217	C	T	3	Nonsynonymous-Arg/R-stop	CGA-TGA	Rv0918
SRR7131250	1024217	C	T	3	Nonsynonymous-Arg/R-stop	CGA-TGA	Rv0918
ERR1633849	1025182	T	G	167	Nonsynonymous-stop-Gly/G	TGA-GGA	Rv0919
ERR1633871	1025182	T	G	167	Nonsynonymous-stop-Gly/G	TGA-GGA	Rv0919
ERR1633888	1025182	T	G	167	Nonsynonymous-stop-Gly/G	TGA-GGA	Rv0919
ERR176677	1024966	A	T	95	Nonsynonymous-Lys/K-stop	AAA-TAA	Rv0919
ERR212038	1024966	A	T	95	Nonsynonymous-Lys/K-stop	AAA-TAA	Rv0919

Table A2.2: Strains and primers used in this study. Top; strains. Middle; plasmid. Bottom; primers.

Annotated strain name	Organism	Parental background	Plasmid at L5 integration site	Plasmid at Tweety integration site (plasmid #)
TacTful	*Msmeg*	mc2155	pUVtetOR-tacT-L5 (FT 2)	None
FT64	*Msmeg*	mc2155	None	pUV15-tacAT-Tw (FT3)
TacTless (ΔtacAT)	*Mtb*	Δ*tacAT*::hygR	None	None
FT-BL3-3	Mtb	Δ*tacAT*::hygR	pPrpsA-Tet-dCas9-sgRNA1-pth(Rv1014c)-KanR (FT 110)	None
FT-BL3-4	Mtb	H37Rv	pPrpsA-Tet-dCas9-sgRNA1-pth(Rv1014c)-KanR (FT 110)	None

Plasmid name	Contents	Selection	Parental vector	Notes
CT 16	pUVtetOR-HivPr-L5	Nourseothracin	Lab vector	L5 integrating vector with tet promoter, driving expression of Hiv protease, contains tet repressor; backbone of cloning vector for Rv0919 (TacT) overexpression)
CT 250	pUV15-eGFP-Tw	Nourseothracin	Lab vector	Tweety integrating vector that expresses eGFP from the UV15 promoter; backbone of cloning vector for Tweety-integrating Rv0918-0919 (TacAT) operon
CT 27	pNit-RecET SacBR	Kanamycin	Lab vector	Nitrile-inducible expression of recombinase ET; used to make mycobacterial strains competent for recombineering (JP XXX)
CT 296	pPrpsA-Tet-dCas9-sgRNA1-KanR	Kanamycin	Gift of Jeremy Rock	For CRISPRi transcriptional repression, optimized for Mtb
CT 216	pET-28a	Kanamycin	Lab vector	For expression in E.coli of C-terminally His-tagged proteins
FT 2	pUVtetOR-tacT-L5	Nourseothracin	CT 16	Adding anhydrous tetracycline (aTC) induces overexpression of *tacT* (Rv0919)
FT 3	pUV15-tacAT-Tw	Kanamycin	CT 250	Constitutive expression of *tacAT* (Rv0918-0919) under UV15 promoter
FT 110	pPrpsA-Tet-dCas9-sgRNA1-pth(Rv1014c)-KanR	Kanamycin	CT 296	Adding anhydrous tetracycline (aTC) induces CRISPRi transcriptional repression of *Mtb pth*
FT 49	pET:eGFP	Kanamycin	Lab vector	T7 expression of eGFP
CLD 34	Rv1014c (Pth) C-term 6x his in pET28a	Kanamycin	CT 216	For expression in E.coli of C-terminally His-tagged Mtb Pth

Table A2.2 continued

Primer name		Sequence (5'->3')	Purpose
FT 27	ClaI-TacT-Fw	ATCGATATGAGCGGCTAC AGCGCG	ClaI+tacT(Rv0919) for insertion into CT16 - Forward
FT 28	EcoRI-TacT-Rv	TGCTTAGAATTCAGTCGCC AATTAGCGCGCGA	EcoRI+tacT(Rv0919) for insertion into CT16 - Reverse
FT-CT16-Fw	CT16-seq-Fw	TCAGTGATAGATAGGCTC TGGGA	For sequencing/PCR confirming CT16 inserts - Forward
FT-CT16-Rv	CT16-seq-Rv	GTCTTAATGACCATGGGCT AGC	For sequencing/PCR confirming CT16 inserts - Reverse
FT 15	TacT-PURExpress-Fw	GCGAATTAATACGACTCAC TATAGGGCTTAAGTATAA GGAGGAAAAAATATGAGC GGCTACAGCGCGCCGCGA CGT	Template for Mtb TacT (Rv0919) expression in PURExpress system - Forward
FT 16	TacT-PURExpress-Rv	AAACCCCTCCGTTTAGAGA GGGGTTATGCTAGTTATC AGTCGCCAATTAGCGCGC GAGC	Template for Mtb TacT (Rv0919) expression in PURExpress system - Reverse
FT 67	Y138F-int-fw	GCCCGCGCGTTCTTCGTC	For making Y138F TacT mutant (internal primer) - Forward
FT 68	Y138F-int-rv	GAAGTCAAAGTGGACGAA GAACGC	For making Y138F TacT mutant (internal primer) - Reverse
FT 61	CT250-TacAT-Fw	CACGATCCGCATGCTTAAT TAAGAAGGAGATATACAT ATGTTGCACCGAGCGGGA GCGGC	For Gibson insertion of tacAT (Rv0918-0919) into CT250 - Forward
FT 62	CT250-TacAT-Rv	TCATCGGCGTCGCTGATAC GTCGCGGCGCGCTGTAGC CGCTCACCCCTCGGTGTCG AAAA	For Gibson insertion of tacAT (Rv0918-0919) into CT250 - Reverse
CLD34-Fw	NcoI to Pth Fw	TATCCATGGCCGAGCCGTT	For insertion of Mtb pth (Rv1014c) into pET28a for C' his tag & E. coli expression - Forward
CLD34-Rv	EcoR1 and Ct 6xhis to Pth Rv	AATGAATTCTCAGTGGTG GTGGTGGTGGTGCCAGGC GTGGACGC	For insertion of Mtb pth (Rv1014c) into pET28a for C' his tag & E. coli expression - Reverse + 6xHis
JPS1	hyg stitch F	AAGGACGACGACGACAAG TAGCGCTCTAGAACTAGT GGATCC	For building dsDNA to generate TacAT knockout
JPS2	hyg stitch R	TCCTTCCCTAGGCCCAAAA AAACTCT AGA CTC GAG GTA CCG G	For building dsDNA to generate TacAT knockout
JPS3	KO Rv0918 F1 (F)	ctatgcgatgaccaaagcgt	For building dsDNA to generate TacAT knockout
JPS4	KO Rv0918 F1 (R)	CTACTTGTCGTCGTCGTCC TTacgacaccacacgttggcc	For building dsDNA to generate TacAT knockout

Table A2.2 continued

JPS5	KO Rv0919 F2 (F)	GTTTTTTTGGGCCTAGGG AAGGAtgcacctaatgctgttgatg	For building dsDNA to generate TacAT knockout
JPS6	KO Rv0919 F2 (R)	gacacttcccgaacgaacag	For building dsDNA to generate TacAT knockout
JPS7	c. KO Rv0918 int F	cagagcctgggtagtagcg	For confirming Rv0918 (TacT) knockout - internal primers
JPS8	c. KO Rv0919 int R	gcgagcgtctttcatcaaca	For confirming Rv0919 (TacT) knockout - internal primers
JPS9	c. KO Rv0918 ext F	ccgttttgctcctgatcgg	For confirming Rv0918 (TacT) knockout - external
JPS10	c. KO Rv0919 ext R	tcgacctcaagccgatctac	For confirming Rv0919 (TacT) knockout - external
FT 221	qPCR 1- amplicon length 138- fw	AGTCGCCACTGGTAGATC A	For qPCR of *pth* knockdown by CRISPRi
FT 222	qPCR 1- amplicon length 138- rv	TCGTGGATGACGATGATG TTG	For qPCR of *pth* knockdown by CRISPRi
FT 223	qPCR 2 - amplicon length 105 - fw	GCAACCCTGGAGCCAATTA	For qPCR of *pth* knockdown by CRISPRi
FT 224	qPCR 2 - amplicon length 105 - rv	AACGCTTGTGTGCCTTGA	For qPCR of *pth* knockdown by CRISPRi
FT 225	qPCR 2 - amplicon length 95 - fw	GCTGGGTACCAAAGACTT TCA	For qPCR of *pth* knockdown by CRISPRi
FT 226	qPCR 2 - amplicon length 95 - rv	GGGTAAAGTTCTCCAACAC AAAC	For qPCR of *pth* knockdown by CRISPRi
FT 434	sgRNA top	GGGAGCTCCAGGGTTGCC GAGGCCGACCA	*Pth* knockdown oligo for sgRNA (PAM = 10)
FT 435	sgRNA bottom	AAACTGGTCGGCCTCGGC AACCCTGGAGC	*Pth* knockdown oligo for sgRNA (PAM = 10)
FT 436	sgRNA top	GGGAATCTGGCGGCCGGA CTCGTTCAT	*Pth* knockdown oligo for sgRNA (PAM = 13)
FT 437	sgRNA bottom	AAACATGAACGAGTCCGG CCGCCAGAT	*Pth* knockdown oligo for sgRNA (PAM = 13)

Appendix II: Supplementary figures and tables accompanying Chapter Three

Figures

Tables

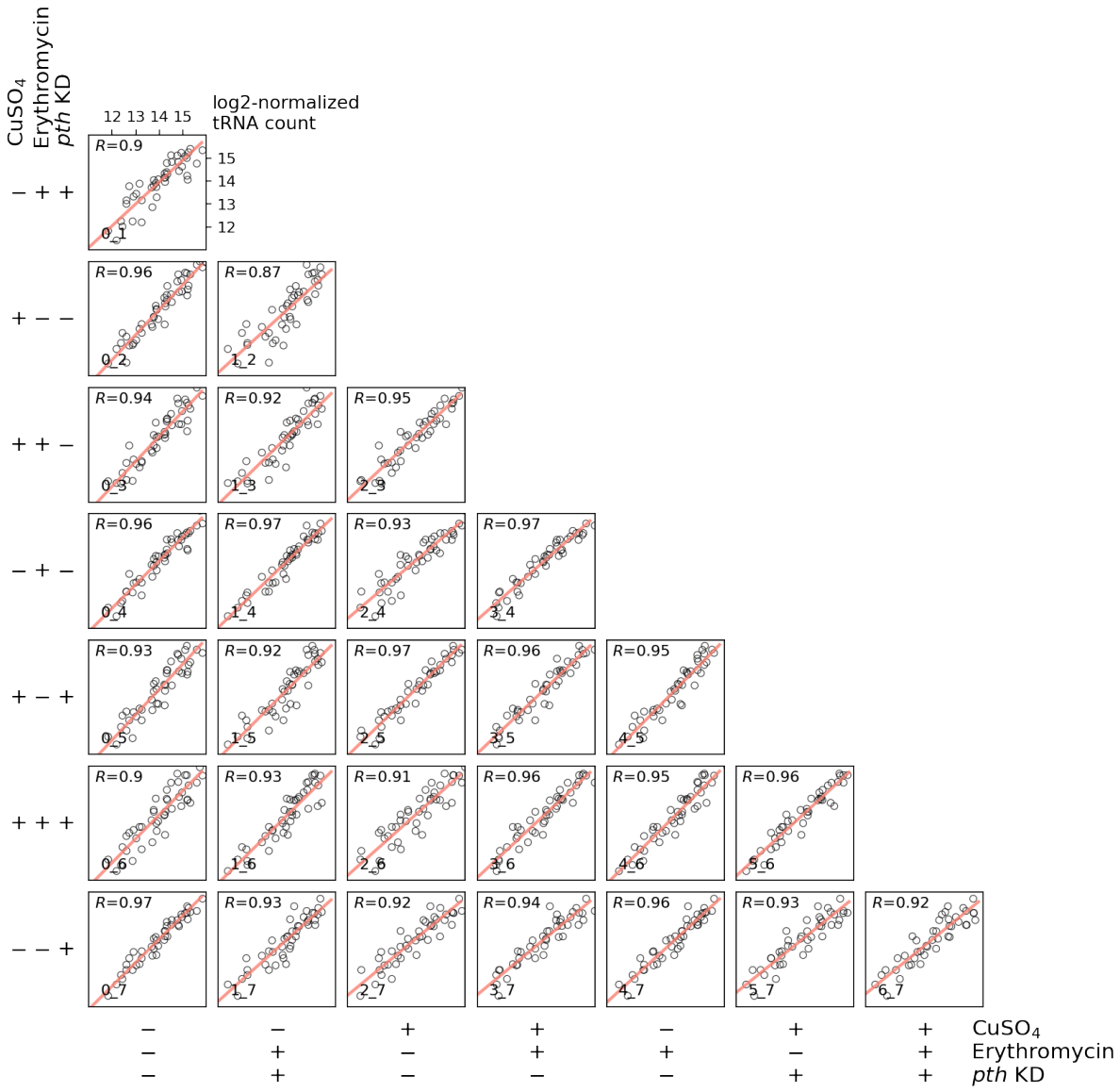

Figure A3.1: Chemical treatments do not bias tRNA counts in $CuSO_4$-tRNAseq. Pairwise linear-regression and Pearson's correlation analysis using the mean tRNA count profiles (Table A3.1) of different treatment groups. Pearson's correlation coefficient is depicted on the top-left corner of each subpanel.

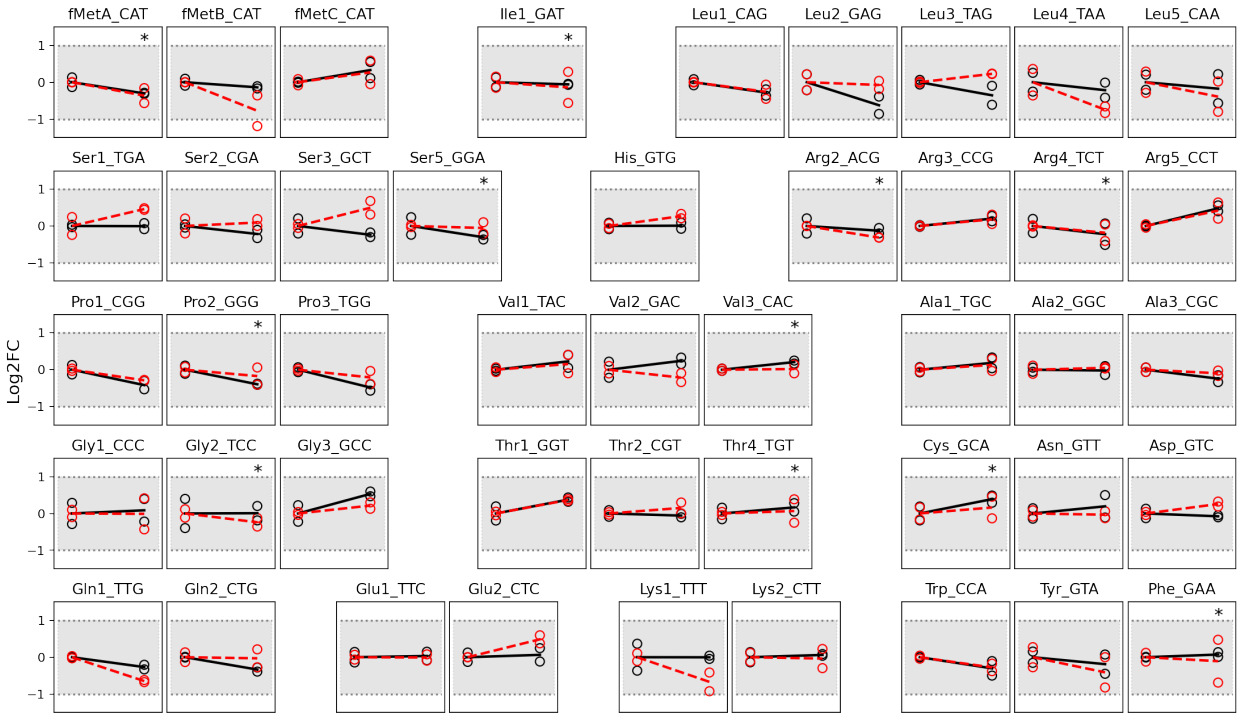

Figure A3.2. Effects of Pth depletion on tRNA abundance. To estimate the effects of Pth depletion on tRNA abundance, log2-transformed tRNA counts from Table A3.1 for $CuSO_4$-treated or $NaIO_4$-only samples were normalized to the average read counts for each corresponding uninduced sample. Normalized read counts of for $CuSO_4$-treated and $NaIO_4$-only were then combined and a non-parametric Mann-Whitney U Test (MWU) was performed to compare tRNA abundance profiles of uninduced (no Pth depletion) and induced (Pth depletion) samples. tRNAs with statistically significant changes (MWU $p<0.05$) in abundance upon Pth depletion are marked by an asterisk. Black: periodate ($NaIO_4$) followed by β-elimination treatments only. Red: copper sulfate (CuSO4) treated samples followed by periodate ($NaIO_4$) and β-elimination treatments. Left: uninduced (no Pth knockdown). Right: induced for Pth knockdown (50ng/mL aTC).

Figure A3.3. Northern blots with arginine- and proline-tRNA probes. Northern blots were performed as described in Methods. Left: RNA blotted using a probe for tRNA-Arg_ACG. Right: RNA blotted using a probe for tRNA-Pro_GGG. $CuSO_4$ treatment was performed where indicated on total RNA samples as described in Methods. Alkali treatment, which also deacylates tRNA, was performed on total RNA where indicated (1 hour at 37C in 100mM Tris pH 9.0). Peptidyl tRNA (blue arrow) is visible in a Pth depleted strain even following $CuSO_4$ treatment, while aminoacyl tRNA is not. KD; knockdown.

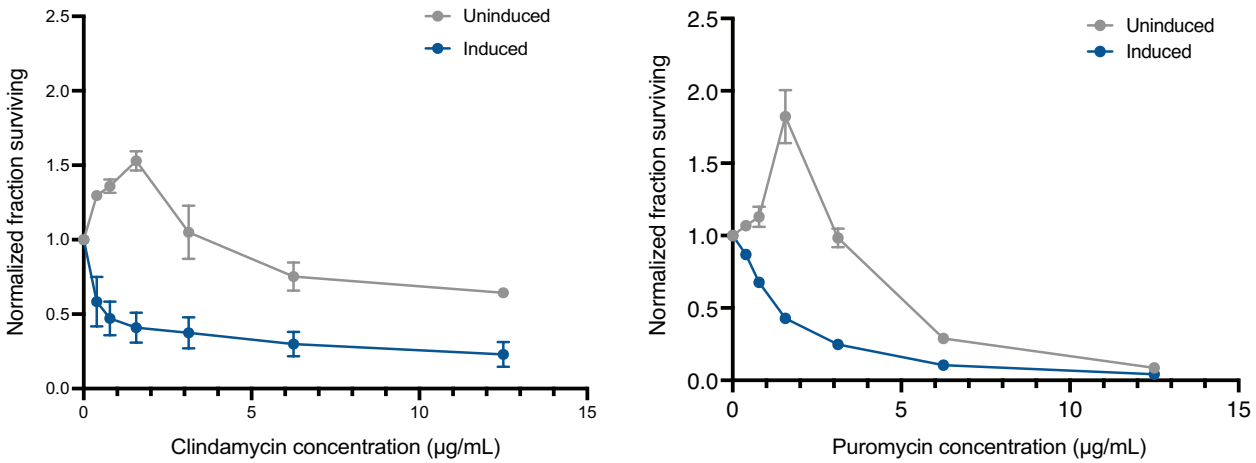

Figure A3.4. Pth depletion increases *Mtb* susceptibility to clindamycin and puromycin. *Mtb* growth in the presence clindamycin (left) or puromycin (right) is plotted across drug concentrations as determined by fluorescence in an Alamar blue assay. Pth CRISPRi strains were grown to mid-log and diluted to an OD_{600} of 0.001 and plated in serial dilutions of antibiotic in 96-well plates. The fraction of *Mtb* cells surviving is plotted by normalizing fluorescence values to control wells with no drug. Results are representative of two biological replicates.

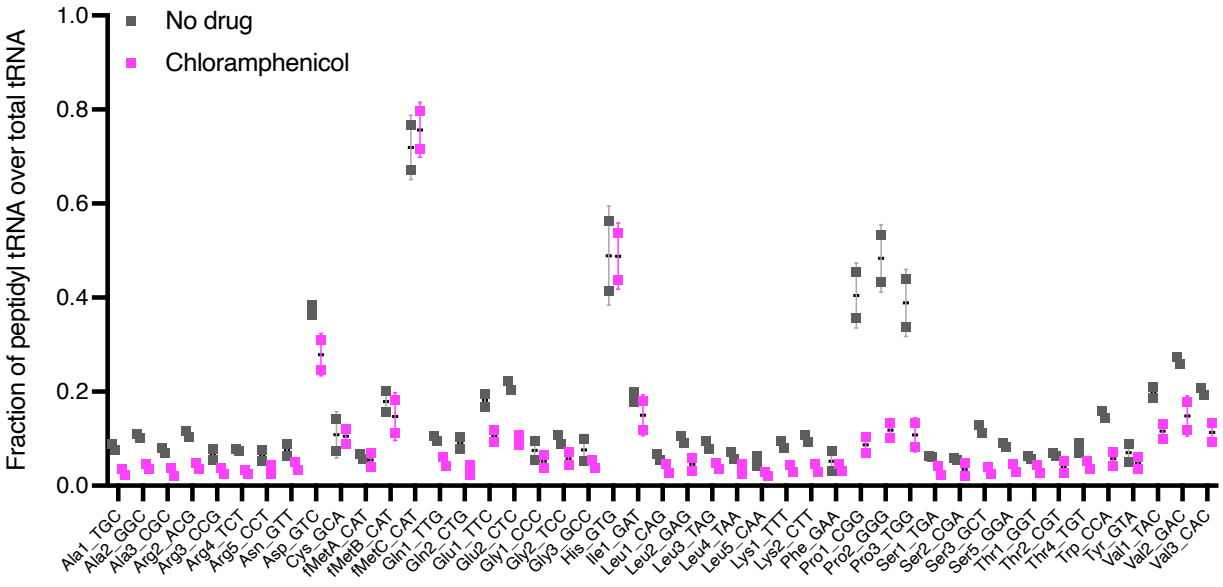

Figure A3.5: Chloramphenicol does not increase peptidyl tRNA drop-off. $CuSO_4$-tRNAseq was performed on *Mtb* strains induced for Pth depletion by CRISPRi in the presence and absence of chloramphenicol (2μg/mL). After 3 days of incubation with inducer (50ng/mL aTC), chloramphenicol was added to cultures and incubated overnight prior to RNA extraction and sample processing. Chloramphenicol treatment (pink) led to a reduction in peptidyl tRNA pools relative to the drug-free control, suggesting that chloramphenicol-induced protein synthesis arrest affects tRNA pools differently from the other ribosome inhibitors tested in this work. Results are from two biological replicates.

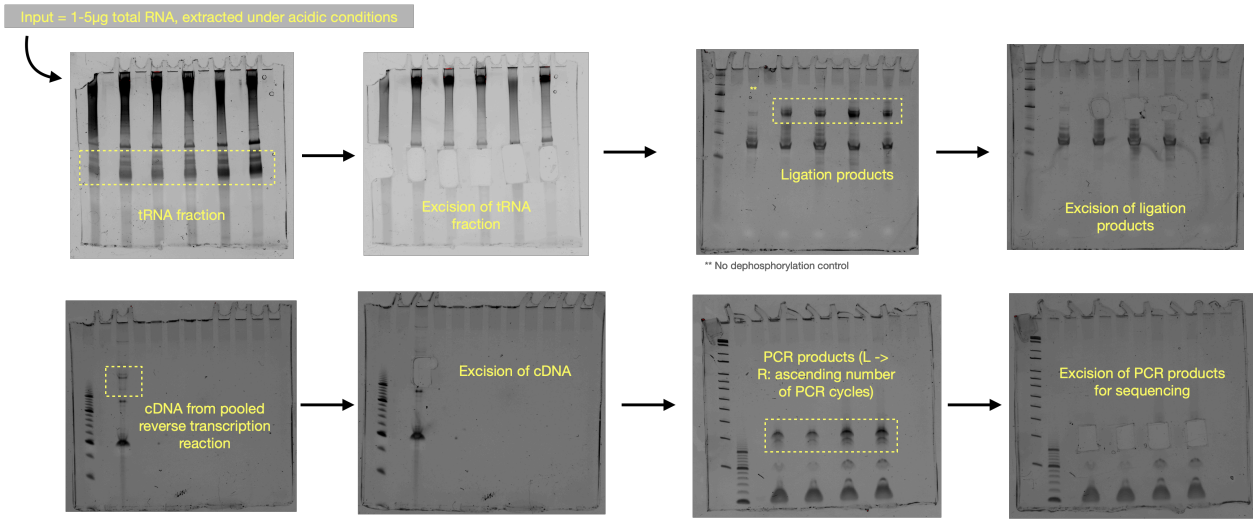

Figure A3.6: Representative images from tRNA sequencing library preparation. The workflow depicted in Figure 3.3 was carried out for each $CuSO_4$-tRNAseq experiment as described in the Methods for Chapter Three. Photos of gels from each step of the tRNA sequencing library preparation process are shown.

Table A3.1. Normalized tRNA counts from *Mtb* $CuSO_4$-tRNAseq experiments. tRNA counts are shown for each tRNA species in reads per million (RPM). Abbreviations: unind = uninduced (no Pth knockdown); ind = induced (Pth knockdown); ery = erythromycin; T1 = treatment 1 ($CuSO_4$), T2 = treatment 2 ($NaIO_4$); T3 = treatment 3 (β-elimination). All treatments were performed as described in Chapter Three.

tRNA	unind-no drug-T1,T2,T3	unind-no drug-T1,T2,T3	unind-no drug-T1,T2,T3	ind-no drug-T1,T2,T3	ind-no drug-T1,T2,T3	ind-no drug-T1,T2,T3	unind-no drug-T2,T3	ind-no drug-T2,T3	ind-ery-T1,T2,T3	ind-ery-T1,T2,T3
Ala1_TGC	14360.02789	14071.13676	15541.83754	16291.18375	15206.04384	18620.8605	15073.96357	16339.13485	14692.53156	16272.81011
Ala2_GGC	36038.6	36540.40076	33815.76651	35460.3464	31884.32895	37626.92651	40394.90159	36507.10415	34194.50321	35560.16874
Ala3_CGC	30248.60056	27506.68549	29954.84687	31234.53575	22744.65521	25885.29176	30051.35347	27517.66674	30622.68443	27886.5348
Arg2_ACG	59577.43559	67591.46694	50813.62883	53965.36007	50927.76964	56425.47441	60248.41458	51664.29445	40275.33598	42900.45061
Arg3_CCG	13954.80332	13681.96412	14129.43897	13986.19612	16796.0644	15191.62353	15587.32886	18345.11116	13746.93326	15094.96612
Arg4_TCT	6664.530599	4848.290868	6320.347265	7260.059904	3876.411235	5797.537538	6639.863238	8082.170117	3961.182792	4321.811553
Arg5_CCT	5147.294419	7745.262869	7634.58686	5710.378956	11320.79916	10135.96328	5480.979223	7499.521396	9885.078022	10630.6629
Asn_GTT	27106.69657	41091.35646	33766.68703	30375.04883	34500.50167	52627.89277	24704.22196	28766.19972	16327.46307	22681.01344
Asp_GTC	46433.0814	40344.83605	33804.85996	44393.80128	35683.44752	34358.51609	44776.29642	44431.12676	30080.35599	35969.34207
Cys_GCA	9780.047873	5947.612635	7721.839281	12436.51517	9489.331036	8295.536934	10489.25576	12818.27186	15896.3815	12368.01546
fMetA_CAT	17238.06472	17354.55355	20820.60902	18361.76585	15243.586	15569.04712	17068.1251	14915.80726	17970.34079	18229.78285
fMetB_CAT	11972.03008	9146.466212	10421.21106	10984.50319	8679.598343	9059.463021	11444.82679	11686.26863	4451.860902	4972.828538
fMetC_CAT	84680.6265	63645.18367	64981.24073	86235.18687	94080.63318	69431.67271	83304.10709	93232.11893	98161.447	93924.23365
Gln1_TTG	8743.426881	7461.566929	7487.348399	7279.593697	6482.278264	5946.691188	9133.835855	8498.347775	4658.462211	5036.884426
Gln2_CTG	26202.00916	29140.66499	29502.22494	29730.43365	22364.81697	24148.62448	26656.02662	24812.51197	22257.31796	22182.94623
Glu1_TTC	18802.42004	17773.73248	21654.9603	18042.7139	21748.684	18528.77433	20349.93553	20692.35315	17370.40238	19025.90603
Glu2_CTC	21363.81627	21230.82211	25319.56199	22776.40318	27486.00819	21382.14851	22728.69746	24471.24629	33328.36696	38285.81214
Gly1_CCC	33725.9928	25711.76311	38271.09327	34698.52845	41153.55992	26934.55527	31545.70391	33094.44736	36292.30112	40770.91915
Gly2_TCC	4962.587406	4038.120733	6991.100253	3457.481443	6114.217949	4663.969796	5233.615091	4036.923282	5020.014502	4706.146881
Gly3_GCC	71115.96962	46338.82206	63247.09886	72073.18661	81795.51599	74841.41076	67674.42136	77642.10386	72789.217	79658.07228
His_GTG	25212.5073	29661.6835	26290.24518	34809.21995	26497.39818	29729.56498	24595.78837	29690.11412	40100.51948	31280.18961
Ile1_GAT	27449.72388	34981.89165	29316.81354	31078.2654	30488.64424	31027.85023	29639.64468	33752.00806	23183.05075	27808.09902
Leu1_CAG	21889.66583	22001.89312	19626.34151	20516.9944	16122.51403	18161.72665	24312.84447	18969.37765	23051.93838	17671.58154
Leu2_GAG	15236.44382	17481.85301	12962.43783	11414.24665	11493.05139	8292.942957	14489.43874	11852.7397	13148.9814	14243.93789
Leu3_TAG	3277.607102	3800.798168	3484.643574	3105.873161	2381.350237	3399.406239	2219.500087	1939.387886	4449.874351	2980.559692
Leu4_TAA	4783.534689	3901.728454	5556.888579	4251.85571	3477.433854	4621.169183	5220.060892	4028.599729	2914.270389	2554.391946
Leu5_CAA	15952.65469	16856.26709	22412.96571	18889.17828	13106.62781	22620.7723	16942.74876	8972.790305	16710.86743	15206.08348
Lys1_TTT	16748.02571	11797.93211	19577.26202	21220.21096	14719.46811	15641.67846	20393.98668	27484.37253	9066.618989	11102.58485
Lys2_CTT	30512.46772	35282.86395	42797.31263	33057.6898	39923.50234	41229.95991	27188.02893	34334.65678	39202.59841	38966.89618
Phe_GAA	18359.50016	19104.01184	19320.95803	21832.26983	19331.99997	21112.37495	21422.41153	25844.63256	22366.57827	18963.15741
Pro1_CGG	51186.45985	54068.62714	45284.00663	37921.60438	34239.17884	40052.29457	50106.48518	39661.7308	26637.66302	29002.93742
Pro2_GGG	32478.27808	40837.66682	35042.75369	20197.94244	29055.41737	28461.11046	32076.01195	22024.12166	16031.46697	18147.42528
Pro3_TGG	10181.50291	14006.57774	12777.02644	6146.633676	10159.20081	9020.553373	9977.584743	6500.695017	7618.423274	7259.231565
Ser1_TGA	3861.884388	6380.4308	6102.216211	4720.666753	5877.187106	6579.621461	3700.296329	4777.719513	11422.66853	7318.058401
Ser2_CGA	5707.069755	8569.072232	8065.39569	7220.992317	6619.196701	7720.971133	4810.046372	6109.488018	13691.30983	9064.561799
Ser3_GCT	5708.954521	16082.46823	12117.18	7188.435994	12352.10416	11324.00453	6002.815885	5693.31036	18168.9959	15697.61438
Ser5_GGA	5744.765064	10814.99842	7776.372044	5729.912749	7113.133643	7741.722945	5253.94639	5360.368234	17618.72126	13003.34529

Table A3.1 continued

Thr1_GGT	29651.12992	23385.82011	17924.91929	23108.47767	27656.05205	25516.9471	28633.2454	26310.75153	28840.74814	27725.74145
Thr2_CGT	12273.59255	12287.12575	13916.76119	10737.07514	12982.22342	12160.56196	11282.1764	10587.55962	12896.68941	14053.07749
Thr4_TGT	8547.411275	10909.56374	8779.774889	8425.576247	11882.4592	10135.96328	9123.670206	9663.645217	9034.834173	9258.036726
Trp_CCA	15999.77383	15931.52744	15879.94067	20295.61141	14782.03836	11252.67017	15768.61627	18245.22852	17781.61844	16795.71531
Tyr_GTA	35322.38913	36744.07989	45463.96475	42746.45136	29926.98419	42995.16094	34793.62885	30048.0269	48670.50071	38717.20894
Val1_TAC	6856.776674	6354.061626	6102.216211	6869.384034	8224.675794	6452.516611	6729.659807	7116.63795	8550.115717	7940.315599
Val2_GAC	23759.35315	27621.25501	20395.25347	23101.9664	29819.51058	26404.08707	23081.10663	22739.94723	26621.77061	31929.89933
Val3_CAC	25180.46629	19925.09336	20826.0623	20660.24222	24190.39613	22872.38803	23650.38299	23239.36042	20236.99554	22830.04143
tRNA	**unind-ery-T1,T2,T3**	**unind-ery-T1,T2,T3**	**unind-no drug-T2,T3**	**unind-no drug-T2,T3**	**unind-ery-T2,T3**	**unind-ery-T2,T3**	**ind-no drug-T2,T3**	**ind-no drug-T2,T3**	**ind-ery-T2,T3**	**ind-ery-T2,T3**
Ala1_TGC	18599.09842	17945.83898	17758.84166	16503.38668	23996.82553	21444.64117	21017.84116	16740.39138	26488.93959	22531.2773
Ala2_GGC	34867.6013	34042.71795	50302.09637	43160.13547	44332.57833	46813.68127	47654.72201	48827.21051	49865.65394	49370.61726
Ala3_CGC	30258.59988	29006.90456	46096.3962	42405.61099	41786.62666	39375.08458	39311.33855	43510.05172	40078.65624	40734.76037
Arg2_ACG	45080.46997	52317.22269	54856.42794	54620.89485	52002.29396	49659.71627	43917.94447	44097.9965	42700.53088	55969.73613
Arg3_CCG	14639.20619	12503.92549	12005.27906	12200.594	16312.6278	14860.27787	14950.33654	12564.91445	20549.69303	14565.19809
Arg4_TCT	4383.933406	5010.001936	7443.318788	7620.029487	4802.261523	5098.617439	5675.178466	7744.836241	5548.967512	5726.544353
Arg5_CCT	8772.759595	7292.594266	5332.458576	5680.968355	8101.281955	6819.770851	8559.550012	6312.388959	12048.61476	7412.498643
Asn_GTT	19980.49411	25479.34009	24858.10625	22072.17794	16981.70043	17968.50332	21443.72152	24421.08819	22386.00599	23950.8552
Asp_GTC	38199.5864	35802.19827	47123.98157	44435.48215	37366.69235	45781.83499	52160.02003	57235.88986	47804.17999	51329.52514
Cys_GCA	11059.3201	10134.43462	4587.134967	5762.43029	13343.79906	9631.97483	7048.965272	4691.799346	9636.890377	7823.573324
fMetA_CAT	18078.83252	16494.37526	21799.76198	21659.52651	15087.44287	16243.12102	14670.93321	19447.07535	13464.62721	15996.83418
fMetB_CAT	5701.722912	5375.664107	9808.21458	9856.894083	7684.197721	6489.918354	7671.008711	4306.962763	6984.994271	3978.106711
fMetC_CAT	92379.00148	83222.12901	67377.40685	59970.6737	70223.66142	76056.37377	95373.32608	61330.12351	79241.65779	85242.6382
Gln1_TTG	6016.49194	6067.410897	5346.190229	5134.772761	4034.710677	3772.159322	3281.214611	3410.079725	3277.3433	4181.999752
Gln2_CTG	20623.07958	28791.80917	28332.97733	23621.29014	22719.50506	20683.4431	21415.3295	29998.01168	22911.38164	28842.0958
Glu1_TTC	20474.66517	17595.66368	16046.19938	17547.70197	16228.63167	16088.06216	17712.10617	15725.91939	18107.94718	14901.73123
Glu2_CTC	32135.79756	28601.66484	24250.09917	24373.14374	27185.78206	32146.52217	31569.99505	36717.68602	43421.04605	35855.57795
Gly1_CCC	28632.56506	30806.82283	34792.95719	39874.94925	19041.05383	24396.39812	27624.79424	49528.46829	16116.52331	23414.81382
Gly2_TCC	4489.9437	4304.489041	5137.163956	6008.151535	3774.033031	3442.306825	4345.270244	5100.153721	4313.083855	2499.334059
Gly3_GCC	71569.99615	71433.18062	63543.22419	67015.12788	71689.24907	72523.85087	71253.65628	80376.32742	64255.943	61569.12139
His_GTG	37731.51017	35073.45508	37195.99646	34236.71503	47226.1002	46588.1411	41244.57728	44763.97759	55324.55706	48751.26474
Ile1_GAT	32850.14385	33098.87935	29207.98877	23704.08752	30337.08516	34028.37295	32001.0376	17811.51987	29205.88221	29473.50651
Leu1_CAG	19726.0694	19825.77273	31315.7975	30935.50351	24631.14113	26727.91962	22779.43721	29721.14314	20149.40683	27083.79237
Leu2_GAG	14874.05977	15204.66327	18045.68063	13421.18758	14372.02755	14592.44892	13696.57057	15956.82134	9311.657835	14438.03899
Leu3_TAG	3711.991232	3926.781528	2953.068262	3022.104229	4486.55193	3308.39235	3512.867717	3483.84007	3432.454205	4355.199218
Leu4_TAA	2857.385166	3051.773462	3615.239083	5952.06299	4089.742624	3253.416934	2943.091414	2599.784919	3027.164423	2460.967089
Leu5_CAA	13652.49499	17566.4107	15074.3035	22484.82938	18160.54267	11185.38274	10560.54244	18658.16035	5909.225096	11229.46408
Lys1_TTT	10817.94281	12884.21415	14085.62449	16285.70971	10986.11457	10037.94713	11358.10021	7989.635068	10882.78119	7723.819202
Lys2_CTT	40068.62943	32925.08227	28956.2418	34101.83543	44193.55026	32841.46782	36697.98178	25589.49482	50476.0904	26215.60264
Phe_GAA	20153.37243	17561.24841	8957.614964	10564.67811	20636.98031	14289.37931	13506.86022	6036.589407	23106.52116	9801.116588
Pro1_CGG	45391.97714	45960.72358	60597.02176	58015.58727	62562.63505	68355.58663	48931.07255	48248.88665	36891.37733	42338.49972
Pro2_GGG	21303.17639	21922.52264	29528.39401	26571.28053	25691.23022	22576.57089	29207.00431	21158.52915	27729.82683	20287.35764

Table A3.1 continued

Pro3_TGG	10532.53048	8964.315674	9198.681761	8853.977479	9781.204562	8597.309306	8811.20659	6911.023644	7880.634654	5380.145422
Ser1_TGA	6013.230085	6411.563528	2592.993805	3629.730134	4075.260533	3937.08557	4156.850447	4281.306991	4548.252	5543.479095
Ser2_CGA	8029.056606	8404.207266	5258.460224	6964.327685	6409.773674	6635.109838	6055.8897	6882.1609	6814.872634	7909.076858
Ser3_GCT	15578.6205	17784.08724	11841.26209	12734.77062	10641.44079	12152.38621	15231.03042	19644.83859	14935.67901	17991.91663
Ser5_GGA	8625.97611	9617.345293	8686.033383	8337.161599	4912.325418	7004.431864	7357.405898	9123.833999	8691.214218	12344.29861
Thr1_GGT	28277.02284	31553.63404	19666.77855	21037.21074	20243.06742	27236.79462	25752.21119	26653.14037	29110.81423	34594.94893
Thr2_CGT	14084.69081	13874.51335	9449.665863	9904.969979	8793.525926	10824.51847	11894.3223	9687.191997	12248.75786	13074.36725
Thr4_TGT	7851.285497	8465.294358	7760.672546	7322.226021	6091.167662	7572.511164	9839.126919	6334.837759	10792.71679	9968.835058
Trp_CCA	17452.55632	18627.26119	11100.5157	11749.21476	16106.98211	13867.90112	10114.65861	8786.032998	11748.40011	12895.68679
Tyr_GTA	36216.37843	41813.68437	36541.45433	53318.83934	35460.84911	33309.46367	24977.23799	44146.10107	14600.43931	31557.38109
Val1_TAC	7220.116513	5301.671291	7029.08059	6438.163714	6621.212209	6800.036086	8904.771215	6291.009148	8691.214218	7119.813471
Val2_GAC	27720.87653	27040.07227	20518.14104	17818.79661	20602.22329	21296.63043	17923.11053	15152.94047	14300.22466	22531.2773
Val3_CAC	23315.74106	20912.43466	24025.05264	23071.08822	26192.31059	23684.53697	25885.78276	21999.82469	30987.15582	19033.30582

Table A3.2: Minimal inhibitory concentrations of antibiotics in *Mtb* Pth proteolytic degradation strains. Minimal inhibitory concentrations are shown for a panel of antibiotics against Pth depletion strains by proteolytic degradation. Pth-tagged control: *pth-flag-DAS* strain used as a parental backbone for generating knockdown strains (by introducing inducible SspB expression plasmids). This strain serves as a control for potential effects of the FLAG or DAS tags on Pth activity even in the absence of induced degradation mediated by SspB.

	Pth-tagged control	**pTetON-6 (-)**	**pTetON-6 (+)**	**pTetON-10 (-)**	**pTetON-10 (+)**
Isoniazid	0.06	0.06	0.06	0.06	0.06
Ethambutol	0.59	0.59	0.59	0.59	0.59
Kanamycin	1.56	2.34	2.34	2.34	2.34
Chloramphenicol	1.2	0.59	0.59	0.59	0.59
Fusidic acid	0.30	0.30	0.30	0.30	0.30
Linezolid	0.15	0.15	0.15	0.15	0.15
Capreomycin	1.56	0.78	0.78	1.56	0.78
Erythromycin	6.25	0.4	0.05	0.4	0.012
Clarithromycin	5	0.08	0.02	0.04	< 0.01

Table A3.3. Strains and primers used in this work. All strains and primers used for the work in Chapter Three are listed below. Top; strains. Middle; plasmids. Bottom; primers

Strain name	Organism	Selection	Source (if published)	Notes
FT-BL3-4	H37Rv	Kanamycin	Tomasi et al. 2022	WT H37Rv with transcriptional repression of *pth* via CRISPRi used for growth curves, MIC assays, and tRNA sequencing
JP-BL3-1 (pTetON-6)	H37Rv	Hygromycin, streptomycin		Removal of aTC induced Pth depletion via proteolytic degradation - pTetON-6
JP-BL3-2 (pTetON-10)	H37Rv	Hygromycin, streptomycin		Removal of aTC induced Pth depletion via proteolytic degradation - pTetON-10
JP-BL3-3 (Pth ctrl.)	H37Rv	Hygromycin, streptomycin		Pth-DAS tagged control (no SspB) used for MIC assays

Name	Source	Selection	Notes
pGMCgS-TetON-6 sspB	Gift of Schnappinger Lab; common lab strain	Streptomycin	Construction of knock-down strains (knocked-down to various degrees) using sspB system
pGMCgS-TetON-10 sspB	Gift of Schnappinger Lab; common lab strain	Streptomycin	Construction of knock-down strains (knocked-down to various degrees) using sspB system
pNit-RecET SacBR	Common lab strain	Kanamycin	For recombineering
pPrpsA-Tet-dCas9-sgRNA1-KanR	Gift of Jeremy Rock	Kanamycin	For CRISPRi transcriptional repression, optimized for Mtb

Primer	Sequence (5' to 3')	Notes
FT 676	tcgggctgacaggatttgaacctgcgaccacttga	tRNA-Pro (GGG) Northern blot probe
FT 689	cgcgcccgaagagattcgaactcccaaccttctga	tRNA-Arg (ACG) Northern blot probe
D701	AGATCGGAAGAGCACACGTCTGAACTCCAGTCACATTACTCGCGATCTCGTATGCCGTCTTCTGCTTG/3ddC/	tRNAseq linker_D701

Table A3.3 continued

D702	AGATCGGAAGAGCACACGTCTGAACTCCAGTCAC TCCGGAGACGATCTCGTATGCCGTCTTCTGCTTG /3ddC/	tRNAseq linker_D702
D703	AGATCGGAAGAGCACACGTCTGAACTCCAGTCAC CGCTCATTCGATCTCGTATGCCGTCTTCTGCTTG/ 3ddC/	tRNAseq linker_D703
D704	AGATCGGAAGAGCACACGTCTGAACTCCAGTCAC GAGATTCCCGATCTCGTATGCCGTCTTCTGCTTG /3ddC/	tRNAseq linker_D704
D705	AGATCGGAAGAGCACACGTCTGAACTCCAGTCAC ATTCAGAACGATCTCGTATGCCGTCTTCTGCTTG/ 3ddC/	tRNAseq linker_D705
D706	AGATCGGAAGAGCACACGTCTGAACTCCAGTCAC GAATTCGTCGATCTCGTATGCCGTCTTCTGCTTG/ 3ddC/	tRNAseq linker_D706
D707	AGATCGGAAGAGCACACGTCTGAACTCCAGTCAC CTGAAGCTCGATCTCGTATGCCGTCTTCTGCTTG /3ddC/	tRNAseq linker_D707
D708	AGATCGGAAGAGCACACGTCTGAACTCCAGTCAC TAATGCGCCGATCTCGTATGCCGTCTTCTGCTTG /3ddC/	tRNAseq linker_D708
RT-univ	/5Phos/AGATCGGAAGAGCGTCGTGTAGGGAAA GAGTGT/iSp18/CAAGCAGAAGACGGCATACGAG ATCG	RT-universal for tRNA sequencing library prep (reverse transcription)
D501	AATGATACGGCGACCACCGAGATCTACACTATAG CCTACACTCTTTCCCTACACGACG	Index-D501 for sequencing
D502	AATGATACGGCGACCACCGAGATCTACACATAGA GGCACACTCTTTCCCTACACGACG	Index-D502 for sequencing
D503	AATGATACGGCGACCACCGAGATCTACACCCTAT CCTACACTCTTTCCCTACACGACG	Index-D503 for sequencing

Table A3.3 continued

D504	AATGATACGGCGACCACCGAGATCTACACGGCTC TGAACACTCTTTCCCTACACGACG	Index-D504 for sequencing
D505	AATGATACGGCGACCACCGAGATCTACACAGGC GAAGACACTCTTTCCCTACACGACG	Index-D505 for sequencing
D506	AATGATACGGCGACCACCGAGATCTACACTAATC TTAACACTCTTTCCCTACACGACG	Index-D506 for sequencing
PCR-univ	CAAGCAGAAGACGGCATACG	PCR-universal-R for tRNA sequencing
JP 1	atggccgagccgttgctc	Amplify region upstream of Pth (Rv1014c) - Fw
JP 2	ctcgtcgttggcggccttgtcgtcgtcgtccttg tagtcccaggcgtggacgcggtttt	Amplify region upstream of Pth (Rv1014c) plus Flag and partial DAS tag - Rv
JP 3	ctacttgtcgtcgtcgtcctttcactagctggcg tccgcgtagttctcggagtagttctcgtcgttggcggccttg	Complete DAS tag and append HygR overlap - Rv
JP 4	gactacaaggacgacgacga	Amplify HygR cassette - Fw
JP 5	tccttccctaggcccaaaaa	Amplify HygR cassette - Rv
JP 6	gttttttgggcctagggaaggataacgacccgcgtgagcaga	Amplify region downstream of Pth (Rv1014c) and append overlap - Fw
JP 7	agtcgctaactcccggctac	Amplify region downstream of Pth (Rv1014c) - Rv
JP 8	gagtccgagtagacggcttg	Confirm recombineering into genome - Fw
JP 9	aactgcatctcaacgccttc	Confirm recombineering into genome - Rv
JP 10	gcgtaggaatcatccgaatc	Confirm recombineering into genome from HygR cassette -Fw
JP 11	gacgaacagggcgatgtcat	Confirm recombineering into genome from HygR cassette -Rv
JP 12	gccagatcgtgctgaacat	Confirm transformation of sspB-containing plasmid - Fw
JP 13	tttttgtgatgctcgtcagg	Confirm transformation of sspB-containing plasmid - Rv

Fin.